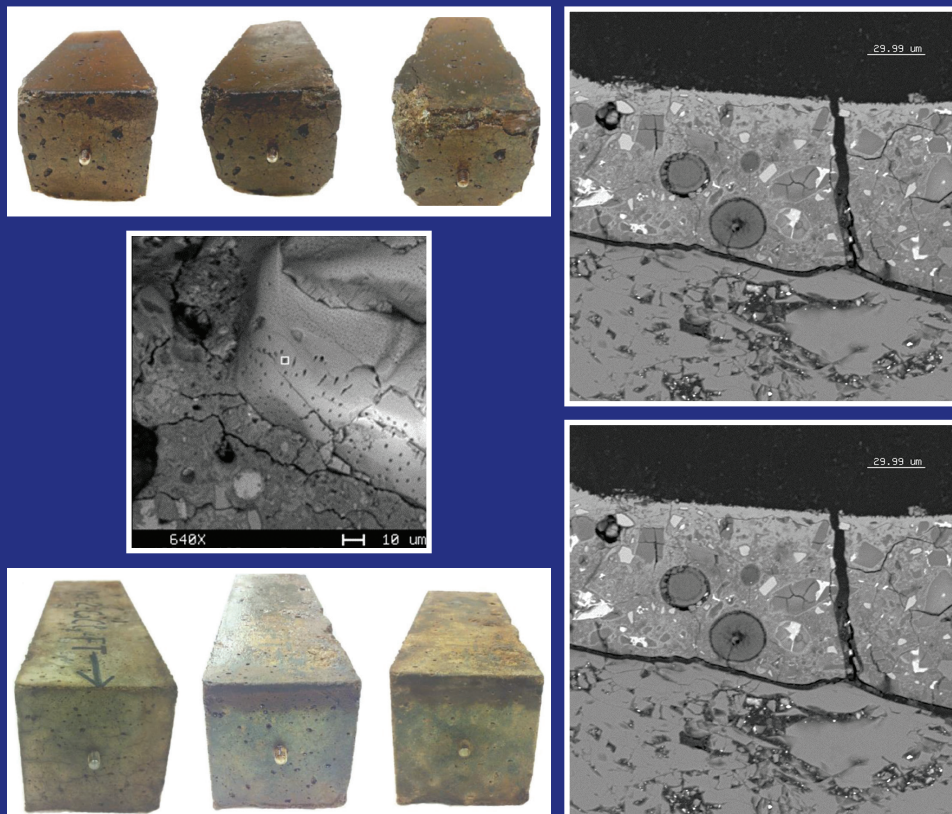


JOINT TRANSPORTATION RESEARCH PROGRAM

INDIANA DEPARTMENT OF TRANSPORTATION
AND PURDUE UNIVERSITY



Investigation of Use of Slag Aggregates and Slag Cements in Concrete Pavements to Reduce the Maintenance Cost



Kho Pin Verian, Parth Panchmatia, Jan Olek

RECOMMENDED CITATION

Verian, K. P., Panchmatia, P., & Olek, J. (2017). *Investigation of use of slag aggregates and slag cements in concrete pavements to reduce the maintenance cost* (Joint Transportation Research Program Publication No. FHWA/IN/JTRP-2017/17). West Lafayette, IN: Purdue University. <https://doi.org/10.5703/1288284316362>

AUTHORS

Kho Pin Verian

Graduate Research Assistant
Lyles School of Civil Engineering
Purdue University

Parth Panchmatia

Graduate Research Assistant
Lyles School of Civil Engineering
Purdue University

Jan Olek, PhD, PE

Professor of Civil Engineering
Lyles School of Civil Engineering
Purdue University
(765) 494-5015
olek@purdue.edu
Corresponding Author

JOINT TRANSPORTATION RESEARCH PROGRAM

The Joint Transportation Research Program serves as a vehicle for INDOT collaboration with higher education institutions and industry in Indiana to facilitate innovation that results in continuous improvement in the planning, design, construction, operation, management and economic efficiency of the Indiana transportation infrastructure. https://engineering.purdue.edu/JTRP/index_html

Published reports of the Joint Transportation Research Program are available at <http://docs.lib.purdue.edu/jtrp/>.

NOTICE

The contents of this report reflect the views of the authors, who are responsible for the facts and the accuracy of the data presented herein. The contents do not necessarily reflect the official views and policies of the Indiana Department of Transportation or the Federal Highway Administration. The report does not constitute a standard, specification or regulation.

COPYRIGHT

Copyright 2017 by Purdue University. All rights reserved
Print ISBN: 978-1-62260-490-6

1. Report No. FHWA/IN/JTRP-2017/17	2. Government Accession No.	3. Recipient's Catalog No.	
4. Title and Subtitle Investigation of Use of Slag Aggregates and Slag Cements in Concrete Pavements to Reduce the Maintenance Cost		5. Report Date December 2017	
		6. Performing Organization Code	
7. Author(s) Kho Pin Verian , Parth Panchmatia , Jan Olek		8. Performing Organization Report No. FHWA/IN/JTRP-2017/17	
9. Performing Organization Name and Address Joint Transportation Research Program Purdue University Mann Hall, Rm 154 203 S Martin Jischke Drive West Lafayette, IN 47907		10. Work Unit No.	
		11. Contract or Grant No. SPR-3310	
12. Sponsoring Agency Name and Address Indiana Department of Transportation State Office Building 100 North Senate Avenue Indianapolis, IN 46204		13. Type of Report and Period Covered Final Report	
		14. Sponsoring Agency Code	
15. Supplementary Notes Prepared in cooperation with the Indiana Department of Transportation and Federal Highway Administration.			
16. Abstract <p>The air-cooled blast furnace slag (ACBFS), the by-product of the pig iron making process, is often used as coarse aggregate in portland cement concrete (PCC) pavements, especially in the areas located in the vicinity of the iron mills. The utilization of this by-product as an aggregate in concrete offers environmental and economic benefits in the form of elimination of waste, decrease in the disposal costs, and reduction in need for mining of the natural materials. However, concerns exist with relation of the influence of these aggregates on the long-term durability of pavement concretes, especially at locations exposed to freezing and thawing environment.</p> <p>The objective of this research was to evaluate the influence of using the ACBFS aggregate (slag aggregate) as a replacement for natural aggregates on the properties of pavement concrete designed to meet the standard specifications of the Indiana Department of Transportation. A total of eight different concrete mixtures, four containing air-cooled blast furnace slag (ACBFS) as coarse aggregate and additional four containing natural dolomite, were used in this study. These mixtures included plain concrete mixture (100% of Type I portland cement), two mixtures with binary binder systems (one containing 20 wt.% of Class C fly ash + 80 wt.% of Type I portland cement and the other containing 25 wt.% slag cement + 75 wt.% of Type I portland cement) and one mixture with a ternary binder system (23% slag cement + 17% of Class C fly ash + 60% of Type I portland cement). Specimens produced from each of these mixtures were ponded with each of the three different types of chloride based deicers (CaCl₂, MgCl₂ and NaCl) while being subjected to either freezing-thawing (FT) cycles or wetting-drying (WD) cycles.</p> <p>The mechanical and durability properties of these concretes were assessed by conducting series of tests prior and after the exposure to FT and WD cycles. In addition, changes in the overall physical appearance of the test specimens were also documented to aid in the evaluation of the effects of given exposure conditions on the deterioration process of concretes. In the case of a plain concrete, the analysis of the data collected during the study (i.e., the observed loss of strength, reduction in the dynamic modulus of elasticity, and physical changes in the appearance of the specimens) indicated that the calcium chloride (CaCl₂) deicer caused the most severe distress, followed by the magnesium chloride (MgCl₂). Specimens exposed to sodium chloride (NaCl) experienced the least damage and performed comparably to those exposed to distilled water (DST). The scanning electron microscopy studies of the microstructure revealed the presence of deposits of Friedel's salt and zones of chloride rich C-S-H in all concretes used in this project, irrespective of the type of deicer the specimen was exposed to. The deposits of brucite (Mg(OH)₂) and of magnesium-silicate hydrate (M-S-H) were found in specimens exposed to MgCl₂ while calcium oxychloride was detected in concretes exposed to CaCl₂ under FT conditions.</p>			
17. Key Words air-cooled blast furnace slag (ACBFS) aggregate, plain concrete, fly ash concrete, slag cement, deicers, freezing and thawing, wetting and drying, pavement concrete, compressive strength, flexural strength, durability, chloride penetration, scanning electron microscopy (SEM)		18. Distribution Statement No restrictions. This document is available to the public through the National Technical Information Service, Springfield, VA 22161.	
19. Security Classif. (of this report) Unclassified	20. Security Classif. (of this page) Unclassified	21. No. of Pages 91	22. Price

EXECUTIVE SUMMARY

INVESTIGATION OF USE OF SLAG AGGREGATES AND SLAG CEMENTS IN CONCRETE PAVEMENTS TO REDUCE THE MAINTENANCE COST

Introduction

This project originated in response to the reported field cases of deterioration of pavement concrete containing air-cooled, blast furnace slag (ACBFS) aggregates. Although the root causes of the observed deterioration were not always entirely clear, some of the concerns appeared to be related to the physical characteristics and chemical composition of the slag aggregates themselves. These included such issues as the perceived variability of specific gravity and porosity of aggregate particles, as well as the fact that such aggregates can contain the soluble calcium sulfide (CaS). The presence of this compound has been linked to the formation of secondary ettringite, which can deposit in the existing air-void system, thus making it less effective in offering freeze-thaw resistance to concrete.

The main purpose of this research was to evaluate the influence of using air-cooled blast furnace slag (ACBFS) coarse aggregate as a replacement for natural dolomite coarse aggregate on the mechanical properties and durability of pavement concrete mixtures. All mixtures containing ACBFS were designed to meet the requirements of Indiana Department of Transportation (INDOT) specifications for pavement concrete. The scope of the study included evaluation and analysis of the effects of ACBFS on concrete properties in the presence of three different types of deicers (CaCl_2 , MgCl_2 , and NaCl). These evaluations were conducted under simulated temperature cycles that represented exposure to freezing-thawing (FT) and wetting-drying (WD) conditions.

Eight different concrete mixtures were produced in the course of this study. These mixtures were prepared using two types of coarse aggregates, ACBFS and (for comparison with the typical INDOT mixtures) dolomite. Four different binder systems were used, including: (a) plain – 100% portland cement (PC); two types of binary binder systems, (b) 20% fly ash (FA) + 80% PC and (c) 25% slag cement (SC) + 75% PC; and a single ternary system, (d) 17% FA + 23% SC + 60% PC.

Each mixture was used to prepare several types of specimens for laboratory testing. The test performed on fresh concrete included determination of slump, unit weight, and entrained air content. The mechanical properties of the hardened concrete were assessed by conducting compressive strength and flexural strength tests. The durability of concrete was assessed by periodically measuring relative dynamic modulus of elasticity (RDME) and by monitoring the length changes of the prismatic specimens. The changes in the physical appearance of specimens exposed to either FT or WD conditions were documented at different stages of the exposure cycles. The depth of chloride ion penetration was measured after completion of the exposure period. The combined effects of the deicer/exposure conditions on the microstructure of the concrete were evaluated using scanning electron microscopy (SEM) analysis on the specimens after completion of the exposure test.

Findings

This study demonstrated that air-cooled blast furnace slag (ACBFS) can safely replace the natural coarse aggregate in a typical pavement concrete. Potential benefits of using ACBFS aggregate in pavement concrete include improved quality of the

paste due to the possibility of internal curing and reduced risk of alkali-silica reaction (ASR) due to the absence of an active form of silica in the aggregate particles. The specific gravity of ACBFS is also lower than that of a typical natural aggregate, thus resulting in a larger volume of concrete for the same weight (an economical benefit). However, it should also be realized that ACBFS has lower resistance to the abrasion compared to dolomite and it contains calcium sulfide, which can dissolve and release sulfide into the pore solution. That sulfide can subsequently oxidize and convert to sulfate, thus increasing the potential for sulfate-related problems. Moreover, in some cases, the leaching of calcium sulfide (CaS) from ACBFS particles was found to create intraparticle porosity, which may weaken the aggregate. With that said, none of these were found to have any measurable negative impact on the durability of concrete under the conditions used in this study. This is mostly because, as discussed below, the durability of concrete was primarily controlled by the type of the binder system and the type of the deicer used.

Under the exposure conditions used in this study (i.e., FT and WD cycles in the presence of the deicers), the durability of pavement concrete was highly improved in cases where part of the portland cement was replaced by either fly ash, slag cement, or a combination of these materials. The observed improvement is attributed to a reduction in the amount of calcium hydroxide present in the hydrated matrix (due to pozzolanic reaction) and to densification of the matrix by formation of additional C-S-H (also due to pozzolanic reaction). Both of these processes reduced the vulnerability of the matrix to chemical attack by chloride-based deicers. In addition, the use of slag cement reduces the total alkali content of the pore solution (especially at later ages), which is beneficial with respect to minimizing the potential for dissolution of calcium sulfide from ACBFS aggregate.

In terms of their role in concrete deterioration, calcium chloride was found to be the most aggressive deicer, followed by magnesium chloride and sodium chloride, respectively.

The mechanisms of deterioration of concrete exposed to CaCl_2 and NaCl deicers were found to be similar. Specifically, in both cases, the deicers reacted with calcium hydroxide, producing expansive compounds that resulted in deterioration of concrete matrix. This, in turn, allowed for more extensive penetration of water and deicers into the concrete matrix. However, the deterioration rate of CaCl_2 was found to be much faster than that of NaCl . The faster deterioration rate observed in the presence of CaCl_2 can be attributed to the formation of calcium oxychloride.

Two most common concrete deterioration mechanisms triggered by the exposure of MgCl_2 involved its reaction with calcium hydroxide and calcium-silicate-hydrate (C-S-H) to produce CaCl_2 and magnesium-silicate-hydrate (M-S-H), respectively. Unlike C-S-H, M-S-H does not have binding capacity and thus reduces the strength of the concrete.

Statistical analysis has proven to be an effective tool in assessing the significance of several different variables (i.e., type of binder system, type of aggregate, type of deicer, and type of exposure conditions) in affecting concrete properties. Moreover, Tukey's multiple comparison method was found to be suitable for differentiating the impact of different levels within a specific factor.

The benefit cost analysis has proven that air-cooled blast furnace slag (ACBFS) is an economically feasible alternative to natural stone to be used as a coarse aggregate in pavement concrete.

Implementation

The results from this study revealed that ACBFS is a viable alternative for natural coarse aggregate to be used in pavement concrete. The usage of fly ash, slag cement, and the combination

of both as partial replacement of portland cement was found to not only improve concrete's strength at later ages, but also to increase concrete durability in the presence of deicers and under the FT/WD exposure conditions used in this study. Among the three types studied, the calcium chloride (CaCl_2) deicer was found to be the most aggressive in terms of inducing damage to the

concrete. The next (in terms of its deteriorative effects) was the magnesium chloride (MgCl_2) deicer, followed by sodium chloride (NaCl). Thus, it is advised that the use of these deicers on plain concrete pavements should be more strictly monitored and restricted to cases where other deicers cannot provide the required safety of roadways.

CONTENTS

1. INTRODUCTION	1
1.1 Background	1
1.2 Literature Review	1
1.3 Research Objectives	2
1.4 Scope of Work	3
1.5 Test Program	3
2. TEST RESULTS AND ANALYSIS.	5
2.1 Aggregate Test Results	5
2.2 Concrete Test Results	5
2.3 Pore Solution Analysis Results	15
3. COST BENEFIT ANALYSIS OF USING SLAG AGGREGATE IN NEW CONCRETE PAVEMENTS	21
3.1 Background	21
3.2 Cost Benefit Analysis Model	21
4. CONCLUSIONS	22
REFERENCES	24
APPENDICES	
Appendix A. Mechanisms of Deicers Deterioration on Pavement Concrete	26
Appendix B. Mill Certificates	28
Appendix C. Test Results	31
Appendix D. SEM Results	60
Appendix E. Pore Solution Analysis	80
Appendix F. Benefit Cost Analysis	81

LIST OF TABLES

Table	Page
Table 1.1 Typical composition of ACBFS	2
Table 1.2 Materials used in the project	3
Table 1.3 Mixture proportions for concrete used in this study	4
Table 1.4 Test performed for this project	4
Table 2.1 Specific gravity and absorptions of aggregates used in this study	5
Table 2.2 Fresh concrete properties, w/cm, and the dosage of admixtures	6
Table 2.3 Tukey pair wise comparison test results of 28-day compressive strength	7
Table 2.4 Tukey pair wise comparison test results of the compressive strength of control 2 (C2) specimens	7
Table 2.5 Changes in the final RDME values with respect to the initial values	9
Table 2.6 The least square (LS) means values for the differences in RDME values of FT and WD specimens exposed to deicers after exposure when compared to the initial RDME values	10
Table 2.7 The results of the analysis of variance (ANOVA) for the differences in RDME values of FT and WD specimens exposed to deicers after exposure when compared to the initial RDME values	10
Table 2.8 The results of Tukey's multiple comparison analysis on the effects of the type of binder system on the change in RDME values of concrete after exposure period when compared the initial RDME values	11
Table 2.9 The results of Tukey's multiple comparison analysis on the effects of the type of deicers on the change in RDME values of concrete after exposure period when compared the initial RDME values	11
Table 2.10 Average chloride penetration depth for different concretes exposed to different deicers	12
Table 2.11 The least square (LS) means values for the chloride ions penetration depth of FT and WD specimens exposed to deicers after the exposure regime	12
Table 2.12 The results of the analysis of variance (ANOVA) for the chloride ions penetration depth of FT and WD specimens exposed to deicers after the exposure regime	13
Table 2.13 The results of Tukey's multiple comparison analysis on the effects of the type of binder system on the chloride ions penetration depth values of concrete specimen after the exposure regime	13
Table 2.14 The results of Tukey's multiple comparison analysis on the effects of the type of deicers on the chloride ions penetration depth values of concrete specimen after the exposure regime	13
Table 3.1 Table summarizing the costs (per lane-mile) for constructing new pavement with 0% ACBFS in base layers	23
Table 3.2 Table summarizing the costs (per lane-mile) for constructing new pavement with 100% ACBFS in base layers	23
Table 3.3 Example of calculation of total cost (per lane-mile) of the project with similar haul distance (60 miles) for ACBFS aggregate and naturally mined dolomite aggregate (0% ACBFS in base)	23
Table 3.4 Example of calculation of total cost (per lane-mile) of the project with similar haul distance (60 miles) for ACBFS aggregate and naturally mined dolomite aggregate (100% ACBFS in base)	23
Table C.1 Compressive strength of different mixtures at 28 days and after the conclusion of exposure condition	32
Table C.2 Chloride penetration depth measurement of different concretes under freezing-thawing (FT) and wetting-drying (WD) condition	35
Table E.1 Oxide composition of cement, class C fly ash and GGBFS used in the study	80

LIST OF FIGURES

Figure	Page
Figure 1.1 Mixture labelling scheme	3
Figure 2.1 The average compressive strengths of control set 1 (C1) and control set 2 (C2) concretes	7
Figure 2.2 Flexural strength at 7 and 56 days of concrete from different mixtures	8
Figure 2.3 An example of cross section of specimen with its location from the original beam	11
Figure 2.4 Physical changes in the appearance of the representative sample of M1-IPC-ACBFS (plain-ACBFS) concrete specimens exposed to CaCl_2 after (from left to right) 35, 59 and 102 FT cycles. Specimen failed after 111 FT cycles	13
Figure 2.5 Physical changes in the appearance of the representative sample of M5-IPC-NA (plain-dolomite) concrete specimens exposed to CaCl_2 after (from left to right) 42, 65, 118 and 139 FT cycles. Specimen failed after 151 FT cycles	14
Figure 2.6 Physical changes in the appearance of the representative sample of M1-IPC-ACBFS (plain-ACBFS) concrete specimens exposed to CaCl_2 after (from left to right) 176, 205 and 281 WD cycles	14
Figure 2.7 Physical changes in the appearance of the representative sample of M5-IPC-NA (plain-dolomite) concrete specimens exposed to CaCl_2 after (from left to right) 176, 205 and 281 WD cycles	14
Figure 2.8 An example of SEM sample and the location from which it was obtained	15
Figure 2.9 Deposits of Friedel's salt and remnants of unreacted binder particles (fly ash and slag cement) found in SEM sample extracted from M4 (ternary-ACBFS) specimen exposed to CaCl_2 after 310 FT cycles (SEM-BSE)	15
Figure 2.10 Deposits of Friedel's salt and remnants of unreacted binder particles (fly ash and slag cement) found in SEM sample extracted from M8 (ternary-dolomite) specimen exposed to MgCl_2 after 310 FT cycles (SEM-BSE)	16
Figure 2.11 SEM-EDX micrographs for specimen from M1 (plain-ACBFS) mixture – exposed to CaCl_2 after 111 FT cycles; (A) and (B) Friedel's salt, (C) & (D) chloride deposits within the paste (SEM-BSE)	16
Figure 2.12 SEM-EDX micrographs of microstructure of specimen removed from the corner of a beam from M5 (plain-dolomite) mixture exposed to CaCl_2 after 151 FT cycles; (A) and (B) chloride deposits within C-S-H, (C) Friedel's salt, (D) deposit of CaCl_2 within C-S-H (SEM-BSE)	17
Figure 2.13 SEM-EDX micrographs of brucite, M-S-H, calcium hydroxide and remnants of un-hydrated cement (C_3A) found in M7 (slag cement-dolomite) specimen exposed to MgCl_2 after 310 FT cycles (SEM-BSE)	17
Figure 2.14 SEM-EDX micrographs of M-S-H, CaCl_2 , CH, calcium carbonate, MgCl_2 and remnants of un-hydrated slag cement found in M3 (slag cement-ACBFS) specimen exposed to MgCl_2 after 226 WD cycles (SEM-BSE)	18
Figure 2.15 Void filled with (A) calcium oxychloride-like phase in sample exposed to CaCl_2 solution and (B) 1000X magnification image of Mg-O-Cl phase surrounded by calcium hydroxide (CH) in M1 (plain-ACBFS) specimen exposed to MgCl_2 after 347 FT cycles (SEM-BSE)	18
Figure 2.16 SEM image showing deposits of calcium sulfide (CaS) inside ACBFS particle (SEM-BSE)	19
Figure 2.17 SEM images showing deposits of calcium sulfide in the particles of ACBFS aggregate and Friedel's salt in the matrix of M3 (slag cement-ACBFS) specimen exposed to NaCl after 310 FT cycles (SEM-BSE)	19
Figure 2.18 CaS deposits and empty voids in ACBFS particle from M4 (ternary-ACBFS) specimen exposed to distilled water (DST) after 310 FT cycles (SEM-BSE)	19
Figure 2.19 SEM-EDX (Energy Dispersive X-Ray) micrographs of ettringite in (A) concrete containing ACBFS and slag cement (M3-DST-FT) and (B) concrete containing natural dolomite as coarse aggregates (SEM-BSE)	20
Figure 2.20 (a) Variation in sodium ion concentration; (b) Variation in potassium ion concentration	21
Figure 2.21 Variation in total alkalis concentration with age in different paste mixtures	21
Figure 2.22 Variation in sulfate ion concentration at with age for different paste mixtures	21
Figure B.1 Cement mill certificate used in this study	28
Figure B.2 Class C fly ash certificate from the producer	29
Figure B.3 Slag aggregate mill certificate	30
Figure C.1 Aggregate gradation curves	31
Figure C.2 Relative dynamic modulus of elasticity (RDME) of control specimens (C2) and specimens exposed to different deicers under freezing-thawing (FT) cycles; (A) M1, (B) M2, (C) M3 and (D) M4	33

Figure C.3 Relative dynamic modulus of elasticity (RDME) of control specimens (C2) and specimens exposed to different deicers under freezing-thawing (FT) cycles; (A) M5, (B) M6, (C) M7 and (D) M8	33
Figure C.4 Relative dynamic modulus of elasticity (RDME) of control specimens (C2) and specimens exposed to different deicers under wetting-drying (WD) cycles; (A) M1, (B) M2, (C) M3 and (D) M4	34
Figure C.5 Relative dynamic modulus of elasticity (RDME) of control specimens (C2) and specimens exposed to different deicers under wetting-drying (WD) cycles; (A) M5, (B) M6, (C) M7 and (D) M8	34
Figure C.6 Chloride penetration depths associated with different deicers in M1-1PC-ACBFS (plain-ACBFS) specimens after: (A) 347 FT cycles and (B) 286 WD cycles	36
Figure C.7 Chloride penetration depths associated with different deicers in M2-.2FA.8PC-ACBFS (fly ash-ACBFS) specimens after: (A) 347 FT cycles and (B) 286 WD cycles	36
Figure C.8 Chloride penetration depths associated with different deicers in M3-.25SC.75PC-ACBFS (slag cement-ACBFS) specimens after: (A) 310 FT cycles and (B) 226 WD cycles	37
Figure C.9 Chloride penetration depths associated with different deicers in M4-.17FA.23SC.6PC-ACBFS (ternary-ACBFS) specimens after: (A) 310 FT cycles and (B) 226 WD cycles	37
Figure C.10 Chloride penetration depths associated with different deicers in M1-1PC-NA (plain-dolomite) specimens after: (A) 350 FT cycles and (B) 286 WD cycles	38
Figure C.11 Chloride penetration depths associated with different deicers in M6-.2FA.8PC-NA (fly ash-dolomite) specimens after: (A) 350 FT cycles and (B) 286 WD cycles	38
Figure C.12 Chloride penetration depths associated with different deicers in M7-.25SC.75PC-NA (slag cement-dolomite) specimens after: (A) 310 FT cycles and (B) 226 WD cycles	39
Figure C.13 Chloride penetration depths associated with different deicers in M8-.17FA.23SC.6PC-NA (ternary-dolomite) specimens after: (A) 310 FT cycles and (B) 226 WD cycles	39
Figure C.14 Physical changes in the appearance of the representative sample of M1-1PC-ACBFS (plain-ACBFS) concrete specimens exposed to CaCl_2 after (from left to right) 35, 59 and 102 FT cycles	40
Figure C.15 Physical changes in the appearance of the representative sample of M1-1PC-ACBFS (plain-ACBFS) concrete specimens exposed to MgCl_2 after (from left to right) 35, 59, 102 and 347 FT cycles	40
Figure C.16 Physical changes in the appearance of the representative sample of M1-1PC-ACBFS (plain-ACBFS) concrete specimens exposed to NaCl after (from left to right) 35, 59, 102 and 347 FT cycles	40
Figure C.17 Physical changes in the appearance of the representative sample of M1-1PC-ACBFS (plain-ACBFS) concrete specimens exposed to distilled water (DST) after (from left to right) 35, 59, 102 and 347 FT cycles	40
Figure C.18 Physical changes in the appearance of the representative sample of M2-.2FA.8PC-ACBFS (fly ash-ACBFS) concrete specimens exposed to CaCl_2 after (from left to right) 35, 59, 102 and 347 FT cycles	40
Figure C.19 Physical changes in the appearance of the representative sample of M2-.2FA.8PC-ACBFS (fly ash-ACBFS) concrete specimens exposed to MgCl_2 after (from left to right) 35, 59, 102 and 347 FT cycles	41
Figure C.20 Physical changes in the appearance of the representative sample of M2-.2FA.8PC-ACBFS (fly ash-ACBFS) concrete specimens exposed to NaCl after (from left to right) 35, 59, 102 and 347 FT cycles	41
Figure C.21 Physical changes in the appearance of the representative sample of M2-.2FA.8PC-ACBFS (fly ash-ACBFS) concrete specimens exposed to distilled water (DST) after (from left to right) 35, 59, 102 and 347 FT cycles	41
Figure C.22 Physical changes in the appearance of the representative sample of M3-.25SC.75PC-ACBFS (slag cement-ACBFS) concrete specimens exposed to CaCl_2 after (from left to right) 18, 191 and 310 FT cycles	41
Figure C.23 Physical changes in the appearance of the representative sample of M3-.25SC.75PC-ACBFS (slag cement-ACBFS) concrete specimens exposed to MgCl_2 after (from left to right) 18, 191 and 310 FT cycles	42
Figure C.24 Physical changes in the appearance of the representative sample of M3-.25SC.75PC-ACBFS (slag cement-ACBFS) concrete specimens exposed to NaCl after (from left to right) 18, 191 and 310 FT cycles	42
Figure C.25 Physical changes in the appearance of the representative sample of M3-.25SC.75PC-ACBFS (slag cement-ACBFS) concrete specimens exposed to distilled water (DST) after (from left to right) 18, 191 and 310 FT cycles	42
Figure C.26 Physical changes in the appearance of the representative sample of M4-.17FA.23SC.6PC-ACBFS (ternary-ACBFS) concrete specimens exposed to CaCl_2 after (from left to right) 18, 191 and 310 FT cycles	43

Figure C.27 Physical changes in the appearance of the representative sample of M4-.17FA.23SC.6PC-ACBFS (ternary-ACBFS) concrete specimens exposed to $MgCl_2$ after (from left to right) 18, 191 and 310 FT cycles	43
Figure C.28 Physical changes in the appearance of the representative sample of M4-.17FA.23SC.6PC-ACBFS (ternary-ACBFS) concrete specimens exposed to NaCl after (from left to right) 18, 191 and 310 FT cycles	43
Figure C.29 Physical changes in the appearance of the representative sample of M4-.17FA.23SC.6PC-ACBFS (ternary-ACBFS) concrete specimens exposed to distilled water (DST) after (from left to right) 18, 191 and 310 FT cycles	44
Figure C.30 Physical changes in the appearance of the representative sample of M5-.1PC-NA (plain-dolomite) concrete specimens exposed to $CaCl_2$ after (from left to right) 42, 65, 118 and 139 FT cycles	44
Figure C.31 Physical changes in the appearance of the representative sample of M5-.1PC-NA (plain-dolomite) concrete specimens exposed to $MgCl_2$ after (from left to right) 42, 65, 139 and 350 FT cycles	44
Figure C.32 Physical changes in the appearance of the representative sample of M5-.1PC-NA (plain-dolomite) concrete specimens exposed to NaCl after (from left to right) 42, 65, 139 and 350 FT cycles	44
Figure C.33 Physical changes in the appearance of the representative sample of M5-.1PC-NA (plain-dolomite) concrete specimens exposed to distilled water (DST) after (from left to right) 42, 65, 139 and 350 FT cycles	45
Figure C.34 Physical changes in the appearance of the representative sample of M6-.2FA.8PC-NA (fly ash-dolomite) concrete specimens exposed to $CaCl_2$ after (from left to right) 42, 65, 139 and 350 FT cycles	45
Figure C.35 Physical changes in the appearance of the representative sample of M6-.2FA.8PC-NA (fly ash-dolomite) concrete specimens exposed to $MgCl_2$ after (from left to right) 42, 65, 139 and 350 FT cycles	45
Figure C.36 Physical changes in the appearance of the representative sample of M6-.2FA.8PC-NA (fly ash-dolomite) concrete specimens exposed to NaCl after (from left to right) 42, 65, 139 and 350 FT cycles	45
Figure C.37 Physical changes in the appearance of the representative sample of M6-.2FA.8PC-NA (fly ash-dolomite) concrete specimens exposed to distilled water (WD) after (from left to right) 42, 65, 139 and 350 FT cycles	45
Figure C.38 Physical changes in the appearance of the representative sample of M7-.25SC.75PC-NA (slag cement - dolomite) concrete specimens exposed to $CaCl_2$ after (from left to right) 3, 87 and 172 FT cycles	46
Figure C.39 Physical changes in the appearance of the representative sample of M7-.25SC.75PC-NA (slag cement - dolomite) concrete specimens exposed to $MgCl_2$ after (from left to right) 3, 87 and 172 FT cycles	46
Figure C.40 Physical changes in the appearance of the representative sample of M7-.25SC.75PC-NA (slag cement - dolomite) concrete specimens exposed to NaCl after (from left to right) 3, 87 and 172 FT cycles	46
Figure C.41 Physical changes in the appearance of the representative sample of M7-.25SC.75PC-NA (slag cement - dolomite) concrete specimens exposed to distilled water (DST) after (from left to right) 3 and 172 FT cycles	47
Figure C.42 Physical changes in the appearance of the representative sample of M8-.17FA.23SC.6PC-NA (Ternary - dolomite) concrete specimens exposed to $CaCl_2$ after (from left to right) 3, 87 and 172 FT cycles	47
Figure C.43 Physical changes in the appearance of the representative sample of M8-.17FA.23SC.6PC-NA (Ternary - dolomite) concrete specimens exposed to $MgCl_2$ after (from left to right) 3, 87 and 172 FT cycles	47
Figure C.44 Physical changes in the appearance of the representative sample of M8-.17FA.23SC.6PC-NA (Ternary - dolomite) concrete specimens exposed to NaCl after (from left to right) 3, 87 and 172 FT cycles	48
Figure C.45 Physical changes in the appearance of the representative sample of M8-.17FA.23SC.6PC-NA (Ternary - dolomite) concrete specimens exposed to distilled water (DST) after (from left to right) 3, 87 and 172 FT cycles	48
Figure C.46 Physical changes in the appearance of the representative sample of M1-1PC-ACBFS (plain-ACBFS) concrete specimens exposed to $CaCl_2$ after (from left to right) 176, 205 and 281 WD cycles	48
Figure C.47 Physical changes in the appearance of the representative sample of M1-1PC-ACBFS (plain-ACBFS) concrete specimens exposed to $MgCl_2$ after (from left to right) 176, 205 and 281 WD cycles	49
Figure C.48 Physical changes in the appearance of the representative sample of M1-1PC-ACBFS (plain-ACBFS) concrete specimens exposed to NaCl after (from left to right) 176, 205 and 281 WD cycles	49
Figure C.49 Physical changes in the appearance of the representative sample of M1-1PC-ACBFS (plain-ACBFS) concrete specimens exposed to distilled water (DST) after (from left to right) 176, 205 and 281 WD cycles	49
Figure C.50 Physical changes in the appearance of the representative sample of M2-.2FA.8PC-ACBFS (fly ash-ACBFS) concrete specimens exposed to $CaCl_2$ after (from left to right) 176, 205 and 281 WD cycles	50

Figure C.51 Physical changes in the appearance of the representative sample of M2-.2FA.8PC-ACBFS (fly ash-ACBFS) concrete specimens exposed to $MgCl_2$ after (from left to right) 176, 205 and 281 WD cycles	50
Figure C.52 Physical changes in the appearance of the representative sample of M2-.2FA.8PC-ACBFS (fly ash-ACBFS) concrete specimens exposed to NaCl after (from left to right) 176, 205 and 281 WD cycles	50
Figure C.53 Physical changes in the appearance of the representative sample of M2-.2FA.8PC-ACBFS (fly ash-ACBFS) concrete specimens exposed to distilled water (DST) after (from left to right) 176, 205 and 281 WD cycles	51
Figure C.54 Physical changes in the appearance of the representative sample of M3-.25SC.75PC-ACBFS (slag cement-ACBFS) concrete specimens exposed to $CaCl_2$ after (from left to right) 0, 90 and 226 WD cycles	51
Figure C.55 Physical changes in the appearance of the representative sample of M3-.25SC.75PC-ACBFS (slag cement-ACBFS) concrete specimens exposed to $MgCl_2$ after (from left to right) 0, 90 and 226 WD cycles	51
Figure C.56 Physical changes in the appearance of the representative sample of M3-.25SC.75PC-ACBFS (slag cement-ACBFS) concrete specimens exposed to NaCl after (from left to right) 0, 90 and 226 WD cycles	52
Figure C.57 Physical changes in the appearance of the representative sample of M3-.25SC.75PC-ACBFS (slag cement-ACBFS) concrete specimens exposed to distilled water (DST) after (from left to right) 0, 90 and 226 WD cycles	52
Figure C.58 Physical changes in the appearance of the representative sample of M4-.17FA.23SC.6PC-ACBFS (ternary-ACBFS) concrete specimens exposed to $CaCl_2$ after (from left to right) 0, 90 and 226 WD cycles	52
Figure C.59 Physical changes in the appearance of the representative sample of M4-.17FA.23SC.6PC-ACBFS (ternary-ACBFS) concrete specimens exposed to $MgCl_2$ after (from left to right) 0, 90 and 226 WD cycles	53
Figure C.60 Physical changes in the appearance of the representative sample of M4-.17FA.23SC.6PC-ACBFS (ternary-ACBFS) concrete specimens exposed to NaCl after (from left to right) 0, 90 and 226 WD cycles	53
Figure C.61 Physical changes in the appearance of the representative sample of M4-.17FA.23SC.6PC-ACBFS (ternary-ACBFS) concrete specimens exposed to distilled water (DST) after (from left to right) 0, 90 and 226 WD cycles	53
Figure C.62 Physical changes in the appearance of the representative sample of M5-1PC-NA (plain-dolomite) concrete specimens exposed to $CaCl_2$ after (from left to right) 176, 205 and 281 WD cycles	54
Figure C.63 Physical changes in the appearance of the representative sample of M5-1PC-NA (plain-dolomite) concrete specimens exposed to $MgCl_2$ after (from left to right) 176, 205 and 281 WD cycles	54
Figure C.64 Physical changes in the appearance of the representative sample of M5-1PC-NA (plain-dolomite) concrete specimens exposed to NaCl after (from left to right) 176, 205 and 281 WD cycles	54
Figure C.65 Physical changes in the appearance of the representative sample of M5-1PC-NA (plain-dolomite) concrete specimens exposed to distilled water (DST) after (from left to right) 176, 205 and 281 WD cycles	55
Figure C.66 Physical changes in the appearance of the representative sample of M6-.2FA.8PC-NA (fly ash-dolomite) concrete specimens exposed to $CaCl_2$ after (from left to right) 176, 205 and 281 WD cycles	55
Figure C.67 Physical changes in the appearance of the representative sample of M6-.2FA.8PC-NA (fly ash-dolomite) concrete specimens exposed to $MgCl_2$ after (from left to right) 176, 205 and 281 WD cycles	55
Figure C.68 Physical changes in the appearance of the representative sample of M6-.2FA.8PC-NA (fly ash-dolomite) concrete specimens exposed to NaCl after (from left to right) 176, 205 and 281 WD cycles	56
Figure C.69 Physical changes in the appearance of the representative sample of M6-.2FA.8PC-NA (fly ash-dolomite) concrete specimens exposed to distilled water (DST) after (from left to right) 176, 205 and 281 WD cycles	56
Figure C.70 Physical changes in the appearance of the representative sample of M7-.25SC.75PC-NA (slag cement-dolomite) concrete specimens exposed to $CaCl_2$ after (from left to right) 0, 90 and 226 WD cycles	56
Figure C.71 Physical changes in the appearance of the representative sample of M7-.25SC.75PC-NA (slag cement-dolomite) concrete specimens exposed to $MgCl_2$ after (from left to right) 0, 90 and 226 WD cycles	57
Figure C.72 Physical changes in the appearance of the representative sample of M7-.25SC.75PC-NA (slag cement-dolomite) concrete specimens exposed to NaCl after (from left to right) 0, 90 and 226 WD cycles	57
Figure C.73 Physical changes in the appearance of the representative sample of M7-.25SC.75PC-NA (slag cement-dolomite) concrete specimens exposed to distilled water (DST) after (from left to right) 0, 90 and 226 WD cycles	57
Figure C.74 Physical changes in the appearance of the representative sample of M8-.17FA.23SC.6PC-NA (ternary-dolomite) concrete specimens exposed to $CaCl_2$ after (from left to right) 0, 90 and 226 WD cycles	58

Figure C.75 Physical changes in the appearance of the representative sample of M8-.17FA.23SC.6PC-NA (ternary-dolomite) concrete specimens exposed to $MgCl_2$ after (from left to right) 0, 90 and 226 WD cycles	58
Figure C.76 Physical changes in the appearance of the representative sample of M8-.17FA.23SC.6PC-NA (ternary-dolomite) concrete specimens exposed to NaCl after (from left to right) 0, 90 and 226 WD cycles	58
Figure C.77 Physical changes in the appearance of the representative sample of M8-.17FA.23SC.6PC-NA (ternary-dolomite) concrete specimens exposed to distilled water (DST) after (from left to right) 0, 90 and 226 WD cycles	59
Figure D.1 SEM-EDX micrographs for M1 (plain-ACBFS) beam exposed to $MgCl_2$ after 347 FT cycles; (A) Mg-O-Cl, (B) M-S-H, (C) and (D) ettringite (SEM-BSE)	60
Figure D.2 SEM-EDX micrographs for M1 (plain-dolomite) beam exposed to $MgCl_2$ after 347 FT cycles; (A) NaCl deposit, (B) Ettringite, (C) Ettringite and Friedel's salt (D) Chloride in paste (SEM-BSE)	61
Figure D.3 SEM-EDX micrographs for M1 (plain-NaCl) specimen exposed to distilled water (DST) after 347 FT cycles; (A) and (B) ettringite, (C) Portlandite/ $Ca(OH)_2$, (D) C-S-H (SEM-BSE)	62
Figure D.4 SEM-EDX micrographs for M2 (fly ash-ACBFS) specimen exposed to $CaCl_2$ after 347 FT cycles; (A) $CaCl_2$, (B) Friedel's salt and ettringite, (C) Ettringite (D) Cl^- intrusion in the paste (SEM-BSE)	63
Figure D.5 SEM-EDX micrographs for M2 (fly ash-ACBFS) specimen exposed to $MgCl_2$ after 347 FT cycles; (A) Cl^- and sulfate in the matrix, (B) Brucite layer, (C) Ettringite and Friedel's salt in void, (D) Mg-O-Cl (SEM-BSE)	64
Figure D.6 SEM-EDX micrographs for M2 (fly ash-ACBFS) specimen exposed to NaCl after 347 FT cycles; (A) Cl^- ingress in the matrix, (B) Friedel's salt, (C) Ettringite and (D) NaCl deposit (SEM-BSE)	65
Figure D.7 SEM-EDX micrographs for M3 (slag cement-ACBFS) specimen exposed to $CaCl_2$ after 310 FT cycles have shown deposits of Friedel's salt, ettringite and $CaCl_2$ deicer in the matrix (SEM-BSE)	66
Figure D.8 SEM-EDX micrographs for M4 (ternary-ACBFS) specimen exposed to $MgCl_2$ after 310 FT cycles (SEM-BSE)	67
Figure D.9 SEM-EDX micrographs for M4 (ternary-ACBFS) specimen exposed to NaCl after 310 FT cycles; (A) and (B) Friedel's salt, (C) ettringite deposit in pore (D) Cl deposits within the matrix (SEM-BSE)	68
Figure D.10 SEM-EDX micrographs for M4 (ternary-ACBFS) specimen exposed to distilled water (DST) after 310 FT cycles (SEM-BSE)	69
Figure D.11 SEM-EDX micrographs for M5 (plain-dolomite) specimen exposed to $CaCl_2$ after 151 FT cycles; (A) and (B) Deposits of Cl within the matrix, (C) & (D) Friedel's salt (SEM-BSE)	70
Figure D.12 SEM-EDX micrographs for M5 (plain-dolomite) specimen exposed to $MgCl_2$ after 350 FT cycles; (A) and (B) Chloride infused M-S-H, (C) & (D) Friedel's salt (SEM-BSE)	71
Figure D.13 SEM-EDX micrographs for M5 (plain-dolomite) specimen exposed to NaCl after 350 FT cycles; (A) and (B) Chloride deposits within C-S-H, (C) & (D) Friedel's salt (SEM-BSE)	72
Figure D.14 SEM-EDX micrographs for M6 (fly ash-dolomite) specimen exposed to $MgCl_2$ after 350 FT cycles; (A) and (B) Chloride infused M-S-H, (C) Cl deposits within C-S-H and (D) Friedel's salt (SEM-BSE)	73
Figure D.15 SEM-EDX micrographs for M7 (slag cement-dolomite) specimen exposed to $CaCl_2$ after 310 FT cycles (SEM-BSE)	74
Figure D.16 SEM-EDX micrographs for M7 (slag cement-dolomite) specimen exposed to $MgCl_2$ after 350 FT cycles; (A) and (B) M-S-H, (C) Friedel's salt and (D) chloride deposits in C-S-H (SEM-BSE)	75
Figure D.17 SEM-EDX micrographs for M8 (ternary-dolomite) specimen exposed to $CaCl_2$ after 310 FT cycles (SEM-BSE)	76
Figure D.18 SEM-EDX micrographs for M8 (ternary-dolomite) specimen exposed to $MgCl_2$ after 310 FT cycles; (A) and (B) brucite, (C) M-S-H and (D) Friedel's salt (SEM-BSE)	77
Figure D.19 SEM-EDX micrographs for M8 (ternary-dolomite) specimen exposed to NaCl after 310 FT cycles; (A) and (B) chloride deposits within the matrix C-S-H, (C) & (D) Friedel's salt (SEM-BSE)	78
Figure D.20 SEM-EDX micrographs for M8 (ternary-dolomite) specimen exposed to distilled water (DST) after 310 FT cycles (SEM-BSE)	79
Figure E.1 Concentration variation of (a) calcium, (b) aluminum and (c) chloride ions	80
Figure F.1 Example of calculation of quantities of raw materials required	81
Figure F.2 Input variables for calculation of cost of concrete pavement	81

LIST OF ABBREVIATIONS

AASHTO:	American Association of State Highway and Transportation Officials
ACBFS:	Air-Cooled Blast Furnace Slag
ASTM:	American Society for Testing Material
BCA:	Benefit Cost Analysis
CA:	Coarse Aggregate
DOT:	Department of Transportation
FA:	Fly Ash
FT:	Freezing and Thawing
INDOT:	Indiana Department of Transportation
NA:	Natural Aggregate
PC:	Portland Cement
QC/QA:	Quality Control/Quality Assurance
SC:	Slag Cement
SEM:	Scanning Electron Microscopy
WD:	Wetting and Drying
DST:	Distilled Water
SEM:	Scanning Electron Microscopy
C-S-H:	Calcium Silicate Hydrate
M-S-H:	Magnesium Silicate Hydrate

1. INTRODUCTION

Concrete, a composite material composed of aggregates, cement and water, is the most widely used man-made material in the world (Chemistry World, 2008). Concrete is being used in a wide range of application, including buildings, bridges, dams and pavements. Although many different types of concrete have been developed for different applications, they all share some common positive features which include: versatility, strength, durability, availability, fire resistance and comparatively low cost (Imbabi, Carrigan, & McKenna, 2012).

A report by Cement Sustainability Initiative (CSI, 2009), has estimated that roughly more than 25 billion tons of concrete were manufactured globally in 2009 and that amount keeps increasing each year. As a result, the demand for concrete's ingredients elevates proportionally to concrete production. Ordinary portland cement (OPC), is a dominant ingredient of concrete (Imbabi et al., 2012) serving as bonding agent once reacted with water through the hydration process. In typical concrete mixture, OPC occupies 10% to 15% of the total volume of concrete (Portland Cement Association, n.d.). That requires manufacturing of high amount of cement in order to fulfill the needs in concrete construction. To meet that high demand, more than 4 billion tons of OPC were produced worldwide in 2013, and this number has increased in the following year (USGS, 2015). Of concern to the cement industry is the fact that every tone of OPC produced releases on average a similar amount of CO₂ into the atmosphere (Chen, Habert, Bouzidi, & Jullien, 2010; Imbabi et al., 2012). Another concern is related to the depletion of fossil fuels, which are used as the major energy source in cement production. Those challenges in cement industry have triggered a strong push toward the innovation in cement production, mainly with respect to reduction, or even elimination, the previously mentioned drawbacks cement production. In this regard, the use of other cementitious materials (i.e., fly ash and slag cement), which are by products of other industry, have been proven to be a viable alternative (Chen, 2006; Hale, Freyne, Bush, & Russell, 2008; Hooton, Stanish, & Prusinski, 2004; Jun-Yuan, Scheetz, & Roy, 1984; Man & Jing, 2012; Verian, 2012; Verian, Panchmatia, Olek, & Nantung, 2015). The development of other type of binders, as the type which result in lower CO₂ emissions, is also being pursued (Solidia Technologies, n.d.).

1.1 Background

Efforts to produce more sustainable concrete pavements have led to the use of alternative materials as a substitute for the generally used concrete ingredients, i.e., cement and natural aggregates. It is estimated that the carbon dioxide (CO₂) emitted from the cement production represents 5%–7% of the global CO₂ emission (Chen et al., 2010). Meanwhile, problems related to the availability of natural aggregates also emerge due to the depletion of existing sources, restrictions on developing

new quarries and the increase in cost of mining and transportation (Verian, 2012). In practice, fly ash and slag cement are commonly used as partial replacement of cement in concrete mixtures. In addition, the air-cooled blast furnace slag (ACBFS) has been used as source of coarse aggregate since at least the 1930s (Morian, Van Dam, & Perera, 2012). Recently however, some concerns arose regarding the use of ACBFS as coarse aggregate in concrete mixtures. These concerns appear to be related to the physical characteristic and the chemical composition of ACBFS (Morian et al., 2012), and include variability of specific gravity and porosity (which, if not properly accounted for, may lead to potential moisture control problems during batching) as well as dissolution of calcium sulfide (CaS) with resulting formation of calcium sulfate (CaSO₄). The presence of CaSO₄ in concrete exposed to water may, in turn, lead to formation of secondary ettringite ($6\text{CaO} \cdot \text{Al}_2\text{O}_3 \cdot 3\text{SO}_3 \cdot 32\text{H}_2\text{O}$) and thaumasite ($\text{Ca}_6[\text{Si}(\text{OH})_6](\text{SO}_4)_2(\text{CO}_3)_2$). Although it is not clear to what extent the formation of secondary ettringite may influence the durability of concrete with ACBFS, some concerns include potential infilling of the air void system, thus reducing its efficiency in providing the FT resistance.

1.2 Literature Review

A review of the literature related to the materials used in this study, i.e., ACBFS coarse aggregate, fly ash, slag cement and deicers are discussed in this chapter. This chapter also provides the information regarding the effect of the aforementioned materials to concrete properties.

1.2.1 Slag Aggregate

Slag is a byproduct of metallurgical operations, and typically contains gangue from the metal ore, flux material and unburned fuel constituents (Morian et al., 2012). The ACBFS is categorized as ferrous slag as it is derived from the production of pig iron. Although the chemical composition of the ACBFS used in this study was not specifically tested, the information provided by the supplier indicates that such material typically contains four major components, which are lime (CaO; 30%–40%), silica (SiO₂; 28%–42%), alumina (Al₂O₃; 5%–22%) and magnesia (MgO; 5%–15%). These oxides account for approximately 95% of ACBFS composition (see Table 1.1) with the remaining 5% consisting of sulfur, manganese, iron, titanium, fluorine, sodium and potassium oxides.

Chesner, Collins, and Mackay (1998) had reported that ACBFS aggregate typically has a high angle of friction (40 to 45 degrees). The L.A. abrasion values of ACBFS aggregate range between 35% and 45%, its hardness ranges from 5 to 6 (Mohs scale) and the California bearing ratio (CBR) is typically greater than 100 due to its angular shape and rough texture (Morian et al., 2012). The typical compacted unit weight of ACBFS (measured according to ASTM C 33 (2011))

TABLE 1.1
Typical composition of ACBFS (Morian et al., 2012).

Component	Percentage
Major components	95
Lime (CaO)	30–40
Silica (SiO ₂)	28–42
Alumina (Al ₂ O ₃)	5–22
Magnesia (MgO)	5–15
Minor components	5
Sulfur (CaS, other sulfides, sulfates)	1–2
Iron (FeO, Fe ₂ O ₃)	0.3–1.7
Manganese (MnO)	0.2–1
Rare components	
Na ₂ O + K ₂ O	0–1
TiO ₂	0–1
V ₂ O ₅	0–1
Cr ₂ O ₃	0–1

ranges between 70 and 85 lb/ft³ (Morian et al., 2012). By comparison, the compacted unit weight of light-weight aggregates typically ranges between 55 and 70 lb/ft³, while that of normal weight aggregates typically ranges between 75 and 110 lb/ft³. Some states (e. q. Illinois, Pennsylvania and Kentucky) require that the compacted unit weight of ACBFS should not be lower than 70 lb/ft³ when it is used in pavement concrete (IDOT, 2012; KYTC, 2008; PennDOT, 2000). Slowly cooled slag will have fewer entrapped pores and higher degree of crystallinity, which is more desirable for ACBFS aggregates (Morian et al., 2012). The absorption of ACBFS coarse aggregate is normally higher (about 1% to 8%) than that of the natural aggregate (about 0.5% to 3%). For use as an aggregate in pavement concrete, the ACBFS with higher density (>2.4) and lower absorption (less than 4%) is more desirable (Morian et al., 2012).

Two chemical properties of ACBFS that are of concern with respect to the use of this material as coarse aggregate in concrete include iron unsoundness and dicalcium silicate unsoundness (Morian et al., 2012). Iron unsoundness becomes a problem only if partially reduced iron oxides in the slag undergo additional oxidation, as this process results in expansive reaction and leads to disintegration of the ACBFS particles (Morian et al., 2012). Testing for iron unsoundness involves immersing pieces of slag in water for a period of 14 days and observing whether any of the particles crack or disintegrate. The dicalcium silicate unsoundness is caused by an increase in volume of the CaO-SiO₂ (C₂S) phase as a result of its inversion from beta form to gamma form during cooling. That volume expansion will damage the ACBFS aggregate particles in a process commonly referred to as falling (Morian et al., 2012). Fortunately, this disruptive transformation process occurs only during the cooling process (in the temperature range from 750°F to 930°F (400°C to 500°C)) and thus it is effectively completed within a few days as the slag reaches ambient temperature (Juckes, 2002).

Once formed, calcium sulfate (CaSO₄) can further react with the existing monosulfate (4CaO, Al₂O₃·SO₃·12H₂O) to produce ettringite (6CaO·Al₂O₃·SO₃·32H₂O) (Mehta, 1983).

Unlike sulfate attack, which occurs in the presence of alkali sulfates and involves the decalcification of C-S-H, no decalcification of C-S-H takes place in the process of ettringite formation since all the calcium ions are supplied by calcium sulfate. As such, the integrity of the hydrated cement phases remain unaffected (Morian et al., 2012). The ettringite produced fills the air void system. This process may initially lead to the strength increase, but it may also compromise the effectiveness of the air-void system with respect to freeze-thaw protection.

The addition of limestone (CaCO₃) to Portland cement provides carbonate, which is required for thaumasite formation. Several researchers have found that relatively high sulfate levels combined with alkaline conditions leads to the formation of thaumasite (Colleparidi, 2003; Crammond, 2003; Gaze & Crammond, 2000; Mehta, 1983). Both of these conditions may exist in concrete made with high-alkali cement and ACBFS, and the potential for thaumasite-related distress increases as the limestone content of cement increases (Morian et al., 2012). Thaumasite formation reduces the binding capacity of hydrated cement in the hardened concrete and causes loss of strength. The expansive disruption that is normally associated with sulfate attack sometimes accompanies the formation of thaumasite, but is not a dominating feature (Crammond, 2002).

To address the potentially adverse effects of calcium sulfide present in ACBFS, the British Standard Institute limits the sulfur content of concrete to maximum of approximately 2% by weight (Morian et al., 2012). The Organization for Economic Co-operation and Development (OECD, 1997) has published a report which states that ACBFS must have a total sulfur content of less than 2% and a sulfate content of less than 0.7% in order for it to be used as concrete aggregate.

1.2.2 Deicers

During winter, concrete pavement subjected to repeated freezing/thawing cycles in the presence of chloride-based deicing chemicals suffer from two types of deterioration: physical (expansion and cracking due to the build-up of internal stresses) and chemical (dissolution of Ca(OH)₂ from concrete matrix and formation of expansive phases (Sumsion & Guthrie, 2013). The details information regarding about the deterioration mechanisms are presented in Appendix A.

1.3 Research Objectives

The main objective of this study was to evaluate the potential of using air-cooled blast furnace slag (ACBFS) as coarse aggregate on pavement concrete subjected to different deicers and exposure conditions.

1.4 Scope of Work

This study covers the evaluation of the influence of multiple aspects (i.e., aggregate, binder system, deicers and exposure condition) to concrete properties. A total of eight different concrete mixtures were produced in this study following Indiana Department Transportation (INDOT, 2010) specification and standard for pavement concrete. The mixtures were prepared using two types of coarse aggregates, ACBFS and dolomite. Four different binder systems were used, included the following: (a) plain – 100% portland cement (PC), two types of binary binder systems (b) 20% fly ash (FA) + 80% PC and (c) 25% slag cement (SC) + 75% PC, and a ternary system (d) 17% FA + 23% SC + 60% PC. More details regarding the scope of the current study is as follows:

- The evaluation and comparison of several properties of ACBFS and dolomite aggregates.
- The evaluation, analysis and comparison of concrete's properties made with two different types of coarse aggregate with different binder systems (plain, binary and ternary) exposed to several types of chloride-based deicing chemical (NaCl, MgCl₂ and CaCl₂) while subjected to freezing-thawing (FT) and wetting-drying (WD) conditions.
- The determination and analysis of chloride ingress (i.e., chloride penetration depth) on concrete specimens after being exposed for a test period to deicers while subjected to

either freezing-thawing (FT) or wetting-drying (WD) conditions.

- The observation and analysis of the physical changes of concrete specimens at different periods of time during the exposure to either deicers or distilled water while subjected to either freezing-thawing (FT) or wetting-drying (WD) conditions.
- The microscopic evaluation and analysis of concrete matrix exposed to either deicers or distilled water while subjected to either freezing-thawing (FT) or wetting-drying (WD) conditions.
- Benefit cost analysis on the application of air-cooled blast furnace slag (ACBFS) as coarse aggregate in pavement concrete.

1.5 Test Program

The materials used in this study are presented in Table 1.2. Mill certificates for the cement, fly ash and safety data sheet for the ACBFS aggregate are provided in Appendix B. A total of eight concrete mixtures (compositions shown in Table 1.3) were produced. The example of labeling scheme of the mixture used for identification of individual mixtures is presented in Figure 1.1.

A comprehensive suite of tests (presented in Table 1.4) was used to assess both the plastic and hardened properties of concretes produced during this study.

TABLE 1.2
Materials used in the project.

Material	Description
Cement (PC)	Type I Portland cement conforming to ASTM C 150
Fly ash (FA)	Class C fly ash met the requirement of ASTM C 618 and AASHTO M 295
Slag cement (SC)	Ground granulated blast furnace slag met the requirement of ASTM C 989 for grade 100
Natural coarse aggregate (NA)	#8 Dolomite, obtained from Delphi Plant, IN., produced by U.S. Aggregates, Inc., INDOT source #2421
Slag aggregate (ACBFS)	#8 Air-cooled blast furnace slag (ACBFS) aggregate, produced by Edw. C. Levy Co.
Fine aggregate	#23 natural siliceous sand produced by Purdy Materials, INDOT source #2109, Lafayette, IN.

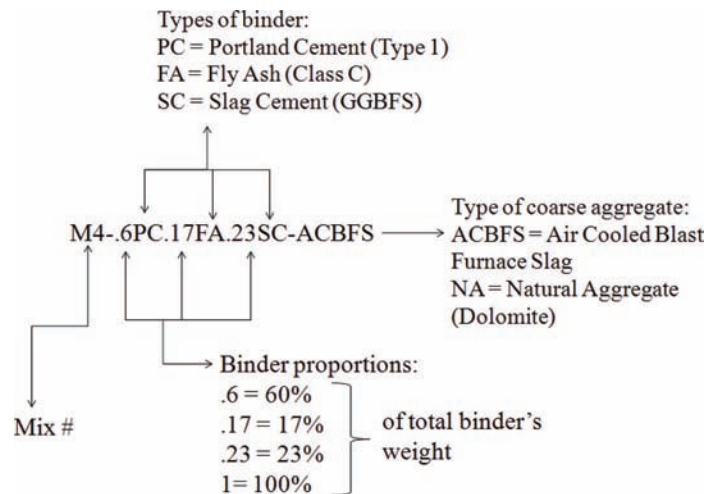


Figure 1.1 Mixture labelling scheme.

Mixture Composition (lbs/yd³)^afl. oz per 100 lbs cementitious.

Standard

– = no specific standard exists.

2. TEST RESULTS AND ANALYSIS

This chapter presents the experimental data and their analysis for the eight laboratory mixtures used in the study. These findings are presented in two sections, aggregate test results (Section 2.1) and concrete test results (Section 2.2).

2.1 Aggregate Test Results

With respect to all aggregate tests, aggregate sources were tested individually and not as a combined blend of materials unless otherwise stated. The results are discussed below and more details are provided in Appendix C.

2.1.1 Sieve Analysis and Fineness Modulus

Sieve analysis test results showed that the fine aggregate used in this project met INDOT specification for #23 aggregate and all coarse aggregates (dolomite and ACBFS) used adhered to the specification for #8's (see Figure C.1 in Appendix C).

2.1.2 Specific Gravity and Absorption

The aggregate test results for specific gravity and absorption are shown in Table 2.1.

As it is indicated in Table 2.1, #8 ACBFS has lower (2.43 vs 2.73) specific gravity and higher absorption than #8 dolomite. The value of ACBFS specific gravity in SSD condition (2.43) and absorption (3.4%) are within the ranges reported by Levy Company which are 2.25–2.83 and 2.3%–3.9% for SSD specific gravity and absorption respectively (Morian et al., 2012, pp. 14–15). Both #8 dolomite and #8 ACBFS satisfied INDOT's requirement for maximum aggregate absorption of 5%.

2.2 Concrete Test Results

Several tests were conducted on the fresh and hardened concrete to characterize the properties, performance and durability of concrete. The results are presented and discussed in the following Sub-chapters. Further details regarding the test results and analysis of the concrete specimens are provided in Appendix D.

2.2.1 Fresh Concrete Test Results

The slump, air content and unit weight were measured within 15 minutes after mixing. The air content of

each mixture was measured using volumetric method. Volumetric method has been reported (Morian et al., 2012) to be more suitable (than the generally used, pressure method) for determining the air content of concrete with ACBFS. The results are presented in Table 2.2.

During the batching process, the w/cm and the amount of admixtures (air entraining agent and water reducers) were varied to meet target values for slump (1.25–3.00 inches) and air content (5.3%–9.3%) set by INDOT for pavement concrete. Despite some variations in the slump and air content among mixtures, all concrete produced in this study satisfied INDOT's slump and air content requirements for pavement concrete.

2.2.2 Hardened Concrete Test Results

The mechanical properties and durability of hardened concrete were evaluated following the procedures described in several ASTM and AASHTO procedures (as identified in Table 1.4).

2.2.2.1 Mechanical Properties. The mechanical properties of concrete evaluated included compressive strength and flexural strength.

2.2.2.1.1 Compressive Strength. The compressive strength data for both, the deicer-exposed specimens and the control specimens were obtained by testing 4 × 8 in. cylindrical specimens following AASHTO T 22 (2011) standard specification. In addition, the compressive strength of 3 × 3 × 3 in. cubes obtained by cutting the deicer-exposed beam specimens at the conclusion of the exposure period was also determined. The cubes were found to have equivalent compressive strength to that of the cylinder when they were tested at the same loading rate (35 ± 7 psi/s). The control specimens consisted of two sets: C1 and C2. The specimens from the first control set (C1) were tested after 28 days of moist curing. The specimens from the second control set (C2) were also moist cured and tested either at the end of the exposure period for given exposure condition (i.e., deicer + environmental cycling combination) or when the corresponding beams failed. The 28-day compressive strength data of the control set C1 and the compressive strength data for control set 2 (C2) are presented in Figure 2.1.

By using Tukey pair wise comparison with 95% confident level ($\alpha = 0.05$), the 28-day compressive strength (control set 1 (C1)) of eight different types of concretes were classified into four different groups as presented in Table 2.3.

TABLE 2.1
Specific gravity and absorptions of aggregates used in this study.

Aggregates	Specific gravity (SSD)	Absorption (%)	INDOT's max. absorption limit (%)
#8 Dolomite	2.73	1.1	5.0
#8 ACBFS	2.43 ^a	3.4 ^a	5.0
#23 Sand	2.56	2.1	—

^aData obtained from aggregate supplier.

TABLE 2.2
Fresh concrete properties, w/cm, and the dosage of admixtures.

Mixture designations	M1-IPC- ACBFS	M2- .8PC.2FA- ACBFS	M3- .75PC.25SC- ACBFS	M4-6PC.17FA. 23SC-ACBFS	M5- IPC- NA	M6- .8PC.2FA- NA	M7- .75PC.25SC- NA	M8-6PC.17FA. 23SC-NA	Target range
Slump (in)	1.9	2.8	1.6	2.3	2.3	2.7	2.7	2.8	1.25–3.00 ^c
Air content (%)	6.9	6.7	6.4	6.5	6.2	6.7	6.4	6.9	6.5 (5.3–9.8) ^d
Unit weight (lbs/ft ³)	136.3	135.6	137.2	135.9	143.4	142.9	142.4	142.6	–
w/cm	0.42	0.42	0.39	0.40	0.42	0.42	0.41	0.40	0.42 (0.39–0.45) ^e
Air entraining agent ^a	1.0	1.0	1.7	1.4	1.0	1.0	1.0	1.0	–
Water reducer ^b	2.0	2.0	6.0	2.0	2.2	2.2	2.6	2.2	–

^afl. oz /100 lbs of cementitious (Microair). Manufacturer's recommended range (0.5–3 fl. oz/100 lbs of cementitious).

^bfl. oz /100 lbs of cementitious (Glenium 3030NS). Manufacturer's suggested range (2–6 fl. oz/100 lbs of cementitious).

^cINDOT's limit for slump (1.25–3.00 in).

^dINDOT's limit for air content based on single sample measurement.

^eINDOT's limit for w/cm (0.42 ± 0.03).

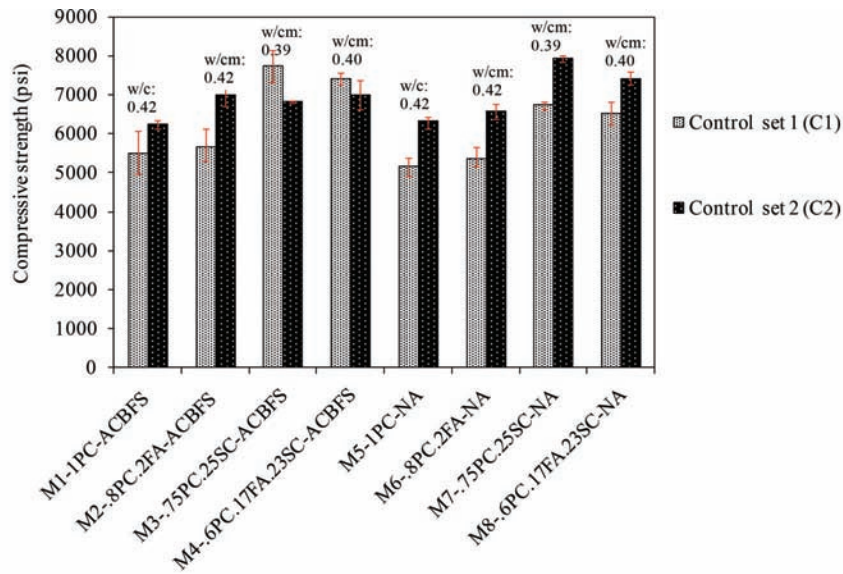
At the confidence level 95%, the 28-day compressive strengths of M3, M4 and M7 concretes are not statistically different as those mixtures were assigned into the same group (A). Similarly, the 28-day compressive strength of M4, M7 and M8 were identified as not being significantly different. The 28-day compressive strength of M3 is significantly different from that of M8 at the 95% confidence level. Table 2.3 shows that the 28-day compressive strengths of M1, M2, M5 and M6 are considered statistically comparable as they were classified into the same group (D). The mixtures with slag cement (M3, M4, M7 and M8) were found to have higher 28-day of compressive strength than the mixtures without slag cement (M1, M2, M5 and M6). This finding indicates that beside the later hydration of slag cement, the lower w/cm of mixtures with slag cement (0.39–0.40) also contributed to generating higher 28-day compressive strength. The compressive strength of concrete made with ACBFS as coarse aggregate was found to be slightly higher (but not significantly different at $\alpha = 0.05$) than the identical concrete made with dolomite coarse aggregate. The internal curing provided by ACBFS can be the reason for slightly higher 28-day compressive strength of ACBFS concretes.

The results of statistical analysis results of the compressive strength of control 2 (C2) specimens are presented in Table 2.4. The compressive strength of control set 2 (C2) specimens from M7, M2, M4 and M3 mixtures are considered statistically similar. On the other hand, the compressive strength values of specimens for control set 2 (C2) mixtures (M3, M6, M8, M5 and M1) are classified in the same group (B), meaning they are comparable. The effect of type of binder system and type of coarse aggregate to the compressive strength of control set 2 (C2) specimens are difficult to ascertain due the lack of specific trend in the results as presented in Table 2.4.

2.2.2.1.2 Flexural Strength. The flexural strength values of control specimens were obtained following the procedure of AASHTO T 97 (2011). The prismatic (6 × 6 × 21 in.) beams were tested after 7 and 56 days of moist curing. The flexural strength test results are summarized in Figure 2.2.

As seen from Figure 2.2, all mixtures used in this study satisfied INDOT's minimum requirement for flexural strength at 7 days (570 psi). In addition, the flexural strength of all mixtures increases with age. The effect of coarse aggregate type on concrete's flexural strength is considered to be insignificant as the flexural strength of concrete made with ACBFS coarse aggregate was found to be comparable (i.e., it was less than 10% different) from the flexural strength of similar concrete made with dolomite.

There is no evidence of fly ash improving concrete's flexural strengths as flexural strength values of plain concretes are comparable to the flexural strength values of concrete containing fly ash (M1 vs. M2 and M5 vs. M6). Concretes with slag cement (M3 and M7) and combination of fly ash and slag cement (M4 and M8) yielded either comparable or higher flexural strengths



For specimen exposed to freezing-thawing (FT) cycles

Specimens of M1-CaCl₂-FT failed at 111 FT cycles, the other M1 specimens were test after 347 FT cycles.
Specimens of M5-CaCl₂-FT failed at 151 FT cycles, the other M5 specimens were test after 350 FT cycles.
Specimens of M2 and M6 were test after 347 and 350 FT cycles, respectively.

For specimen exposed to wetting-drying (WD) cycles

M1, M2, M5 and M6 specimens were test after 286 WD cycles.
M3, M4, M7 and M8 specimens were test after 226 WD cycles.

Figure 2.1 The average compressive strengths of control set 1 (C1) and control set 2 (C2) concretes.

TABLE 2.3
Tukey pair wise comparison test results of 28-day compressive strength.

Mix #	28-day compressive strength (psi), C1	Tukey grouping	
M3-.75PC.25SC-ACBFS	7740	A	
M4-.6PC.17FA.23SC-ACBFS	7415	A	B
M7-.75PC.25SC-NA	6739	A	B
M8-.6PC.17FA.23SC-NA	6525	C	B
M2-.8PC.2FA-ACBFS	5655	C	D
M1-1PC-ACBFS	5488		D
M6-.8PC.2FA-NA	5374		D
M5-1PC-NA	5160		D

TABLE 2.4
Tukey pair wise comparison test results of the compressive strength of control 2 (C2) specimens.

Mix #	Control 2 compressive strength (psi), C2	Tukey grouping	
M7-.75PC.25SC-NA	7380	A	
M2-.8PC.2FA-ACBFS	6998	A	
M4-.6PC.17FA.23SC-ACBFS	6988	A	
M3-.75PC.25SC-ACBFS	6825	A	B
M6-.8PC.2FA-NA	6569		B
M8-.6PC.17FA.23SC-NA	6480		B
M5-1PC-NA	6325		B
M1-1PC-ACBFS	6243		B

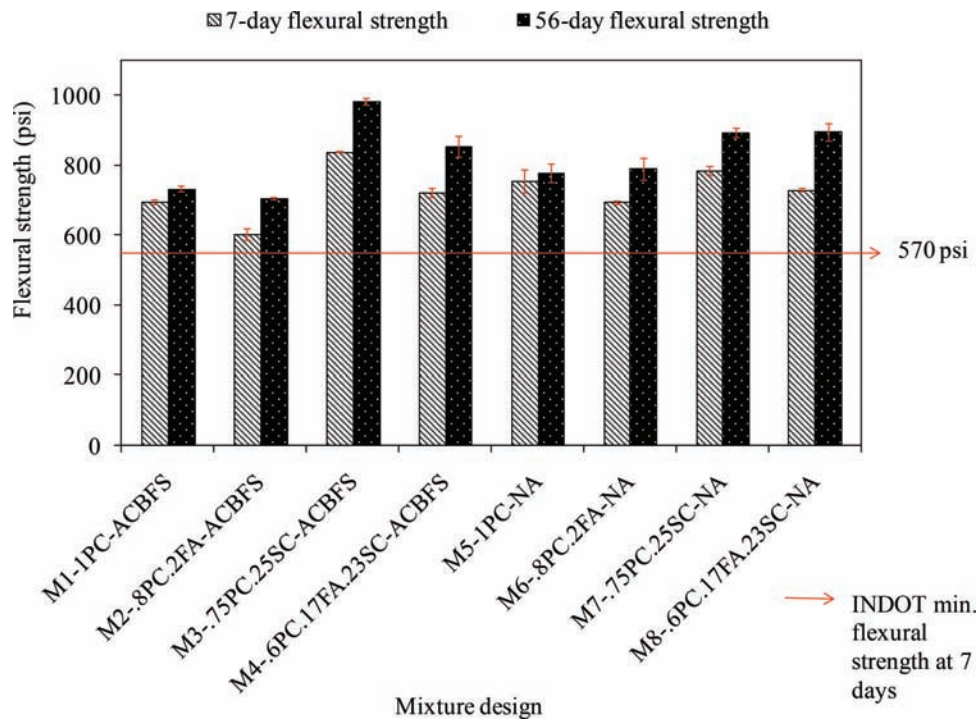


Figure 2.2 Flexural strength at 7 and 56 days of concrete from different mixtures.

than plain concretes (M1 and M5). However, it should be remembered that the effects of slag cement (and the combination of fly ash and slag cement) on the flexural strength might be influenced (skewed) by lower w/cm of those concretes.

2.2.2.2 Durability Properties. Several tests were conducted to evaluate the durability properties of different concrete mixtures. These tests included the determination of changes in dynamic modulus of elasticity (DME) (by measuring resonant frequency), chloride penetration depth measurements, and SEM analysis of the microstructure of concrete samples exposed to freezing/thawing and wetting/drying cycles in the presence of deicing solutions.

2.2.2.2.1 Relative Dynamic Modulus of Elasticity (RDME). The results for the relative dynamic modulus of elasticity (RDME) of concretes exposed to deicers undergoing FT and WD cycles are presented as the percent change in the final reading of RDME (after the completion of exposure regime) with respect to the initial (i.e., obtained before initiation of the exposure) value of RDME. The values of changes in RDME for all concrete mixtures in this study (along with the exposure conditions) used, are presented in Table 2.5. The detailed results of the RDME measurements for all concrete mixtures used in this study are presented in Figure C.2 to Figure C.5 in Appendix C.

The specimen was classified for having comparable final RDME value with respect to the initial value, if the Δ RDME was in the range of $\pm 2\sigma$ from the average. In data set with normal distribution, this range (average $\pm 2\sigma$) covers 95% data from the population

(Montgomery, 2013). The values of mean (μ) and standard deviation (σ) of the Δ RDME are 0.99% and 7.13%, respectively.

The results highlighted in Table 2.5 indicate that CaCl_2 deicer had the most severe effect with respect to reducing the RDME of plain concretes (M1 and M5) as the reductions in RDME were shown to be statistically significant. This observation applies to M1 specimens exposed to CaCl_2 under FT and WD conditions and M5 specimens exposed to CaCl_2 and FT condition). It should be noted that M1- CaCl_2 -FT and M5- CaCl_2 -FT specimens failed, respectively, after 111 and 151 FT cycles.

The effect of MgCl_2 and NaCl on the RDME is not as significant as that of CaCl_2 . The aggressivity of MgCl_2 however, was noticeable in plain specimen with dolomite (M5). This might be due to the contribution of magnesium ions leached out from dolomite aggregate to detrimental chemical reactions with concrete's hydration products. The results presented in Table 2.5 indicate that the majority of control specimens (i.e., C2 series, continuously moist cured for up to 350 days) have experienced increase in the values of RDME. This is to be expected, as the specimens were kept in the curing chamber with $23 \pm 2^\circ\text{C}$ and $>95\%$ RH, and such conditions promote additional hydration. The fact that the other specimens have showed inferior performance, in terms of RDME, compared to the control specimens, indicates that there was a negative effect of the applied exposure conditions (i.e., deicers + FT or deicers + WD) with respect to concrete performance.

The LS mean values from the data presented in Table 2.6 for each factor are summarized in Table 2.6. The significance of each factor in the changes of RDME

TABLE 2.5
Changes in the final RDME values with respect to the initial values.

		M1-1PC-ACBFS		M2-8PC.2FA-ACBFS		M3-.75PC.25SC-ACBFS		M4-.6PC.17FA.23SC-ACBFS	
Exposure condition	Deicer	Δ RDME (%)		Δ RDME (%)		Δ RDME (%)		Δ RDME (%)	
Freezing-thawing (FT)	CaCl ₂	↓	[-18.3]	↔	[-6.3]	↔	[0.4]	↔	[3.7]
	MgCl ₂	↔	[4.8]	↔	[-7.3]	↔	[-4.2]	↔	[3.4]
	NaCl	↔	[6.8]	↔	[4.7]	↔	[3.9]	↔	[5.6]
	DST	↔	[12.5]	↔	[7.5]	↔	[9.3]	↔	[11.1]
Wetting-drying (WD)	CaCl ₂	↓	[-17.2]	↔	[0.6]	↔	[-3.3]	↔	[0.4]
	MgCl ₂	↔	[-2.1]	↔	[-0.5]	↔	[-3.1]	↔	[3.5]
	NaCl	↔	[1.9]	↔	[2.9]	↔	[0.2]	↔	[5.8]
	DST	↔	[1.0]	↔	[2.2]	↔	[3.0]	↔	[3.2]
Control specimen set 2 (C2)		↔	[13.1]	↔	[9.6]	↔	[10.1]	↔	[14.1]
		M5-1PC-NA		M6-8PC.2FA-NA		M7-.75PC.25SC-NA		M8-.6PC.17FA.23SC-NA	
Exposure condition	Deicer	Δ RDME (%)		Δ RDME (%)		Δ RDME (%)		Δ RDME (%)	
Freezing-thawing (FT)	CaCl ₂	↓	[-24.6]	↔	[3.4]	↔	[-0.5]	↔	[-1.9]
	MgCl ₂	↓	[-19.4]	↔	[-0.6]	↔	[3.5]	↔	[2.3]
	NaCl	↔	[4.9]	↔	[12.8]	↔	[2.2]	↔	[0.8]
	DST	↔	[11.1]	↔	[13.9]	↔	[8.0]	↔	[4.7]
Wetting-drying (WD)	CaCl ₂	↔	[-5.6]	↔	[0.8]	↔	[1.1]	↔	[-1.2]
	MgCl ₂	↔	[-8.4]	↔	[0.0]	↔	[1.0]	↔	[-1.6]
	NaCl	↔	[1.9]	↔	[2.8]	↔	[5.9]	↔	[3.4]
	DST	↔	[2.0]	↔	[4.1]	↔	[4.3]	↔	[3.3]
Control specimen set 2 (C2)		↔	[11.0]	↑	[19.1]	↔	[8.8]	↔	[12.1]

Notes:

- ↑ = statistically significant increase (more than 2σ above the average).
- ↓ = statistically significant decrease (more than 2σ below the average).
- ↔ = statistically comparable (within $\pm 2\sigma$ from the average).
- [xx] = percent change of RDME.

For specimens exposed to freezing-thawing (FT) cycles:

- M1-CaCl₂-FT specimens failed after 111 FT cycles, the other M1 specimens were tested after 347 FT cycles.
- M5-CaCl₂-FT specimens failed after 151 FT cycles, the other M5 specimens were tested after 350 FT cycles.
- M2 and M6 specimens were tested after 347 and 350 FT cycles, respectively.

For specimens exposed to wetting-drying (WD) cycles:

- M1, M2, M5 and M6 specimens were tested after 286 WD cycles.
- M3, M4, M7 and M8 specimens were tested after 226 WD cycles.

was analyzed using ANOVA and the results are presented in Table 2.7.

The values highlighted in bold indicate the main effects and interaction effects that have significant (p -value <0.05) influence on the response variable (i.e., Δ RDME). Both binder (X1) and deicer (X4) types were found to have a significant influence to the change of RDME. The other two factors, type of aggregate and type of exposure conditions were found to not have a significant effect on the change in RDME. Three interaction effects were also found to have a significant influence on the Δ RDME (i.e., X1*X4, X3*X4 and X1*X2*X3).

Tukey's multiple comparison method was used to analyze the level of influence of the type of binder on the Δ RDME. The results of this analysis are presented in Table 2.8.

The results shown in Table 2.6 and Table 2.8 indicate that incorporation of fly ash, slag cement (and the combination of both materials) into concrete has a significant positive influence on concrete's performance in terms of the Δ RDME values. Specifically, the results indicate that the binary and the ternary binder system used in this study have relatively similar impact on concrete's performance in terms of the Δ RDME.

The Tukey's multiple comparison method was also used to analyze the impact of the type of deicers on the Δ RDME. The results are presented in Table 2.9.

The results in Table 2.9 indicate that CaCl₂ and MgCl₂ have statistically significantly different effects on Δ RDME compared to NaCl and distilled water (DST). This also implies that CaCl₂ have statistically comparable effects on Δ RDME compared to MgCl₂.

2.2.2.2.2 Chloride Penetration Depth. The depth of chloride ion penetration into the specimens was determined after completion of the FT and WD exposures. This was accomplished by cutting the specimen in the direction perpendicular to the long axis and spraying the resulting cross-section with the 0.1 mol/L solution of silver nitrate. An example of cut cross sections sprayed with silver nitrate and the position from which it was cut from a beam specimen is presented in Figure 2.3. The cross sections of the beams illustrating the depth of chloride penetration are presented in Figure C.6 to Figure C.13 in the Appendix C.

The reaction of silver nitrate with chloride ions results in formation of grayish-colored layer of silver

chloride. The thickness of this layer was measured (using a digital caliper) at several locations (indicated by arrows added to pictures of cross sections shown in Figure 2.3). These measurements were used to calculate the average depth of chloride penetration as presented in Table 2.10. It should also be noted that the area outside of the grayish-colored zone is typically not entirely chloride free but its existing chloride levels are too low (typically below 0.01%) to be detected by this colorimetric method.

The average of chloride penetration depth of specimens from each concrete mixture exposed to NaCl, CaCl₂ and MgCl₂ were analyzed using analysis of variance (ANOVA). The LS means and the ANOVA results of the average chloride penetration depth are presented in Table 2.11 and Table 2.12, respectively.

Results presented in Table 2.12 indicate there are three main effects (i.e., type of binder, exposure condition and type of deicer) that have a significant impact on the chloride penetration depth at 95% confidence level. Along with those main effects, four interaction effects (i.e., X1*X3, X1*X4, X1*X2*X3 and X1*X3*X4) are also found to have statistically significant influences on the response variable (i.e., chloride penetration depth).

Tukey's multiple comparison analysis results on the effects of type of binder system and the type of deicers on the chloride penetration depth are presented in Table 2.13 and Table 2.14, respectively.

Tukey's multiple comparison analysis results indicate that both the binary (20%FA+80%PC and 25%SC+75%PC) and the ternary (17%FA+23%SC+60%PC) binder systems used in this study have statistically significant influence on reducing the ion chloride penetration depth when compared to that of plain (100%PC) concrete. This happens due to the densification of concrete matrix as the results of pozzolanic reaction and the latent hydration reactions which are promoted by fly ash and slag cement, respectively.

TABLE 2.6

The least square (LS) means values for the differences in RDME values of FT and WD specimens exposed to deicers after exposure when compared to the initial RDME values.

Type of binder (X1)	LS mean
100% PC	-3.04
20%FA+80%PC	2.56
25%SC+75%PC	1.54
17%FA+23%SC+60%PC	2.91
Aggregate type (X2)	LS mean
ACBFS	1.13
Dolomite	0.86
Exposure condition (X3)	LS mean
Freezing-thawing (FT)	1.60
Wetting-drying (WD)	0.38
Type of deicers (X4)	LS mean
CaCl ₂	-4.28
MgCl ₂	-2.23
NaCl	4.16
DST ^a	6.33

^aDistilled water.

TABLE 2.7

The results of the analysis of variance (ANOVA) for the differences in RDME values of FT and WD specimens exposed to deicers after exposure when compared to the initial RDME values.

Source	DF	Sum of squares	Mean square	F value	p-value
Binder type (X1)	3	363.56	121.19	14.13	0.0009
Aggregate type (X2)	1	1.18	1.18	0.14	0.719
Exposure condition (X3)	1	23.64	23.64	2.76	0.1312
Deicer type (X4)	3	1226.40	408.80	47.66	<.0001
X1*X2	3	170.49	56.83	6.63	0.0118
X1*X3	3	4.99	1.66	0.19	0.8978
X1*X4	9	578.89	64.32	7.50	0.0031
X2*X3	1	24.13	24.13	2.81	0.1278
X2*X4	3	45.90	15.30	1.78	0.2201
X3*X4	3	218.58	72.86	8.49	0.0054
X1*X2*X3	3	153.58	51.19	5.97	0.016
X1*X2*X4	9	151.92	16.88	1.97	0.1638
X1*X3*X4	9	152.63	16.96	1.98	0.1622
X2*X3*X4	3	6.98	2.33	0.27	0.8447
R ²	0.98				

TABLE 2.8

The results of Tukey's multiple comparison analysis on the effects of the type of binder system on the change in RDME values of concrete after exposure period when compared the initial RDME values.

Binder system	100% PC	20%FA+80%PC	25%SC+75%PC	17%FA+23%SC+60%PC
100% PC		0.002	0.0073	0.0013
20%FA+80%PC	0.002		0.7619	0.9866
25%SC+75%PC	0.0073	0.7619		0.5763
17%FA+23%SC+60%PC	0.0013	0.9866	0.5763	

TABLE 2.9

The results of Tukey's multiple comparison analysis on the effects of the type of deicers on the change in RDME values of concrete after exposure period when compared the initial RDME values.

Type of deicers	CaCl ₂	MgCl ₂	NaCl	DST
CaCl ₂		0.2637	<0.0001	<0.0001
MgCl ₂	0.2637		0.0008	<0.0001
NaCl	<0.0001	0.0008		0.2257
DST	<0.0001	<0.0001	0.2257	

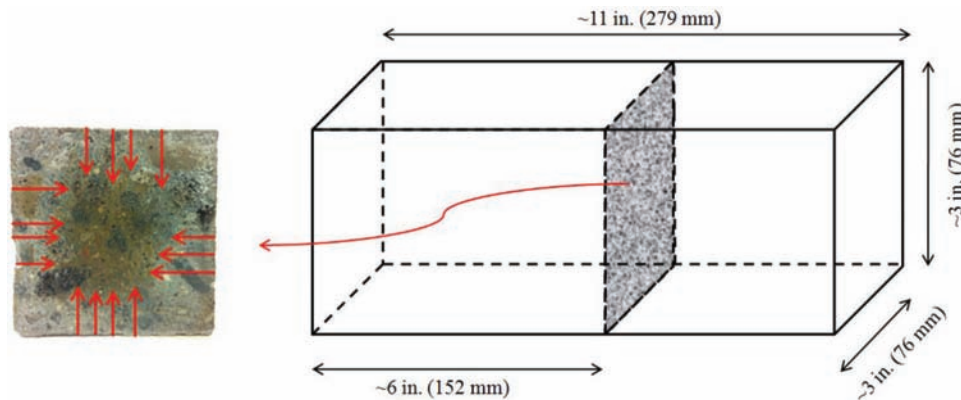


Figure 2.3 An example of cross section of specimen with its location from the original beam.

The results presented in Table 2.14 have indicated that the effects of each type of deicers used in this study (i.e., NaCl, MgCl₂ and CaCl₂) on the chloride penetration depth are significantly different among the type of deicers. Among the deicers, the chloride penetration depth on the specimens exposed to MgCl₂ was found to be the lowest, followed by that of CaCl₂. The formation of brucite (Mg(OH)₂) in the area near concrete's surfaces as the result of chemical reaction between magnesium ion with portlandite contributes to the lower chloride ingress in the matrix.

2.2.2.2.3 Physical Changes in the Appearance of Concrete Specimens. Pictures of the prismatic specimens were taken at different stages of exposures to capture the physical changes in the appearance of the specimens and to document any signs of deteriorations of the FT and WD specimens exposed to deicers. Plain concrete (M1 and M5) specimens exposed to CaCl₂ have demonstrated severe deterioration as shown from Figure 2.4 to Figure 2.7.

Figure 2.4 clearly shows the first sign of deterioration were observed as early as after about 35 FT cycles.

After undergoing 102 FT cycles, the specimen shows a very extensive damage (in the form of cracking and spalling). In fact the damage to this specimen started to exponentially accelerate with each of additional FT cycle to the point that it failed (that is it was impossible to obtain consistent readings of resonant frequency) after 111 FT cycles. The deterioration started at the corner and propagated along the edges. Cracks visible on the surface tend to be parallel to the length of the specimen. The changes in physical appearance of this specimen were accompanied by reduction of the values of relative dynamic modulus of elasticity (RDME) which decreased approximately 20% after 111 FT cycles. At the same time, the RDME values of the rest M1 specimens have slightly increase over time. In fact, after 347 FT cycles, that increase was about 3%–10% with respect to the initial RDME values (see Figure C.2(A), Appendix C).

Similar to M1 specimens showed in Figure 2.4, M5 specimens exposed to CaCl₂ under FT condition had started to deteriorate at 42 FT cycles as shown in Figure 2.5. The deterioration started at the corner and

TABLE 2.10
Average chloride penetration depth for different concretes exposed to different deicers.

Exposure condition	Deicers	Average chloride penetration depth (mm)									
		M1-1PC-ACBFS (plain - ACBFS)	M2-8PC-2FA-ACBFS (fly ash - ACBFS)	M3-75PC-25SC-ACBFS (slag cement - ACBFS)	M4-17FA-23SC-6PC-ACBFS (ternary - ACBFS)	M5-1PC-NA (plain - dolomite)	M6-8PC-2FA-NA (fly ash - dolomite)	M7-75PC-25SC-NA (slag cement - dolomite)	M8-17FA-23SC-6PC-NA (ternary - dolomite)		
Freezing-thawing (FT)	NaCl	19.2	17.8	13.7	13.8	20.0	16.6	13.9	11.8		
	CaCl ₂	17.4	12.4	12.9	14.5	19.8	10.5	11.8	13.0		
	MgCl ₂	8.4	4.9	8.3	9.3	16.1	5.0	10.6	6.6		
Wetting-drying (WD)	NaCl	21.6	19.4	14.6	21.9	16.8	21.6	16.5	18.2		
	CaCl ₂	23.3	12.5	14.3	14.3	17.7	15.2	13.6	12.3		
	MgCl ₂	10.6	14.1	12.2	12.0	10.5	13.7	12.3	13.1		

Notes:

For specimens exposed to freezing-thawing (FT) cycles:

- M1-CaCl₂-FT specimens failed after 111 FT cycles, the other M1 specimens were tested after 347 FT cycles.
- M5-CaCl₂-FT specimens failed after 151 FT cycles, the other M5 specimens were tested after 350 FT cycles.
- M2 and M6 specimens were tested after 347 and 350 FT cycles, respectively.

For specimens exposed to wetting-drying (WD) cycles:

- M1, M2, M5 and M6 specimens were tested after 286 WD cycles.
- M3, M4, M7 and M8 specimens were tested after 226 WD cycles.

TABLE 2.11

The least square (LS) means values for the chloride ions penetration depth of FT and WD specimens exposed to deicers after the exposure regime.

Type of binder (X1)	LS mean
100% PC	16.78
20%FA+80%PC	13.64
25%SC+75%PC	12.89
17%FA+23%SC+60%PC	13.40
Aggregate type (X2)	LS mean
ACBFS	14.31
Dolomite	14.05
Exposure condition (X3)	LS mean
Freezing-thawing (FT)	12.85
Wetting-drying (WD)	15.51
Type of deicers (X4)	LS mean
CaCl ₂	14.72
MgCl ₂	10.48
NaCl	17.34

then propagated to the edges of the specimen. The damages of the specimen were very comprehensive after 139 FT cycles and eventually the specimen failed at 151 FT cycles. The superiority of dolomite aggregate compared to ACBFS is indicated by the fact that M5 specimens could withstand up to 151 FT cycles while M1 specimens were failed at 111 FT cycles under the exposure of CaCl₂ deicer.

Figure 2.6 shows that M1 specimen under the exposure of CaCl₂+WD had experienced extensive damaged after 176 WD cycles. The damages were progressively increased as the corners and edges of the specimens crumbled after 281 WD cycles. However, unlike M1 specimens exposed to CaCl₂+FT condition which failed at 111 FT cycles, M1 specimens exposed to CaCl₂+WD condition did not fail even after 286 WD cycles (as shown by the RDME reading in Figure C.4(A), Appendix C). This indicates that FT temperature cycle has higher degree of severity in damaging concrete than WD cycle despite of higher deicer concentration used in WD condition (10.5 molar vs. 5.5 molar).

Comparing the damage of M1 specimen showed in Figure 2.6 to the damage of M5 specimen showed in Figure 2.7, one can tell that the damage of M5 specimen does not as severe as what occurred on M1 specimen. This finding is similar to the specimen exposed to CaCl₂+FT condition which the dolomite specimens (M5) have maintained longer stable RDME readings (151 FT vs. 111 FT cycles) than the specimens made with ACBFS coarse aggregate (M1) before they failed.

Following the specimens exposed to CaCl₂, only M5 specimens exposed to MgCl₂ under FT condition had experienced minor damaged. No observable damages were found on the rest of the specimens (i.e., FF and WD specimens exposed to NaCl and distilled water).

TABLE 2.12

The results of the analysis of variance (ANOVA) for the chloride ions penetration depth of FT and WD specimens exposed to deicers after the exposure regime.

Source	DF	Sum of squares	Mean square	F value	p-value
Binder type (X1)	3	112.02	37.34	22.58	0.0011
Aggregate type (X2)	1	0.80	0.80	0.48	0.5126
Exposure condition (X3)	1	85.33	85.33	51.59	0.0004
Deicer type (X4)	2	383.05	191.53	115.79	<.0001
X1*X2	3	9.73	3.24	1.96	0.2214
X1*X3	3	42.15	14.05	8.49	0.014
X1*X4	6	80.45	13.41	8.11	0.0112
X2*X3	1	3.20	3.20	1.94	0.2134
X2*X4	2	9.73	4.86	2.94	0.1288
X3*X4	2	11.15	5.58	3.37	0.1044
X1*X2*X3	3	39.86	13.29	8.03	0.016
X1*X2*X4	6	16.35	2.73	1.65	0.2796
X1*X3*X4	6	52.17	8.69	5.26	0.0317
X2*X3*X4	2	0.67	0.34	0.20	0.8219
R ²	0.99				

TABLE 2.13

The results of Tukey's multiple comparison analysis on the effects of the type of binder system on the chloride ions penetration depth values of concrete specimen after the exposure regime.

Binder system	100% PC	20%FA+80%PC	25%SC+75%PC	17%FA+23%SC+60%PC
100% PC		0.004	0.0013	0.0027
20%FA+80%PC	0.004		0.5278	0.9651
25%SC+75%PC	0.0013	0.5278		0.7718
17%FA+23%SC+60%PC	0.0027	0.9651	0.7718	

TABLE 2.14

The results of Tukey's multiple comparison analysis on the effects of the type of deicers on the chloride ions penetration depth values of concrete specimen after the exposure regime.

Type of deicers	CaCl ₂	MgCl ₂	NaCl
CaCl ₂		0.0002	0.0029
MgCl ₂	0.0002		<0.0001
NaCl	0.0029	<0.0001	



Figure 2.4 Physical changes in the appearance of the representative sample of M1-1PC-ACBFS (plain-ACBFS) concrete specimens exposed to CaCl₂ after (from left to right) 35, 59 and 102 FT cycles. Specimen failed after 111 FT cycles.

The complete sets of pictures demonstrating the extend of physical changes in the specimens from eight different mixtures, exposed to different deicers (CaCl₂,

MgCl₂ and NaCl) and distilled water (DST) under freezing-thawing (FT) and wetting-drying (WD) cycles is presented Appendix C (Figure C.14 to Figure C.77).



Figure 2.5 Physical changes in the appearance of the representative sample of M5-1PC-NA (plain-dolomite) concrete specimens exposed to CaCl_2 after (from left to right) 42, 65, 118 and 139 FT cycles. Specimen failed after 151 FT cycles.



Figure 2.6 Physical changes in the appearance of the representative sample of M1-1PC-ACBFS (plain-ACBFS) concrete specimens exposed to CaCl_2 after (from left to right) 176, 205 and 281 WD cycles.



Figure 2.7 Physical changes in the appearance of the representative sample of M5-1PC-NA (plain-dolomite) concrete specimens exposed to CaCl_2 after (from left to right) 176, 205 and 281 WD cycles.

2.2.3 Scanning Electron Microscopy (SEM) Observations

Once the exposure of the beam specimens was completed (either after completion of FT/WD cycles or upon premature failure), part of the beams were sawed-off and used to prepare the specimens for SEM analysis. The location of the sample taken for SEM

analysis and the example of finished SEM specimen are shown in Figure 2.8.

From each specimen exposed to deicers, the SEM samples were taken from the corner of the beams, considering the extent of chloride penetration and associated potential changes in the microstructure due to chemical reactions involving chloride.

The deposits of Friedel's salt ($C_3A \cdot CaCl_2 \cdot 10H_2O$) (Figure 2.9, Figure 2.10, Figure 2.11(A) and (B)) and chloride (Figure 2.11(C) and (D), Figure 2.12(A) and (B)) were observed in all SEM specimens despite of the different types of coarse aggregate, binder system and exposure conditions. In addition, remnants of unreacted binders beside OPC (fly ash, slag cements or combination of both) were also found in the specimens which binder system containing fly ash (M2 and M6), slag cement (M3 and M7) and combination of both fly ash and slag cement (M4 and M8) as shown in Figure 2.9 and Figure 2.10.

Specimens exposed to magnesium chloride solution show evidence of brucite ($Mg(OH)_2$) and magnesium silicate hydrate (M-S-H) formation (see Figure 2.13 and Figure 2.14). The formation of M-S-H, which is not cementitious, reduced the strength of the matrix. In addition, the physical appearance of M-S-H itself which found to possess cracks (as shown in Figure 2.13), also implies as weaker region than C-S-H. Calcium oxychloride like phase was detected in specimens exposed to calcium chloride (Figure 2.15).

The SEM analysis on concrete with ACBFS coarse aggregate indicated the presence of calcium sulfide

(CaS) within the aggregate particles as shown in Figure 2.16 to Figure 2.18.

In some cases, the dissolution of calcium sulfide from ACBFS leaves empty voids in the ACBFS near the aggregate-matrix interface as shown in Figure 2.18. These empty spaces potentially weaken ACBFS's matrix as multiple cracks propagate through the empty voids. Furthermore, once the sulfide released from ACBFS converts into sulfate, it can contribute to formation of ettringite, which causes cracking due to localized heterogeneous expansion experienced by concrete in the region where ettringite is formed (Collepardi, 2003).

Ettringite formation was not exclusively observed in concrete containing ACBFS, but was also detected in concrete made with dolomite. However, the frequency of ettringite detected (using SEM) in the matrix of concrete with natural dolomite was lower than that in concrete with ACBFS aggregates. Ettringite is expansive, and therefore its formation can increase the crack width (of the pre-existing micro-cracks) or fill in the available spaces. Pores filled with ettringite reduce the freeze-thaw durability of concrete. In a sulfate depleted environment, the ettringite forms into monosulfate. The morphology and energy dispersive X-ray signature of ettringite in concrete containing ACBFS and natural dolomite are shown in Figure 2.19 (A) and (B), respectively. The completed set of SEM results in this study are presented in Appendix D.

2.3 Pore Solution Analysis Results

The variation in the concentration of sodium and potassium ion in the pore solution with age is presented in Figure 2.20 (A) and (B), respectively.

Figure 2.20 indicates that for mixtures without slag cement (Mix 1 and Mix 2), both sodium and potassium

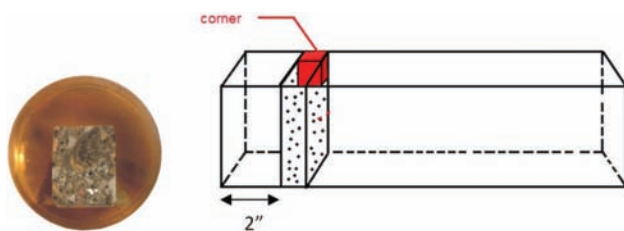


Figure 2.8 An example of SEM sample and the location from which it was obtained.

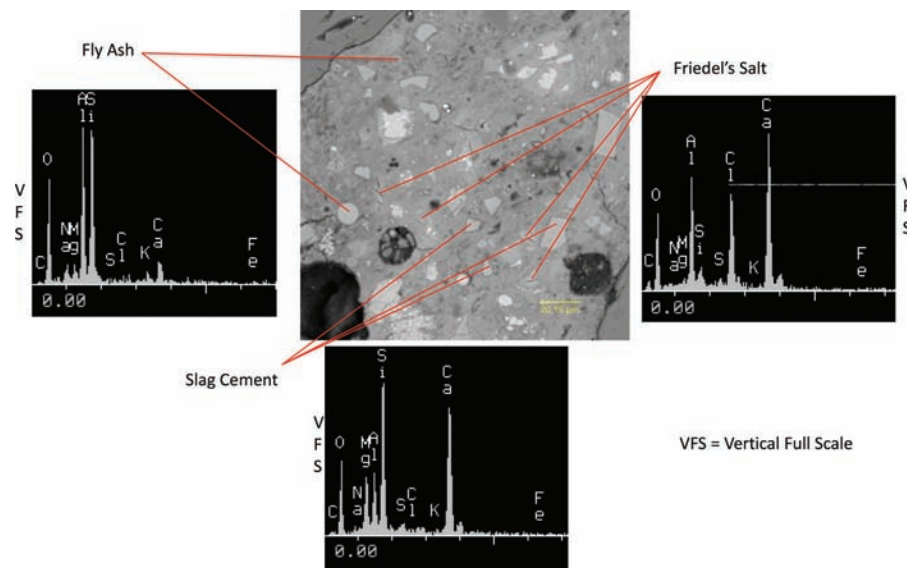


Figure 2.9 Deposits of Friedel's salt and remnants of unreacted binder particles (fly ash and slag cement) found in SEM sample extracted from M4 (ternary-ACBFS) specimen exposed to $CaCl_2$ after 310 FT cycles (SEM-BSE).

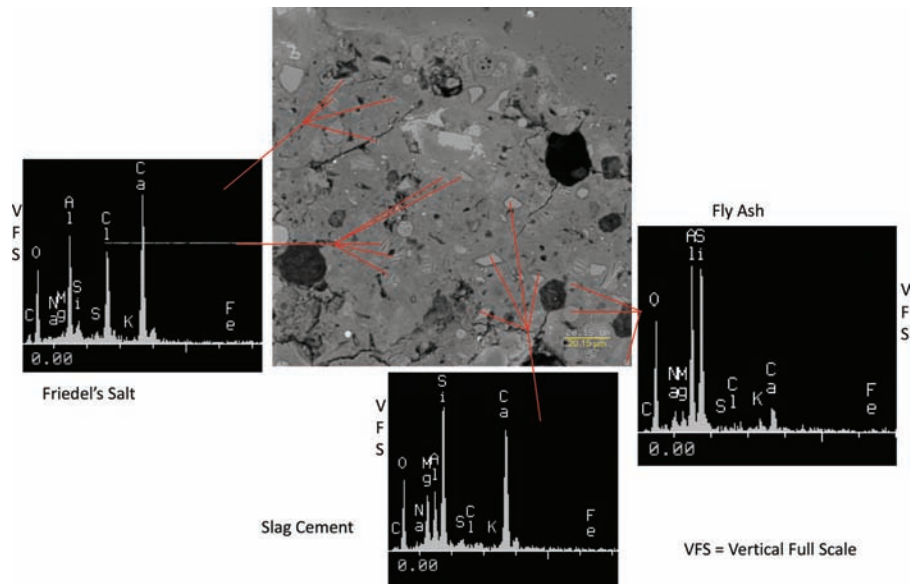


Figure 2.10 Deposits of Friedel's salt and remnants of unreacted binder particles (fly ash and slag cement) found in SEM sample extracted from M8 (ternary-dolomite) specimen exposed to MgCl_2 after 310 FT cycles (SEM-BSE).

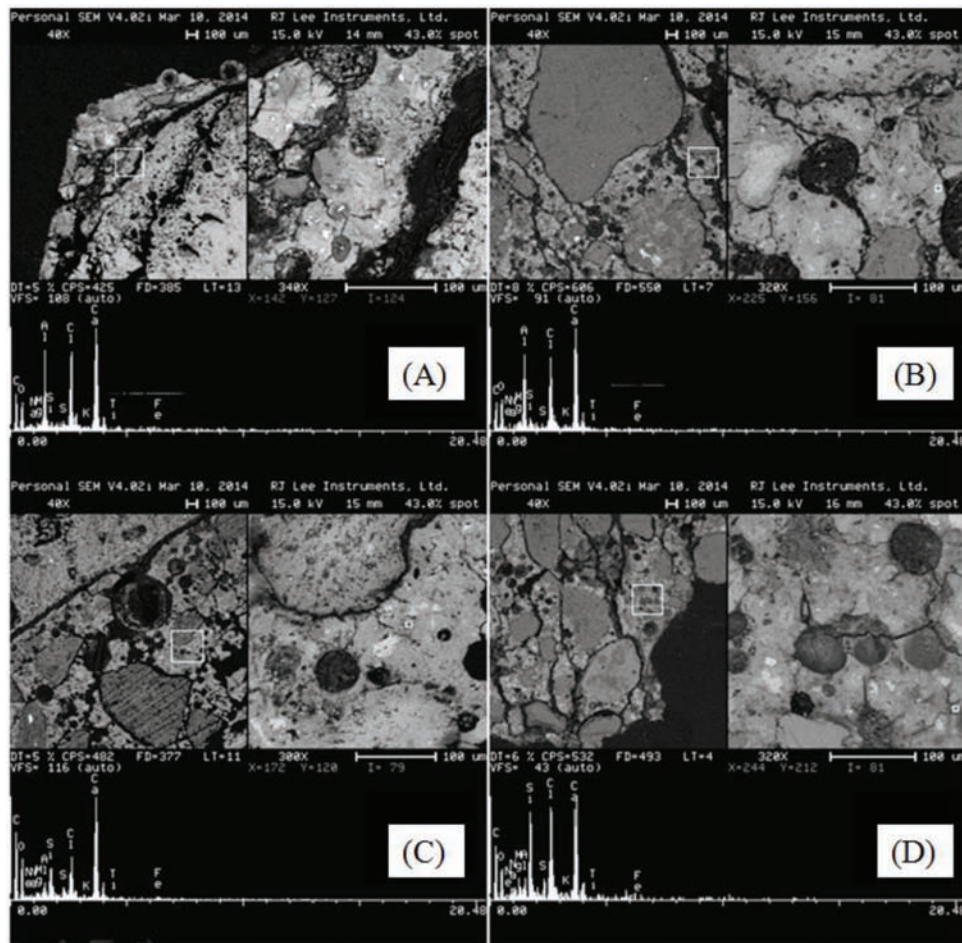


Figure 2.11 SEM-EDS micrographs for specimen from M1 (plain-ACBFS) mixture – exposed to CaCl_2 after 111 FT cycles; (A) and (B) Friedel's salt, (C) & (D) chloride deposits within the paste (SEM-BSE).

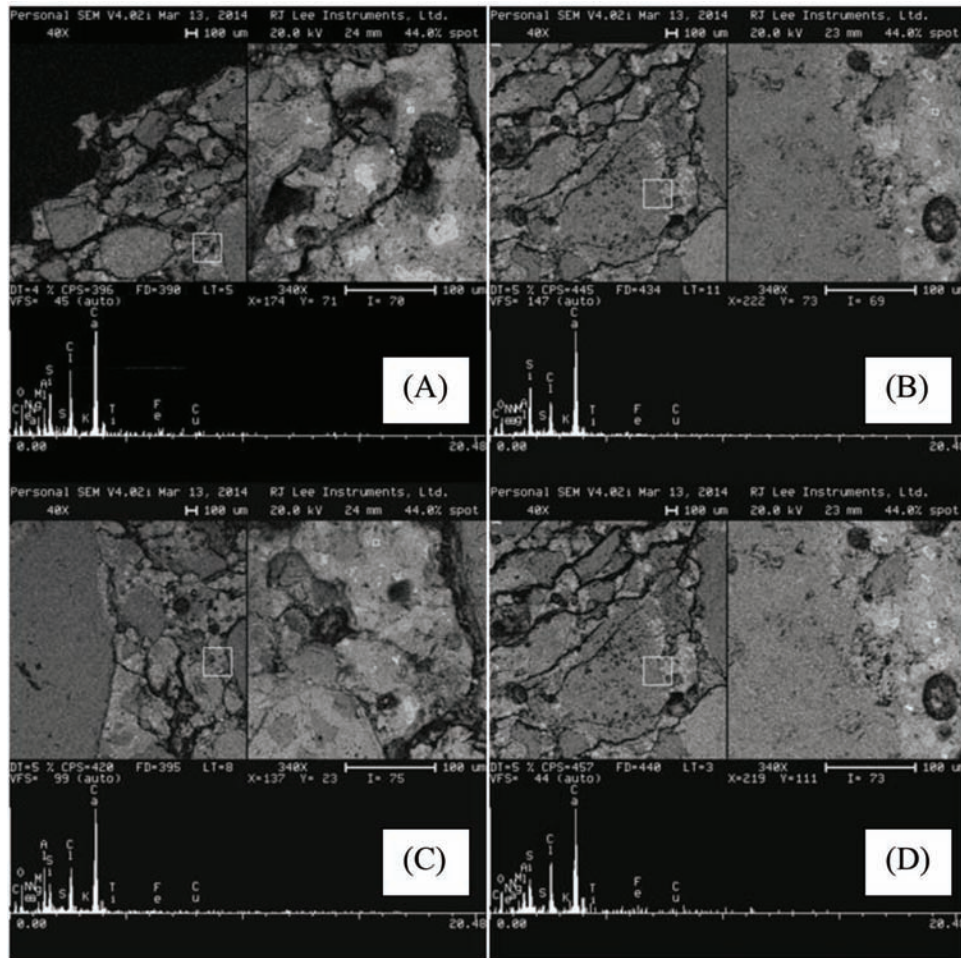


Figure 2.12 SEM-EDX micrographs of microstructure of specimen removed from the corner of a beam from M5 (plain-dolomite) mixture exposed to CaCl_2 after 151 FT cycles; (A) and (B) chloride deposits within C-S-H, (C) Friedel's salt, (D) deposit of CaCl_2 within C-S-H (SEM-BSE).

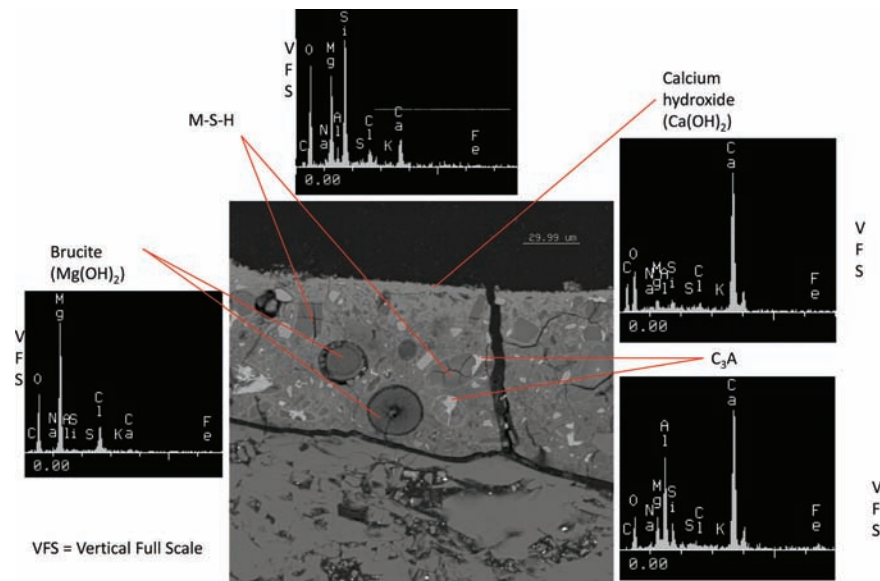


Figure 2.13 SEM-EDX micrographs of brucite, M-S-H, calcium hydroxide and remnants of un-hydrated cement (C_3A) found in M7 (slag cement-dolomite) specimen exposed to MgCl_2 after 310 FT cycles (SEM-BSE).

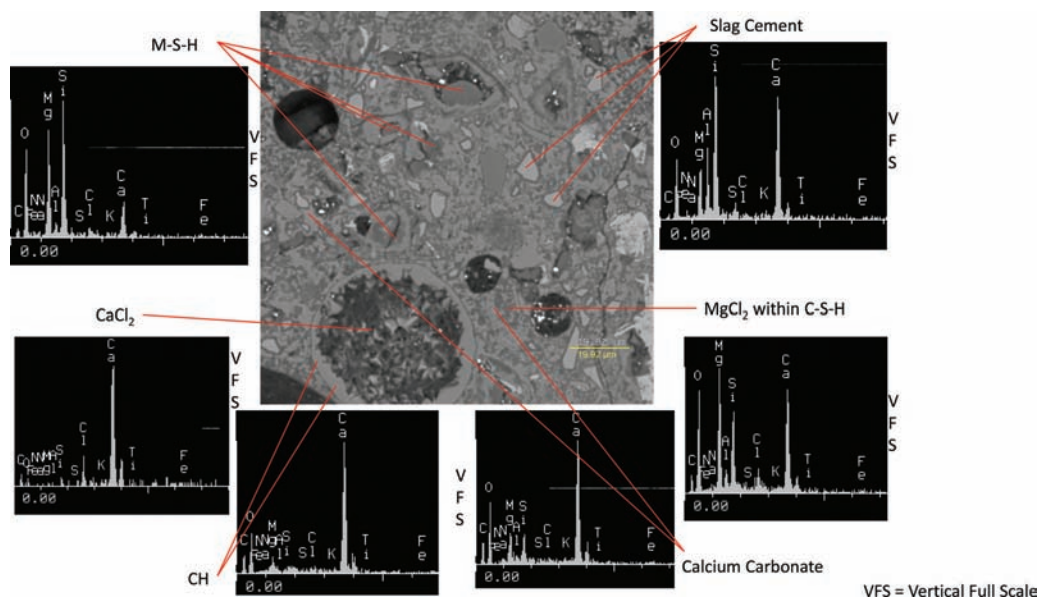


Figure 2.14 SEM-EDX micrographs of M-S-H, CaCl₂, CH, calcium carbonate, MgCl₂ and remnants of un-hydrated slag cement found in M3 (slag cement-ACBFS) specimen exposed to MgCl₂ after 226 WD cycles (SEM-BSE).

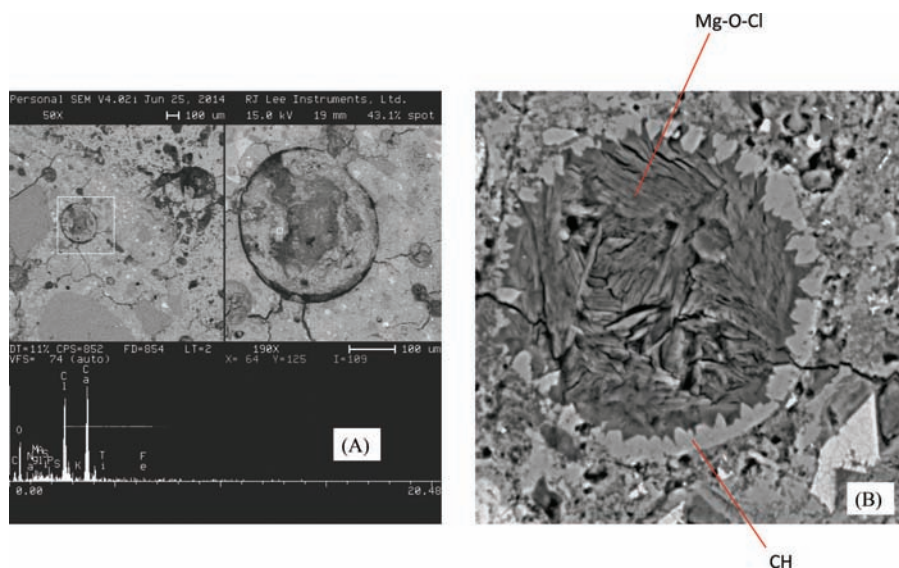


Figure 2.15 Void filled with (A) calcium oxychloride-like phase in sample exposed to CaCl₂ solution and (B) 1000X magnification image of Mg-O-Cl phase surrounded by calcium hydroxide (CH) in M1 (plain-ACBFS) specimen exposed to MgCl₂ after 347 FT cycles (SEM-BSE).

ion concentrations increase with age. This is not desirable as it increased the pH of the pore solution, making the condition more favorable with respect to the dissolution of calcium sulfide found in the ACBFS aggregate. The opposite trend was found in the mixtures containing slag cement (Mix 3 and Mix 4). For these mixtures, the sodium and potassium ion concentrations decreased with time. Analysis of the total alkali content (i.e., combined sodium and potassium ions concentration) shown in Figure 2.21 indicates that mixtures containing slag cement (M3 and M4) not

only showed a decreasing trend in total alkali content with age, but also have less than 70% of the total alkali content of mixtures M1 and M2. This finding suggests that using binder system utilized in mixtures M3 and M4 would be beneficial with respect to minimizing the dissolution of calcium sulfide from ACBFS aggregates.

The variation of sulfate ion (SO_4^{2-}) concentration in the pore solution with age for the four types of paste mixtures is presented in Figure 2.22. It can be seen that replacing part of the portland cement with either fly

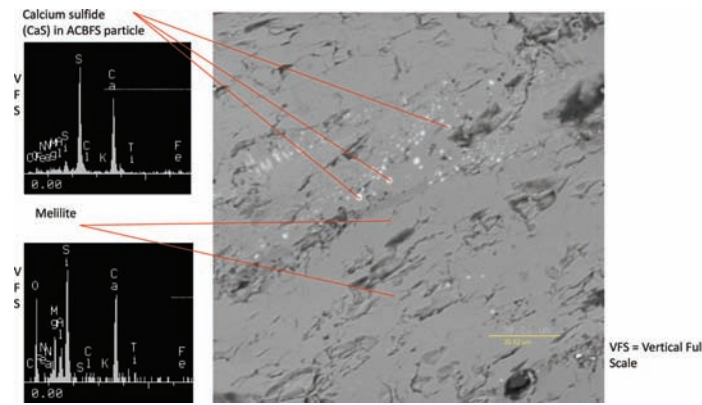


Figure 2.16 SEM image showing deposits of calcium sulfide (CaS) inside ACBFS particle (SEM-BSE).

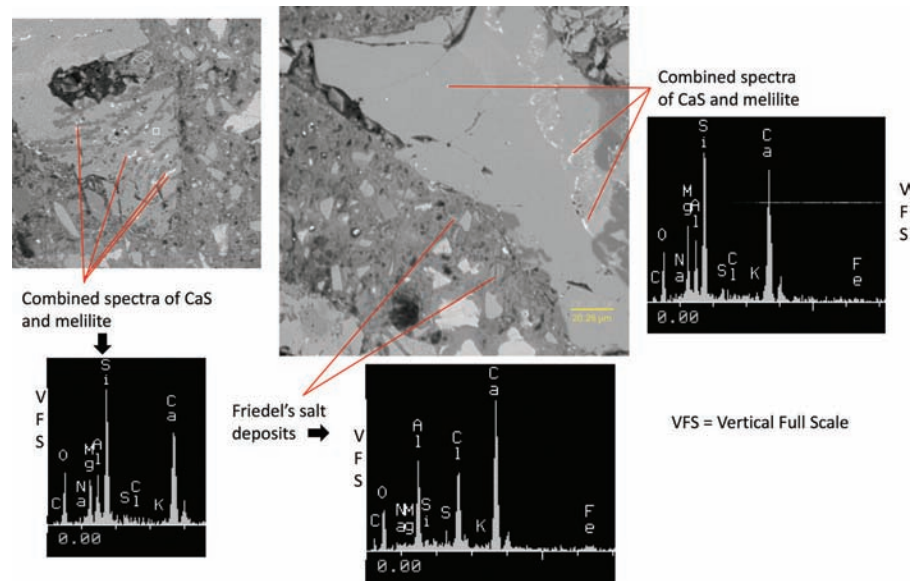


Figure 2.17 SEM images showing deposits of calcium sulfide in the particles of ACBFS aggregate and Friedel's salt in the matrix of M3 (slag cement-ACBFS) specimen exposed to NaCl after 310 FT cycles (SEM-BSE).

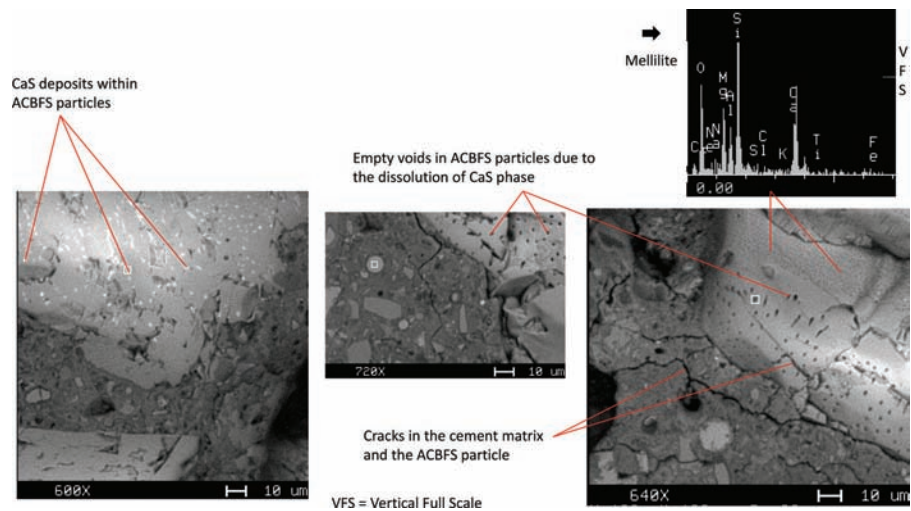


Figure 2.18 CaS deposits and empty voids in ACBFS particle from M4 (ternary-ACBFS) specimen exposed to distilled water (DST) after 310 FT cycles (SEM-BSE).

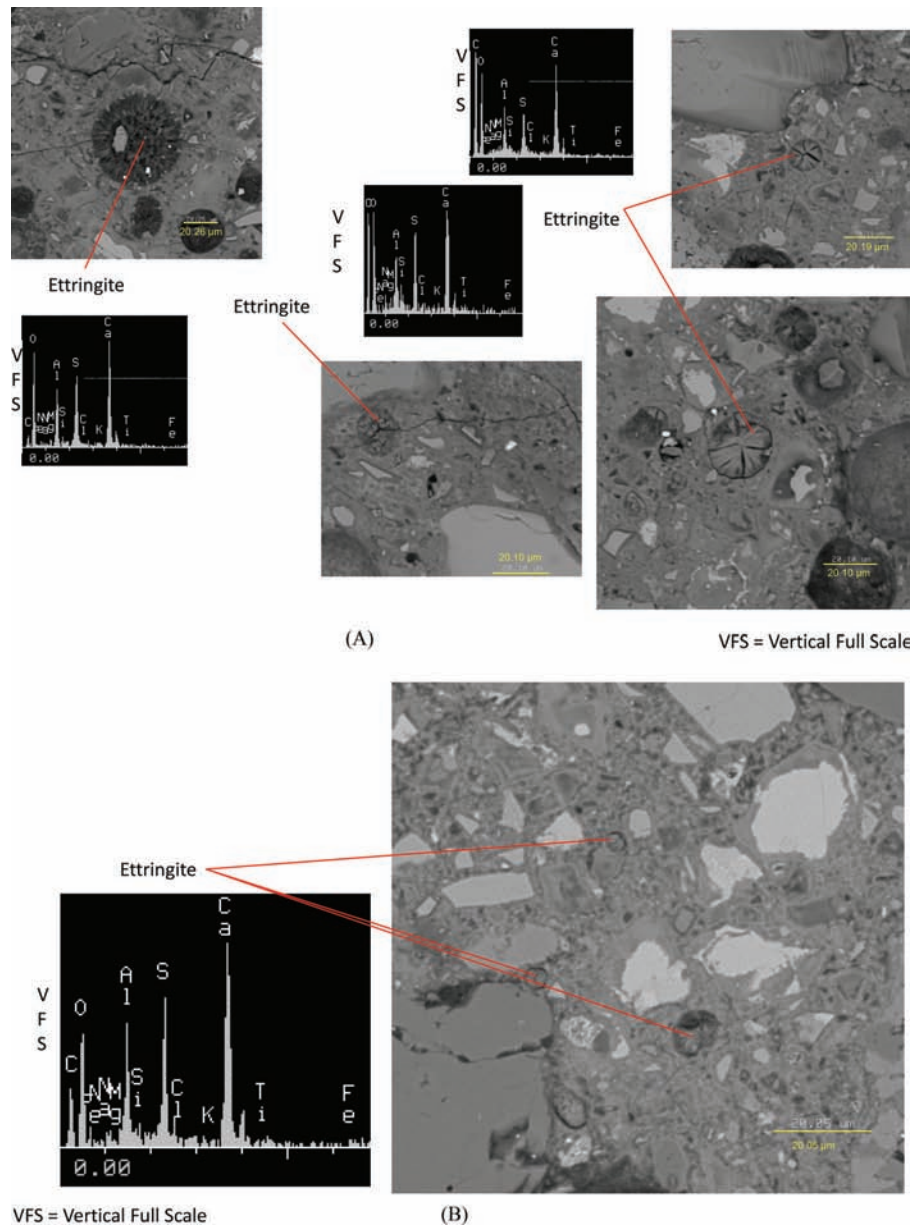
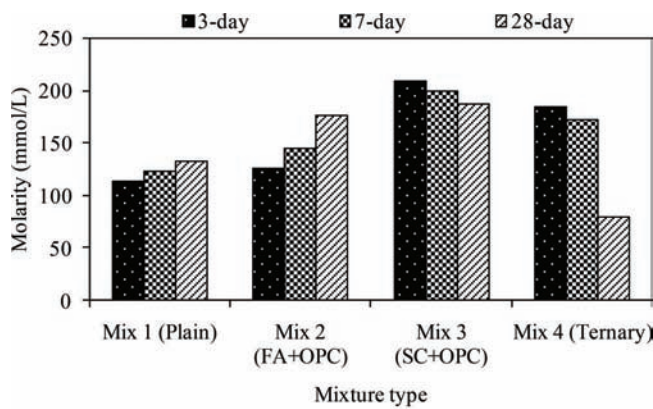


Figure 2.19 SEM-EDX (Energy Dispersive X-Ray) micrographs of ettringite in (A) concrete containing ACBFS and slag cement (M3-DST-FT) and (B) concrete containing natural dolomite as coarse aggregates (SEM-BSE).

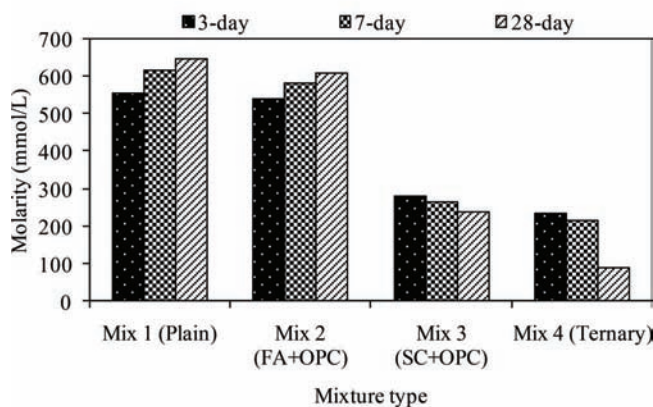
ash, slag, or combination of these two materials results in the reduction of sulfate ion content in the pore solution. This finding is supported by the fact that OPC has the highest amount of sulfur oxide (see Table E.1) compared to class C fly ash and slag cement (see Table E.1)

used in this study and thus replacing part of the cement with other materials results in the dissolution effect.

The plots for calcium, aluminum, and chloride ion concentration detected in the pore solution are included in the Figure E.1, Appendix E.



(A) Sodium (Na⁺) ion concentration



(B) Potassium (K⁺) ion concentration

Figure 2.20 (a) Variation in sodium ion concentration; (b) Variation in potassium ion concentration.

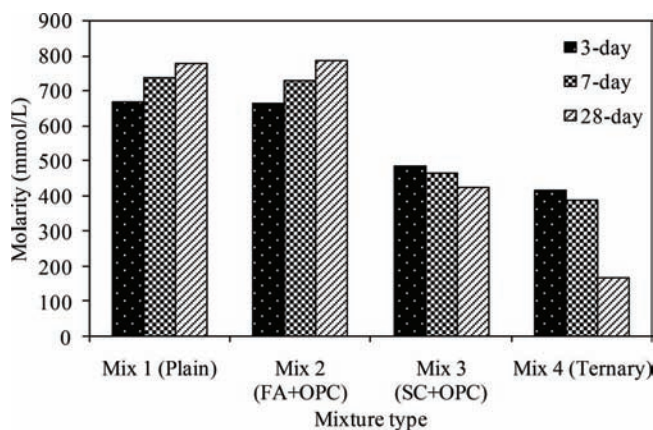


Figure 2.21 Variation in total alkalis concentration with age in different paste mixtures.

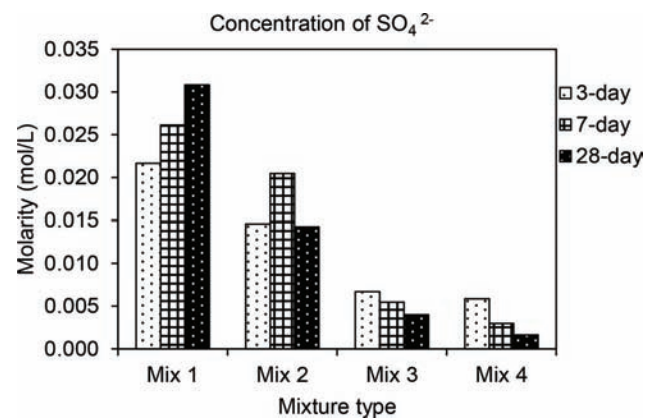


Figure 2.22 Variation in sulfate ion concentration at with age for different paste mixtures.

3. COST BENEFIT ANALYSIS OF USING SLAG AGGREGATE IN NEW CONCRETE PAVEMENTS

3.1 Background

With the shrinking availability of good quality natural aggregates, use of reclaimed aggregates such as air-cooled blast furnace slag (ACBFS) aggregate is becoming increasingly popular in industrial states where such materials may be abundantly available. This project has demonstrated that concrete mixtures incorporating ACBFS aggregate can be successfully used for paving applications in the state of Indiana. Today, the cost of slag aggregate is similar to that of naturally mined dolomite aggregate (INDOT #8 size). However, this can be expected to change in the near future as the deposits of good quality natural aggregate in the existing quarries are diminishing. A major cost benefit associated with using ACBFS aggregate instead of naturally mined coarse aggregate in concrete arises from the savings associated with disposing slag (waste product of iron and steel industries) in landfills.

The feasibility of using slag aggregate in base layers of a concrete pavement was not studied in this project; however, the cost benefit analysis presented here has an option to calculate cost benefits associated with using ACBFS aggregate in base layers of a concrete pavement. Furthermore, this analysis does not include the costs associated with the environmental damage caused due to mining and land filling operations. Similar approach in analyzing the benefit cost on pavement concrete with recycled aggregate was done in SPR 3309 project study sponsored by INDOT (Verian, Whiting, Olek, Jain, & Snyder, 2013).

3.2 Cost Benefit Analysis Model

The costs benefit model is presented as a supplemental Excel worksheet (available for download at <https://doi.org/10.5703/1288284316362>) to provide flexibility to the user with respect to updating the parameters of pavement structure and/or cost of raw materials. This model considers the use of ACBFS aggregates and supplementary cementitious materials such as fly ash

and ground granulated blast furnace slag (GGBFS) in concrete.

3.2.1 Input Parameters

The input parameters used for this cost benefit analysis are expected to change either with each project, location or over time. Input parameters such as amount of aggregate needed will vary from project to project. Although certain parameters, such as landfill costs or new aggregate costs, are common for different project in Indiana, they can be expected to change over time. Figure F.1 of Appendix F shows an example of how the model estimates the quantity of raw material needed to build a new concrete pavement.

The cells marked in yellow are project specific variables and their values will change depending on the requirements of the project. The cells highlighted in blue are the values calculated by the model. The values used in this example are those for a typical concrete pavement structure. In calculating the quantity of raw materials required in the base layers, the weights of one cubic yard of aggregates were assumed as follows:

1. #8 natural aggregate is 1.5t/cy
2. #53 natural aggregate is 1.4 t/cy
3. ACBFS aggregate is 1.33 t/cy

The next part of the model deals with the calculations of the costs associated with the use of all 8 concrete mixtures tried during the course of this study (see Table 3.1). The model also provides for partial or complete replacement of natural aggregate by ACBFS aggregate in base layers of the pavement structure (see Table 3.2 for the example of the case of complete replacement). All the input variables used for this part of the model are highlighted in yellow in Figure F.2, Appendix F. The values used in this table are the average values of the range of cost of each particular material. For example, the cost of #8 dolomite aggregate varies between \$8.5–10.5/ton and therefore the average value of \$9.5/ton is used for calculations. The major portion of the cost of fly ash and GGBFS generally arise from their availability and transportation from the source and therefore huge variations are expected for those values depending on the proximity of the concrete production plant and the source. Landfill costs and hauling costs are more or less similar but are expected to change over time. Hauling distances used for calculation of the cost of raw materials required for constructing a concrete pavement are shown in Figure F.2 of Appendix F. The values for hauling distances were arrived at using engineering judgment. For example, the hauling distance between slag production plant and disposal site is generally expected to be a small number. Most assumptions made and values used for this example are also listed in the Figure F.2 of Appendix F. The cost of #53 and #8 ACBFS aggregates are assumed to be the same for this cost benefit analysis model.

3.2.2 Output Values

Table 3.1 and Table 3.2 show the final costs of building concrete pavement for all the eight mixtures tested during the course of this study without ACBFS aggregate in base layers and with 100% of base material consisting of ACBFS aggregate respectively. The purpose of this cost benefit analysis is to demonstrate the economic benefits associated with replacing naturally mined coarse aggregate (dolomite) with ACBFS aggregates. Therefore, the costs associated with hauling sand, cement, fly ash and GGBFS from source to concrete production plant and concrete from production plant to job site are not included in this analysis.

Concrete incorporating slag aggregates (Mixes 1–4) cost slightly less than concrete with dolomite as coarse aggregate. However, hauling cost of aggregates contributes 32%–37% (for the input values used in this example) of the cost of concrete and therefore the hauling distances used for calculation will significantly alter the output. The total cost of raw materials required for constructing pavement with 100% ACBFS aggregate in base layers of the pavement structure is approximately 4% lower than the costs associated with pavement incorporating 0% ACBFS aggregate in the base layers. However, since the hauling distance has huge implications on the total cost, a project site or concrete production plant located close to the ACBFS aggregate source would benefit significantly from using ACBFS in concrete as well as in the base layers.

Table 3.3 and Table 3.4 present the costs of concrete and a total cost of the raw materials required for the project when the hauling distances are same for both ACBFS aggregates and naturally mined dolomite aggregate. The difference in the cost of concrete produced using ACBFS aggregate and naturally mined dolomite aggregate is more pronounced when the haul distance is similar. In addition, the total cost of the project also reduces significantly when ACBFS aggregate is used in base layers (100%) when the haul distance is similar.

However, in real life, ACBFS aggregate source are located mostly in industrial areas and are therefore farther away from most construction projects than sources of naturally mined aggregates. Therefore, the initial cost of constructing concrete pavements with ACBFS aggregate as coarse aggregate can be higher than using naturally mined dolomite aggregate. However, inclusion of the costs associated with environmental pollution due to mining operations in the model could potentially lead to a different picture.

4. CONCLUSIONS

The conclusions drawn from the study are as follows:

- This study demonstrated that air-cooled blast furnace slag (ACBFS) can be safely used as coarse aggregate in pavement concrete, as replacement for natural coarse aggregate. Potential benefits on using ACBFS aggregate in pavement concrete include improved quality of the

TABLE 3.1

Table summarizing the costs (per lane-mile) for constructing new pavement with 0% ACBFS in base layers.

	Mix 1	Mix 2	Mix 3	Mix 4	Mix 5	Mix 6	Mix 7	Mix 8
Cost of concrete	\$95,705	\$92,640	\$90,249	\$89,379	\$101,053	\$97,612	\$97,690	\$94,928
Cost of base (#8)	\$28,380	\$28,380	\$28,380	\$28,380	\$28,380	\$28,380	\$28,380	\$28,380
Cost of base (#53)	\$52,155	\$52,155	\$52,155	\$52,155	\$52,155	\$52,155	\$52,155	\$52,155
Total cost	\$176,240	\$173,174	\$170,784	\$169,913	\$181,588	\$178,146	\$178,224	\$175,462

TABLE 3.2

Table summarizing the costs (per lane-mile) for constructing new pavement with 100% ACBFS in base layers.

	Mix 1	Mix 2	Mix 3	Mix 4	Mix 5	Mix 6	Mix 7	Mix 8
Cost of concrete	\$95,705	\$92,640	\$90,249	\$89,379	\$101,053	\$97,612	\$97,690	\$94,928
Cost of base (#8)	\$24,383	\$24,383	\$24,383	\$24,383	\$24,383	\$24,383	\$24,383	\$24,383
Cost of base (#53)	\$48,767	\$48,767	\$48,767	\$48,767	\$48,767	\$48,767	\$48,767	\$48,767
Total cost	\$168,855	\$165,790	\$163,399	\$162,529	\$174,203	\$170,762	\$170,840	\$168,078

TABLE 3.3

Example of calculation of total cost (per lane-mile) of the project with similar haul distance (60 miles) for ACBFS aggregate and naturally mined dolomite aggregate (0% ACBFS in base).

	Mix 1	Mix 2	Mix 3	Mix 4	Mix 5	Mix 6	Mix 7	Mix 8
Cost of concrete	\$90,161	\$87,096	\$85,081	\$83,903	\$101,053	\$97,612	\$97,690	\$94,928
Cost of base (#8)	\$28,380	\$28,380	\$28,380	\$28,380	\$28,380	\$28,380	\$28,380	\$28,380
Cost of base (#53)	\$52,155	\$52,155	\$52,155	\$52,155	\$52,155	\$52,155	\$52,155	\$52,155
Total cost	\$170,696	\$167,630	\$165,616	\$164,438	\$181,588	\$178,146	\$178,224	\$175,462

TABLE 3.4

Example of calculation of total cost (per lane-mile) of the project with similar haul distance (60 miles) for ACBFS aggregate and naturally mined dolomite aggregate (100% ACBFS in base).

	Mix 1	Mix 2	Mix 3	Mix 4	Mix 5	Mix 6	Mix 7	Mix 8
Cost of concrete	\$90,161	\$87,096	\$85,081	\$83,903	\$101,053	\$97,612	\$97,690	\$94,928
Cost of base (#8)	\$21,652	\$21,652	\$21,652	\$21,652	\$21,652	\$21,652	\$21,652	\$21,652
Cost of base (#53)	\$43,305	\$43,305	\$43,305	\$43,305	\$43,305	\$43,305	\$43,305	\$43,305
Total cost	\$155,118	\$152,053	\$150,039	\$148,860	\$166,011	\$162,569	\$162,647	\$159,885

paste (due to possibility of internal curing) and reduced risk of alkali-silica reaction (ASR) due to the absence of an active form of silica. The specific gravity of ACBFS is also lower than that of a typical natural aggregate, thus resulting in larger volume of concrete for the same weight. However, one should keep in mind that ACBFS has lower resistance to the abrasion compared to dolomite and that it contains calcium sulfide, which under certain conditions, can dissolve and release sulfide which, upon oxidizing in the pore solution, will convert to sulfate, thus increasing the potential for sulfate attack. Moreover, in some cases the leaching of sulfide from ACBFS particles was found to create intraparticle porosity, which may weaken the aggregate.

- Under the exposure conditions used in this study (i.e., FT and WD cycles in the presence of the deicers), the durability of pavement concrete was highly improved in cases when part of the portland cement was replaced by either fly ash, slag cement or combination of these materials. The observed improvement is attributed to reduction of the amount of calcium hydroxide present in the hydrated matrix (due to pozzolanic reaction) and

densification of the matrix by formation of additional C-S-H (also due to pozzolanic reaction). Both of these processes reduced the vulnerability of the matrix to chemical attack by chloride-based deicers. In addition, the use of slag cement reduces the total alkali content of the pore solution (especially at later ages), which is beneficial with respect to minimizing the potential for dissolution of calcium sulfide from ACBFS aggregate.

- In terms of their role in concrete deterioration, calcium chloride was found to be the most aggressive deicer, followed by magnesium chloride and then by sodium chloride.
- The mechanisms of deterioration of concrete exposed to CaCl_2 and NaCl deicers were found to be similar, specifically, in both cases the deicers reacted with calcium hydroxide which leads to deterioration of concrete matrix. This in turn, enables liquids to penetrate further into concrete matrix. However, the deterioration rate of CaCl_2 was found to be much faster than that of NaCl . The faster deterioration rate observed in the presence of CaCl_2 can be attributed to the formation of calcium oxychloride.

- Two most common concrete deterioration mechanisms triggered by the exposure of MgCl_2 involved its reaction with calcium hydroxide and C-S-H to produce CaCl_2 and M-S-H, respectively. Unlike C-S-H, M-S-H does not have binding capacity and thus reduces the strength of concrete.
- Statistical analysis has proven to be an effective tool in assessing the significance of several different variables (i.e., type of binder system, type of aggregate, type of deicer and exposure conditions) with respect to affecting concrete properties. Moreover, Tukey's multiple comparison method was found to be suitable for differentiating the impact of different levels within a specific factor.
- The benefit cost analysis has proven that air-cooled blast furnace slag (ABCFS) is economically feasible to be used as coarse aggregate in pavement concrete.

REFERENCES

- AASHTO T 22. (2011). *Standard method of test for compressive strength of cylindrical concrete specimens*. Washington, DC: American Association of State Highway and Transportation Officials.
- AASHTO T 97. (2011). *Flexural strength of concrete (using simple beam with third-point loading)*. Washington, DC: American Association of State Highway and Transportation Officials.
- ASTM C 33. (2011). *Standard specification for concrete aggregates*. West Conshohocken, PA: ASTM International.
- Chatterji, S. (1978). Mechanism of the CaCl_2 attack on portland cement concrete. *Cement and Concrete Research*, 8(4), 461–467. [https://doi.org/10.1016/0008-8846\(78\)90026-1](https://doi.org/10.1016/0008-8846(78)90026-1)
- Cement Sustainability Initiative (CSI). (2009). *Recycling concrete*. Conches-Geneva, Switzerland: World Business Council for Sustainable Development. Retrieved September 2015 from <http://www.wbcsdcement.org/pdf/CSI-RecyclingConcrete-Summary.pdf>
- Chemistry World. (2008, March). The concrete conundrum. *Chemistry World*. Retrieved September 2015 from http://www.rsc.org/images/Construction_tcm18-114530.pdf
- Chen, W. (2006). *Hydration of slag cement theory, modeling and application* (Doctoral dissertation). Enschede, Netherlands: University of Twente.
- Chen, C., Habert, G., Bouzidi, Y., & Jullien, A. (2010). Environmental impact of cement production: Detail of the different processes and cement plant variability evaluation. *Journal of Cleaner Production*, 18(5), 478–485. <https://doi.org/10.1016/j.jclepro.2009.12.014>
- Chesner, W., Collins, R., & Mackay, M. (1998). *User guidelines for waste and byproduct materials in pavement construction* (Publication No. FHWA-RD-97-148). Washington, DC: Federal Highway Administration.
- Collepardi, M. (2003). A state-of-the-art review on delayed ettringite attack on concrete. *Cement and Concrete Composites*, 25(4–5), 401–407. [https://doi.org/10.1016/S0958-9465\(02\)00080-X](https://doi.org/10.1016/S0958-9465(02)00080-X)
- Collepardi, M., Coppola, L., & Pistolesi, C. (1994). Durability of concrete structures exposed to CaCl_2 based deicing salts. *ACI Special Publication*, 145, 107–120.
- Crammond, N. J. (2002). The occurrence of thaumasite in modern construction—A review. *Cement and Concrete Composites*, 24(3–4), 393–402. [https://doi.org/10.1016/S0958-9465\(01\)00092-0](https://doi.org/10.1016/S0958-9465(01)00092-0)
- Crammond, N. J. (2003). The thaumasite form of sulfate attack in the UK. *Cement and Concrete Composites*, 25(8), 809–818. [https://doi.org/10.1016/S0958-9465\(03\)00106-9](https://doi.org/10.1016/S0958-9465(03)00106-9)
- Farnam, Y., Washington, T., & Weiss, J. (2015). The influence of calcium chloride salt solution on the transport properties of cementitious materials. *Advances in Civil Engineering*, 2015, 1–13. <https://doi.org/10.1155/2015/929864>
- Farnam, Y., Weise, A., Bentz, D., Davis, J., & Weiss, J. (2015). Damage development in cementitious materials exposed to magnesium chloride deicing salt. *Construction and Building Materials*, 93, 384–392. <https://doi.org/10.1016/j.conbuildmat.2015.06.004>
- Gaze, M. E., & Crammond, N. J. (2000). The formation of thaumasite in a cement:lime:sand mortar exposed to cold magnesium and potassium sulfate solutions. *Cement and Concrete Composites*, 22(3), 209–222. [https://doi.org/10.1016/S0958-9465\(00\)00002-0](https://doi.org/10.1016/S0958-9465(00)00002-0)
- Hale, W. M., Freyne, S. F., Bush, T. D., & Russell, B. W. (2008). Properties of concrete mixtures containing slag cement and fly ash for use in transportation structures. *Construction and Building Materials*, 22(9), 1990–2000. <https://doi.org/10.1016/j.conbuildmat.2007.07.004>
- Harnik, A., Meier, A. B., & Rosli, U. (1980). Combined influence of freezing and deicing salt on concrete—Physical aspects. In P. Sereda & G. Litvan (Eds.), *Durability of building materials and components* (STP691-EB; pp. 474–484). West Conshohocken, PA: ASTM International.
- Hobbs, D. W. (2001). Concrete deterioration: Causes, diagnosis, and minimising risk. *International Materials Reviews*, 46(3), 117–144. <https://doi.org/10.1179/095066001101528420>
- Hooton, R. D., Stanish, K., & Prusinski, J. (2004). The effect of ground, granulated blast furnace slag (slag cement) on the drying shrinkage of concrete—A critical review of the literature. In *Eighth CANMET/ACI International Conference on Fly Ash, Silica Fume, Slag and Natural Pozzolans in Concrete, supplementary papers volume*. Farmington Hills, MI: American Concrete Institute.
- Hudec, S. P., MacInnis, P. P., & McCann, C. (1994). Investigation of alternate concrete deicers. *ACI Special Publication*, 145, 65–84. <https://doi.org/10.14359/4541>
- IDOT. (2012). *Standard specifications for road and bridge construction*. Springfield, IL: Illinois Department of Transportation.
- Imbabi, M. S., Carrigan, C., & McKenna, S. (2012). Trends and development in green cement and technology. *International Journal of Sustainable Built Environment*, 1(2), 194–216. <http://doi.org/10.1016/j.ijse.2013.05.001>
- INDOT. (2010). *2010 standard specifications*. Indianapolis, IN: Indiana Department of Transportation.
- Janusz, A. (2010). *Investigation of deicing chemicals and their interactions with concrete materials* (Master's thesis). West Lafayette, IN: Purdue University.
- Juckes, L. M. (2002). Dicalcium silicate in blast-furnace slag: A critical review of the implications for aggregate stability. *Mineral Processing and Extractive Metallurgy*, 111(3), 120–128. <http://dx.doi.org/10.1179/037195502766647039>
- Jun-Yuan, H., Scheetz, B. E., & Roy, D. M. (1984). Hydration of fly ash-portland cement. *Cement and Concrete Research*, 14(4), 505–512. [https://doi.org/10.1016/0008-8846\(84\)90126-1](https://doi.org/10.1016/0008-8846(84)90126-1)
- KYTC. (2008). *Standard specification for road and bridge construction*. Lexington, KY: Kentucky Transportation Cabinet.
- Lee, H., Cody, R. D., Cody, A. M., & Spry, P. G. (2000). Effects of various deicing chemicals on pavement concrete deterioration. In *Proceedings of Mid-Continent*

- Transportation Symposium* (pp. 151–155). Ames, IA: Iowa State University.
- Man, Z. W., & Jing, B. A. H. (2012). Effect of ground granulated blast-furnace slag (GGBFS) and silica fume (SF) on chloride migration through concrete subjected to repeated loading. *Science China Technological Sciences*, 55(11), 3102–3108. <https://doi.org/10.1007/s11431-012-5027-y>
- Marchand, M., Sellevold, J., & Pigeon, E. J. (1994). The deicer salt scaling deterioration of concrete—An overview. *ACI Special Publication*, 145, 1–46.
- Mehta, P. K. (1983). Mechanism of sulfate attack on portland cement concrete—Another look. *Cement and Concrete Research*, 13(3), 401–406. [https://doi.org/10.1016/0008-8846\(83\)90040-6](https://doi.org/10.1016/0008-8846(83)90040-6)
- Montgomery, D. C. (2013). *Design and analysis of experiment* (8th ed.). New York, NY: John Wiley & Sons.
- Morian, D., Van Dam, T., & Perera, R. (2012). *Use of air-cooled blast furnace slag as coarse aggregate in concrete pavements* (Publication No. FHWA-HIF-12-008). Washington, DC: Federal Highway Administration. Retrieved from <https://www.fhwa.dot.gov/pavement/concrete/pubs/hif12008.pdf>
- OECD. (1997). *Recycling strategies for road works*. Paris, France: Organization for Economic Co-Operation and Development.
- PennDOT. (2000). *Pennsylvania Department of Transportation construction specifications*. Harrisburg, PA: Pennsylvania Department of Transportation.
- Peterson, K., Julio-Betancourt, G., Sutter, L., Hooton, R. D., & Johnston, D. (2008). *The deleterious chemical effects of concentrated deicing solutions on portland cement concrete*. Houghton, MI: Michigan Tech Transportation Institute.
- Peterson, K., Julio-Betancourt, G., Sutter, L., Hooton, R. D., & Johnston, D. (2013). Observations of Chloride Ingress and calcium oxychloride formation in laboratory concrete and mortar at 5°C. *Cement and Concrete Research*, 45, 79–90. <https://doi.org/10.1016/j.cemconres.2013.01.001>
- Portland Cement Association. (n.d.). How concrete is made. Retrieved September 2015 from <http://www.cement.org/cement-concrete-basics/how-concrete-is-made>
- Shi, C. (2001). Formation and stability of $3\text{CaO} \cdot \text{CaCl}_2 \cdot 12\text{H}_2\text{O}$. *Cement and Concrete Research*, 31(9), 1373–1375. [https://doi.org/10.1016/S0008-8846\(01\)00576-2](https://doi.org/10.1016/S0008-8846(01)00576-2)
- Solidia Technologies. (n.d.). Retrieved October 2015 from <http://solidiatech.com/>
- Sumsion, E. S., & Guthrie, W. S. (2013). *Physical and chemical effects of deicers on concrete pavement: Literature review* (Report No. UT-13.09). Salt Lake City, UT: Utah Department of Transportation, Research Division. Retrieved from <https://www.udot.utah.gov/main/uconowner.gf?n=8081525197623431>
- Sutter, L. (2005). Investigation of the long-term effects of magnesium chloride and other concentrated salt solutions on pavement and structural portland cement concrete: Phase I results. *Transportation Research Record*, 1979, 60–68. <https://doi.org/10.3141/1979-10>
- USGS. (2015, January). *U.S. Geological Survey, Mineral commodity summaries, January 2015*. Retrieved September 2015 from <http://minerals.usgs.gov/minerals/pubs/commodity/cement/mcs-2015-cemen.pdf>
- Verian, K. P. (2012). *Using recycled concrete as coarse aggregate in pavement concrete* (Master's thesis). West Lafayette, IN: Purdue University. Retrieved from <http://docs.lib.purdue.edu/dissertations/AAI1530423/>
- Verian, K. P., Panchmatia, P., Olek, J., & Nantung, T. (2015). Pavement concrete with air-cooled blast furnace slag as coarse aggregates: Effects of deicers and freeze-thaw cycles. *Transportation Research Record*, 2508, 55–64. <https://doi.org/10.3141/2508-07>
- Verian, K. P., Whiting, N. M., Olek, J., Jain, J., & Snyder, M. B. (2013). *Using recycled concrete as aggregate in concrete pavements to reduce materials Cost* (Joint Transportation Research Program Publication No. FHWA/IN/JTRP-2013/18). West Lafayette, IN: Purdue University. <https://doi.org/10.5703/1288284315220>

APPENDIX A. MECHANISMS OF DEICERS DETERIORATION ON PAVEMENT CONCRETE

A.1 Physical Deterioration

During freezing and thawing cycles, concrete experiences expansion and internal stress which lead to scaling and internal micro-cracking (Chatterji, 1978; Collepari, Coppola, & Pistolesi, 1994; Harnik, Meier, & Rosli, 1980; Hudec, MacInnis, & McCann, 1994; Janusz, 2010; Marchand, Sellevold, & Pigeon, 1980; Sutter, 2005). Several different physical mechanisms of deterioration have been introduced to explain the development of the pressure within the pore system during freezing and thawing cycles but it is still not clear which one is dominantly found from all experiment from the literature (Janusz, 2010).

Hydraulic Pressure Theory

This theory was proposed by Powers in 1949 (as described by Marchand et al., 1994). According to this theory, when the temperature of saturated cement paste drops below 0°C, ice crystals begin to form in larger capillaries. The formation of ice crystals results in about 9% of volume increase and forces the unfrozen pore water to escape from the larger capillaries into the surrounding paste. This generates an internal stress which, if not accommodated by sufficient air voids system, can lead to the freeze/thaw damage of concrete matrix (Harnik et al., 1980; Sumsion & Guthrie, 2013).

Osmotic Pressure Theory

Based on this theory, only pure water freezes in the larger capillaries, with a more concentrated solution remaining in the smaller pores. In order to maintain a thermodynamic equilibrium, unfrozen water from the smaller pores migrates to the larger pores causing growth of ice crystals and increasing pressure in the pore structure (Harnik et al., 1980; Sumsion & Guthrie, 2013).

Thermal Shock

Proposed by Harnik et al. (1980), this theory stated that heat required for melting of ice and snow is extracted mostly from the concrete when thawing takes place. Because of the great loss of heat, the temperature of the surface (usually only a few millimeters below the surface) rapidly decreases causing thermal shock (OECD, 1997; PennDOT, 2000).

Layer by Layer Deterioration

According to this theory, stress is created because of a different concentration of salt solutions between layers. The concentration of deicers in the layer underneath the surface is much higher than that near the

surface and achieves its maximum depth around 10 mm. In this layer, freezing practically does not occur. A different situation exists in the outer layer, which contains a low concentration of deicing salts. This is due to washing out of the salts caused by precipitation such as rain. In fact, as the temperature of the concrete pavement surface drops below 0°C, ice crystals can form in the outer layer. Variable deformations of the different layers cause stress, which leads to the concrete cracking (Hobbs, 2001; Marchand et al., 1994).

Growth of the Salt Crystals

The growth of salt crystals occurs when the solution in the larger pore reaches a supersaturated state (Hobbs, 2001). It is commonly known that application of salts increases the degree of concrete saturation (Farnam, Washington, & Weiss, 2015; Farnam, Weise, Bentz, Davis, & Weiss, 2015). The formation of salt crystals starts in the largest pores when the solution reaches super saturation. Then, salt molecules are drawn out of the smaller pores into the larger pores leading to the growth of crystallization pressure. This mechanism is most prominent in case of surface scaling failure (Marchand et al., 1994).

Supercooling

Harnik et al. (1980) asserted that super cooling is the result of freeze/thaw cycles and the presence of sodium chloride, which reduces the freezing point of water in the concrete pores. Thus, at a temperature near 0°C, water does not freeze, resulting in a decrease in the hydraulic pressure. However, when water finally starts freezing (i.e., with no chlorides present), the rate of freezing is much higher than with normal freezing, inducing a greater magnitude of hydraulic pressure and destructive effect. In addition, a higher osmotic pressure occurs during and after freezing when sodium chloride is present in the pore solution (Harnik et al., 1980; Sutter, 2005).

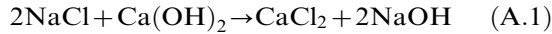
A.2 Chemical Deterioration

The salt that ingresses into concrete matrix may react with various products of cement hydration resulting in either the deterioration of the matrix or loss of corrosion protection of steel reinforcement. The role of three different deicers: calcium chloride (CaCl_2), magnesium chloride (MgCl_2) and sodium chloride (NaCl) on chemical changes observed in hydrated cement matrix are described below.

Effects of Sodium Chloride (NaCl) on Concrete Properties

It is commonly known that long-term application of NaCl leads to the removal of calcium hydroxide

(Ca(OH)₂) according to the Equation A.1 (Janusz, 2010) below.



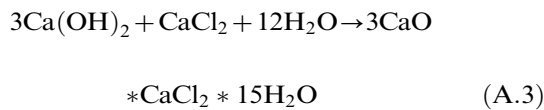
The removal of Ca(OH)₂ increases the porosity near the exposed surface. Moreover, the product of this reaction, calcium chloride, can interact with the aluminate phases (C₃A) present in the cement paste and form chloroaluminate crystals (Equation A.2; Chatterji, 1978; Collepardi et al., 1994).



Formation chloroaluminate crystals can affect the long-term frost durability on concrete surfaces in service (Marchand et al., 1994).

Effects of Calcium Chloride (CaCl₂) on Concrete Properties

Concrete deterioration due to CaCl₂ exposure was reported to be related with formation of 3CaO.CaCl₂.12H₂O, which is an unstable complex salt (Farnam, Washington, et al., 2015; Farnam, Weise, et al., 2015). Another form of the complex salt which is known for its destructive effect is known as calcium oxychloride (Collepardi et al., 1994) which formation is presented in Equation A.3. It is reported that calcium oxychloride forms at room temperature when for CaCl₂ concentration above 12% by mass in the solution (Farnam, Washington, et al., 2015). Other studies have reported that calcium oxychloride can form at temperature above water's freezing point and it's unstable at room temperature and low level of relative humidity (Farnam, Weise, et al., 2015; Shi, 2001).

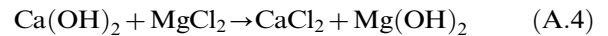


Since calcium hydroxide comprises 20%–25% of the volume of the hydration product in concrete matrix (Sumsion & Guthrie, 2013), the consumption of

calcium hydroxide promotes a more porous concrete microstructure (Lee, Cody, Cody, & Spry, 2000). As the presence of calcium hydroxide is a prerequisite to oxychloride formation, the use of fly ash and slag cement as partial cement replacement helps to mitigate the formation of oxychloride as those cementitious materials convert Ca(OH)₂ into additional C-S-H.


Effects of Magnesium Chloride (MgCl₂) on Concrete Properties

Magnesium chloride was also found to contribute to concrete deteriorations. The most dominant deterioration effect associated with the exposure of concrete to MgCl₂ is the formation of calcium chloride (CaCl₂) and magnesium silicate hydrate (M-S-H) by reaction with calcium hydroxide and calcium silicate hydrate (C-S-H) (Farnam, Washington, et al., 2015; Janusz, 2010; Lee et al., 2000; Peterson, Julio-Betancourt, Sutter, Hooton, & Johnston, 2008; Peterson, Julio-Betancourt, Sutter, Hooton, & Johnston, 2013; Verian et al., 2015). The formation of aforementioned components through chemical reaction of MgCl₂ with the hydration products is shown in Equation A.4 and Equation A.5, respectively.



The formation of brucite (Mg(OH)₂) usually takes place near the surface of concrete specimen which exposed to MgCl₂ deicer (Farnam, Washington, et al., 2015; Peterson et al. 2008; 2013). Brucite has been reported to slow down concrete deterioration by hindering ingress of chloride solution into the concrete due to its dense and homogeneous nature (Farnam, Washington, et al., 2015; Peterson et al. 2008; 2013). The formation of non-cementitious M-S-H through the dissolution of C-S-H produced significant concrete crumbling due to the loss of binding capacity of the matrix. The formation of CaCl₂ (as shown in Equation A.4) will ultimately lead to its reaction with Ca(OH)₂ and thus formation of oxychloride (as shown in Equation A.5).

APPENDIX B. MILL CERTIFICATES



BUZZI UNICEM USA
 PO Box 482-Greencastle, IN 46135-(765) 653-9766

This is to certify that **Type I** meets ASTM C-150 Specifications for Portland Cement and CSA A3000.

Chemical Data		Physical Data	
ASTM C114		ASTM C185	
Silicon Dioxide (SiO ₂)	18.94	Air Entrained (%)	9.8
Aluminum Oxide (Al ₂ O ₃)	5.65	ASTM C204	
Ferric Oxide (Fe ₂ O ₃)	3.29	Fineness (cm ² /gm)	3750
Calcium Oxide (CaO)	63.20	ASTM C151	
Magnesium Oxide (MgO)	3.13	Autoclave Expansion (%)	0.082
Sulfur Trioxide (SO ₃)	3.43	Compressive Strength, PSI	
Loss on Ignition	1.13	ASTM C109 Mortar Cubes	
Sodium Oxide	0.34	1-Day	2790
Potassium Oxide	0.78	3-Day	4060
Insoluble Residue	0.35	7-Day	4690
Total Alkali as Na ₂ O	0.86	28-Day	
POTENTIAL COMPOUND COMPOSITION		ASTM C191	
		Setting Time:	
Tricalcium Silicate (C ₃ S)	61	Vicat	
Dicalcium Silicate (C ₂ S)	8	Initial, Min.	112
Tricalcium Aluminate (C ₃ A)	9	Final, Min.	225
Tricalcium Aluminoferrite (C ₄ AF)	10		

Silo	Bill of Lading	Tons	Date	Silo	Bill of Lading	Tons	Date
							11/19/2010

STATE OF INDIANA)
 COUNTY OF PUTNAM)
 Before me the undersigned, a Notary Public for Putnam County,
 State of Indiana personally appeared John J. Wachal and acknowledged
 the execution of the foregoing instrument this 18th day of November 2010.

Philip A. Clodfelter, Notary Public
 My commission expires May 8, 2015.

To:

John J. Wachal

John J. Wachal
 Quality Manager

Figure B.1 Cement mill certificate used in this study.

Analytical Testing Service Laboratories, Inc.
P.O. Box 1118, Joplin, Missouri 64802
(417) 782-6573

Headwaters Resources, Inc
P.O. Box 3734
Alpharetta, GA 30023
1-770-475-8095

February 02, 2010

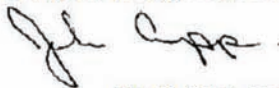
Attn: Carolyn Grant

Re: 9747- Schahfer 15 Fly Ash Sample 2000 Ton Composite - 12/1-31/09

	ASTM C-618 Class "C" <u>Requirements</u>	<u>Actual</u>
Fineness (+325 Mesh)	34% Max	11.00%
Moisture Content	3% Max	0.12%
Specific Gravity	****	2.62
Specific Gravity Variation	5% Max	0.73%
Loss on Ignition	6% Max	0.37%
Soundness	0.8% Max	0.01%
S.A.I., 7 Days	75% Min	97.20%
S.A.I., 28 Days	75% Min	101.80%
Water Req. % Control	105% Max	93.40%
Silica SiO ₂	****	36.90%
Aluminum Oxide Al ₂ O ₃	****	20.14%
Ferric Oxide Fe ₂ O ₃	****	7.01%
Total	50% Min	64.05%
Sulfur Trioxide SO ₃	5% Max	1.58%
Calcium Oxide CaO	****	24.60%
Magnesium Oxide MgO	****	5.47%
Available Alkalies as Na ₂ O	****	1.21%

We certify the above was tested in accordance with ASTM C-618 and AASHTO M295

Analytical Testing Service Laboratories, Inc.



John K. Cupp, Manager

Figure B.2 Class C fly ash certificate from the producer.

MATERIAL SAFETY DATA SHEET

TRADE NAME: Blast Furnace Slag

SYNONYMS: Air Cooled, ACBF, BF Slag

I. PRODUCT AND COMPONENT DATA

Component(s):	CAS Registry	% (Approx.)	ACGIH TLV-TWA
Blast Furnace Slag	65996-69-2	100	None Known

Composition of BF Slag Normal Range

SiO₂: 32 - 42%
Al₂O₃: 7 - 11%
CaO: 35 - 45%
MgO: 7 - 15%
FeO: 0.1 - 0.7%
S: 1.0 - 2.5%

These constituents usually exist as an isomorphous mixture with the following general formula: $\text{Ca}_2(\text{MgFeAl})(\text{SiAl})_2\text{O}_7$

This formula represents the melilite mineral series.

Some of the constituents may also occur as separate compounds such as those listed below:
CaCO₃, CaS, Fe, Fe₂O₃, CaSO₄ · 2H₂O

II. PHYSICAL DATA

SOLUBILITY: CaS, CaCO₃

FLASH POINT: None

STABILITY: Stable

FLAMMABLE LIMITS: None

SPECIFIC GRAVITY: 2.3-2.4 Air Cooled

APPEARANCE & ODOR: Grayish, vesicular, stony material, may have slight sulfurous odor when exposed to heat greater than 200 degrees F.

Figure B.3 Slag aggregate mill certificate.

APPENDIX C. TEST RESULTS

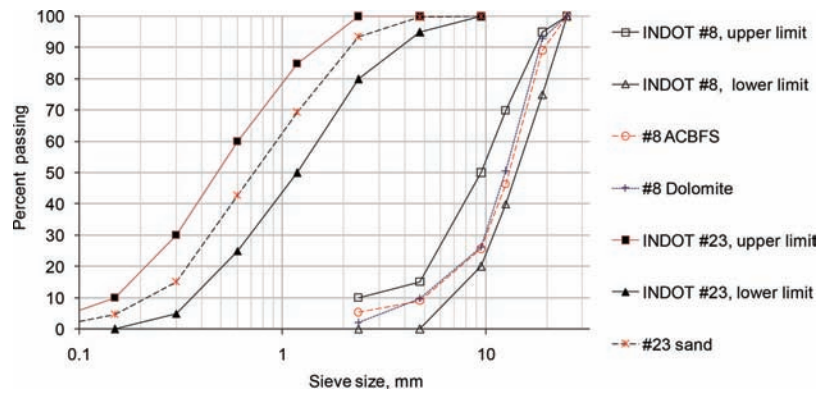


Figure C.1 Aggregate gradation curves.

TABLE C.1
Compressive strength of different mixtures at 28 days and after the conclusion of exposure condition.

Exposure condition	Deicers	Average compressive strength (psi)							
		M1-1PC-ACBFS (plain - slag aggregate)	M2-.8PC.2FA-ACBFS (fly ash - slag aggregate)	M3-.75PC.25SC-ACBFS (slag cement - slag aggregate)	M4-.6PC.17FA.23SC-ACBFS (fly ash + slag cement - slag aggregate)	M5-1PC-NA (plain - dolomite)	M6-.8PC.2FA-NA (fly ash - dolomite)	M7-.75PC.25SC-NA (slag cement - dolomite)	M8-.6PC.17FA.23SC-NA (fly ash + slag cement - dolomite)
Freezing-thawing (FT)	CaCl ₂	3780	4900	6810	6898	3588	4223	5830	5930
	MgCl ₂	4010	6380	6693	6595	5410	5723	5970	5843
	NaCl	6255	6165	7255	6763	5533	5800	6040	6293
Wetting-drying (WD)	DST (distilled water)	7323	6618	6958	6978	5910	6048	5703	6243
	CaCl ₂	3538	5213	4485	5478	6065	5865	8178	6905
	MgCl ₂	5300	5573	4830	5568	6860	5935	8225	6568
Moist cured	NaCl	4943	6208	4625	5443	7055	5928	8170	6728
	DST (distilled water)	5253	5158	5078	5823	7810	5728	8033	7365
	Control 2 (C2)	6243	6998	6825	6988	6325	6569	7380	6480
	Control 1 (C1)	5488	5655	7740	7415	5160	5374	6739	6525

Notes:

Freezing-thawing (FT):

- Specimens of M1-CaCl₂-FT failed after 111 FT cycles, the other M1 specimens were tested after 347 FT cycles.
- Specimens of M5-CaCl₂-FT failed after 151 FT cycles, the other M5 specimens were tested after 350 FT cycles.
- Specimens of M2 and M6 were tested after 347 and 350 FT cycles, respectively.
- Specimens of M3 and M4 were tested after 191 FT cycles.
- Specimens of M7 and M8 were test after 172 FT cycles

Wetting-drying (WD):

- Specimens of M1, M2, M5 and M6 were test after 286 WD cycles.
- Specimens of M3, M4, M7 and M8 were test after 226 WD cycles.

Control C1: compressive strength of specimens after 28 days of moist cured.

Control C2: compressive strength of moist cured specimens and tested either at the end of the exposure period for given exposure condition (i.e., deicer + environmental cycling combination) or when the corresponding beams failed.

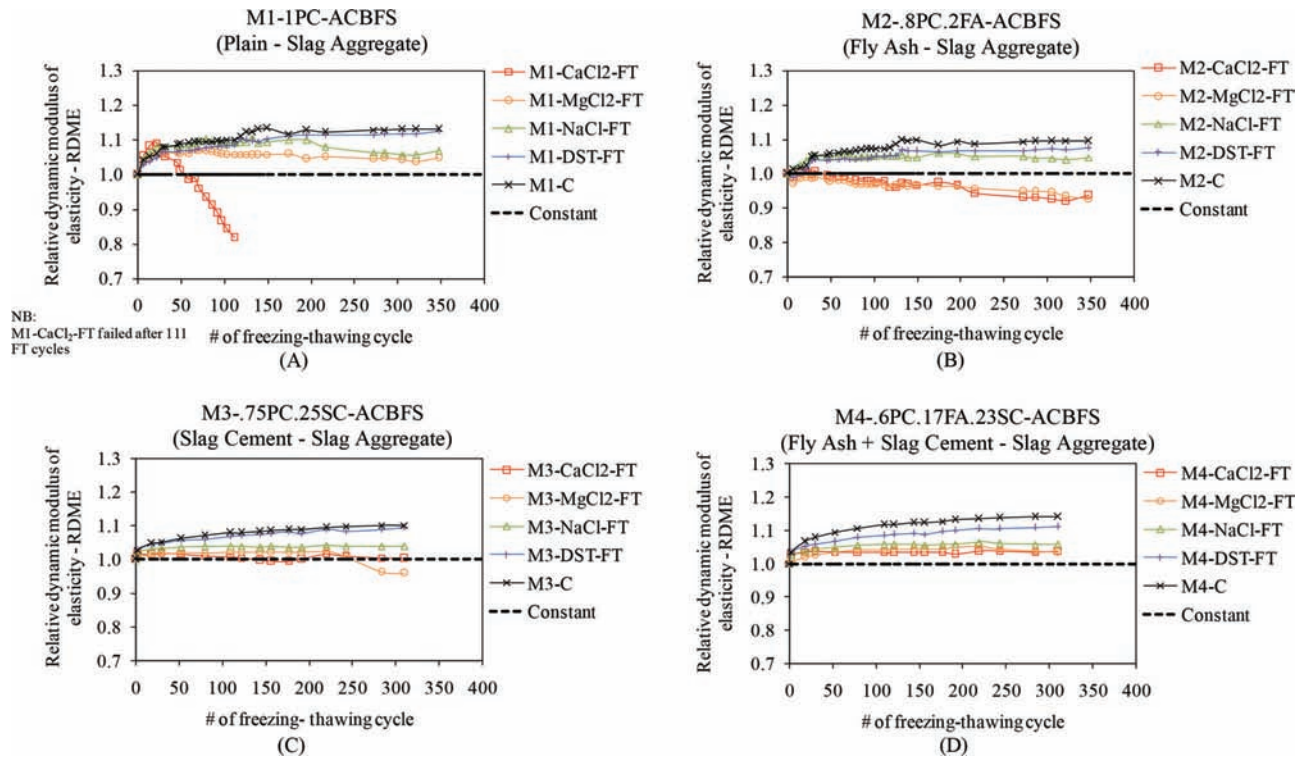


Figure C.2 Relative dynamic modulus of elasticity (RDME) of control specimens (C2) and specimens exposed to different deicers under freezing-thawing (FT) cycles; (A) M1, (B) M2, (C) M3 and (D) M4.

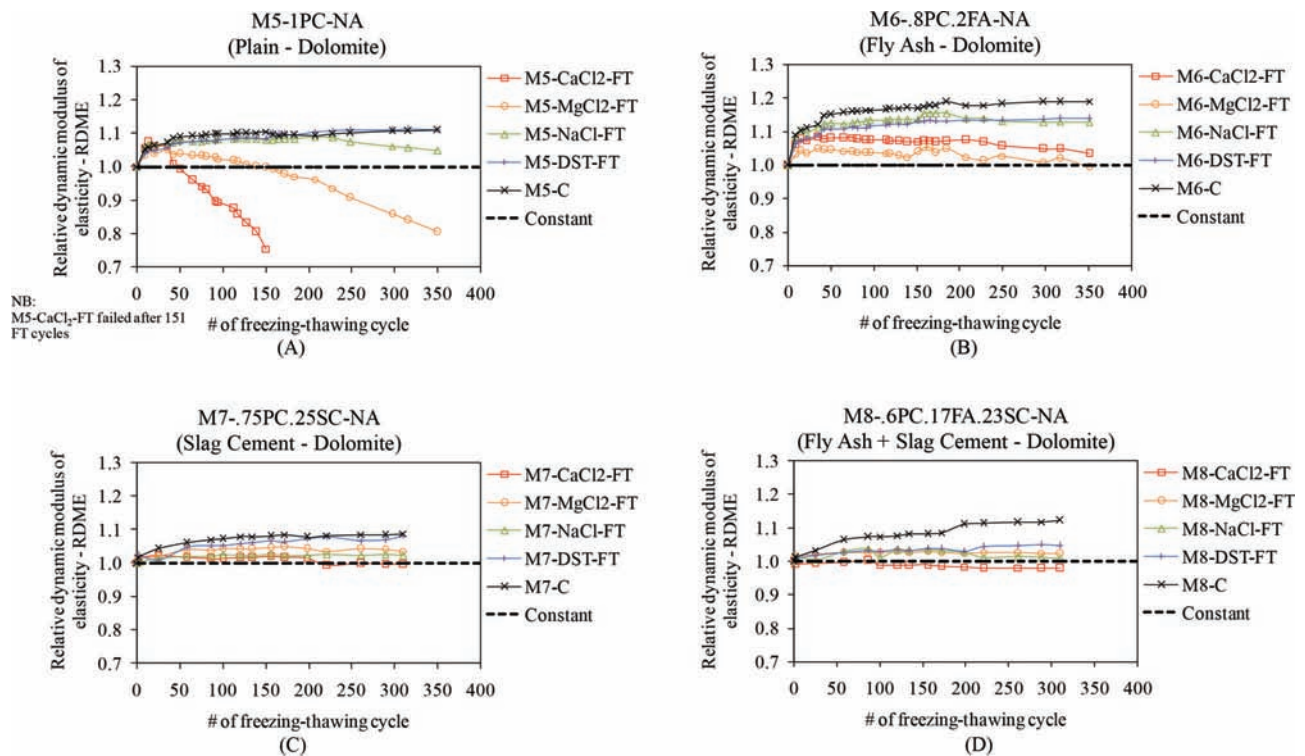


Figure C.3 Relative dynamic modulus of elasticity (RDME) of control specimens (C2) and specimens exposed to different deicers under freezing-thawing (FT) cycles; (A) M5, (B) M6, (C) M7 and (D) M8.

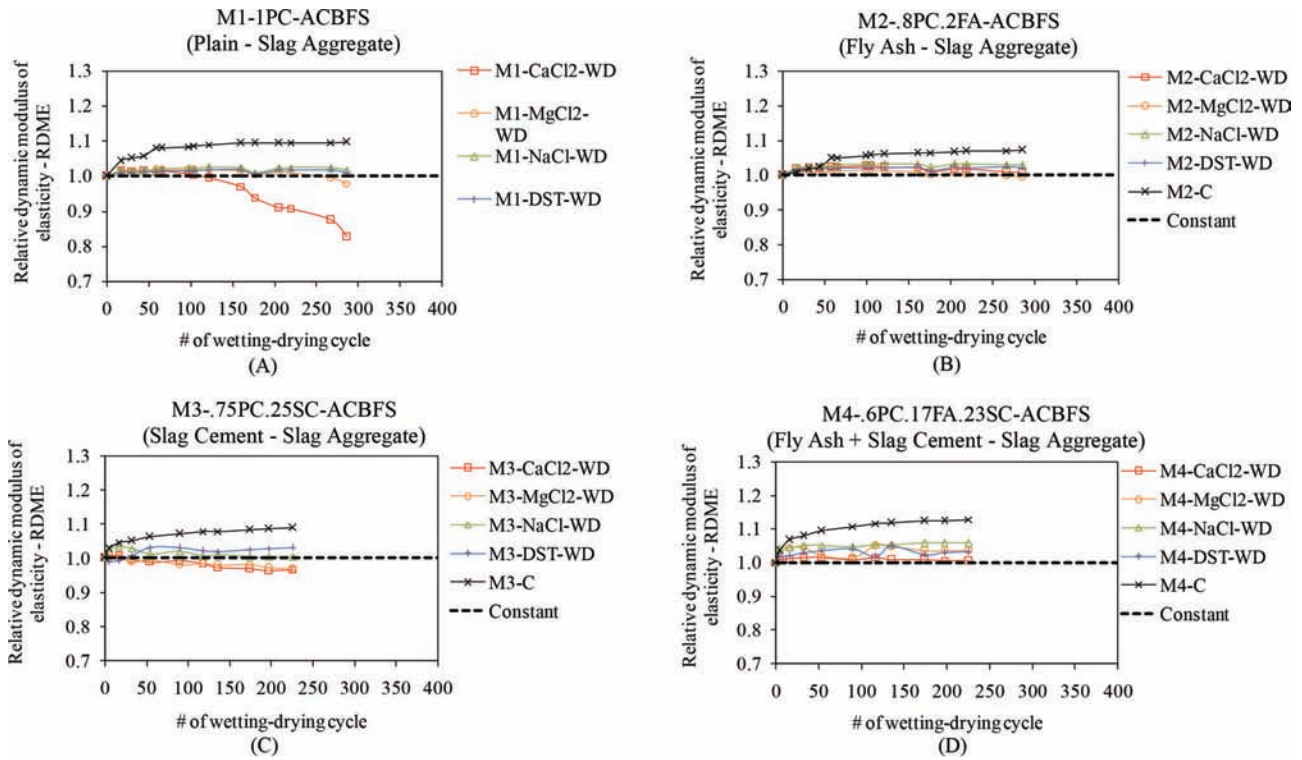


Figure C.4 Relative dynamic modulus of elasticity (RDME) of control specimens (C2) and specimens exposed to different deicers under wetting-drying (WD) cycles; (A) M1, (B) M2, (C) M3 and (D) M4.

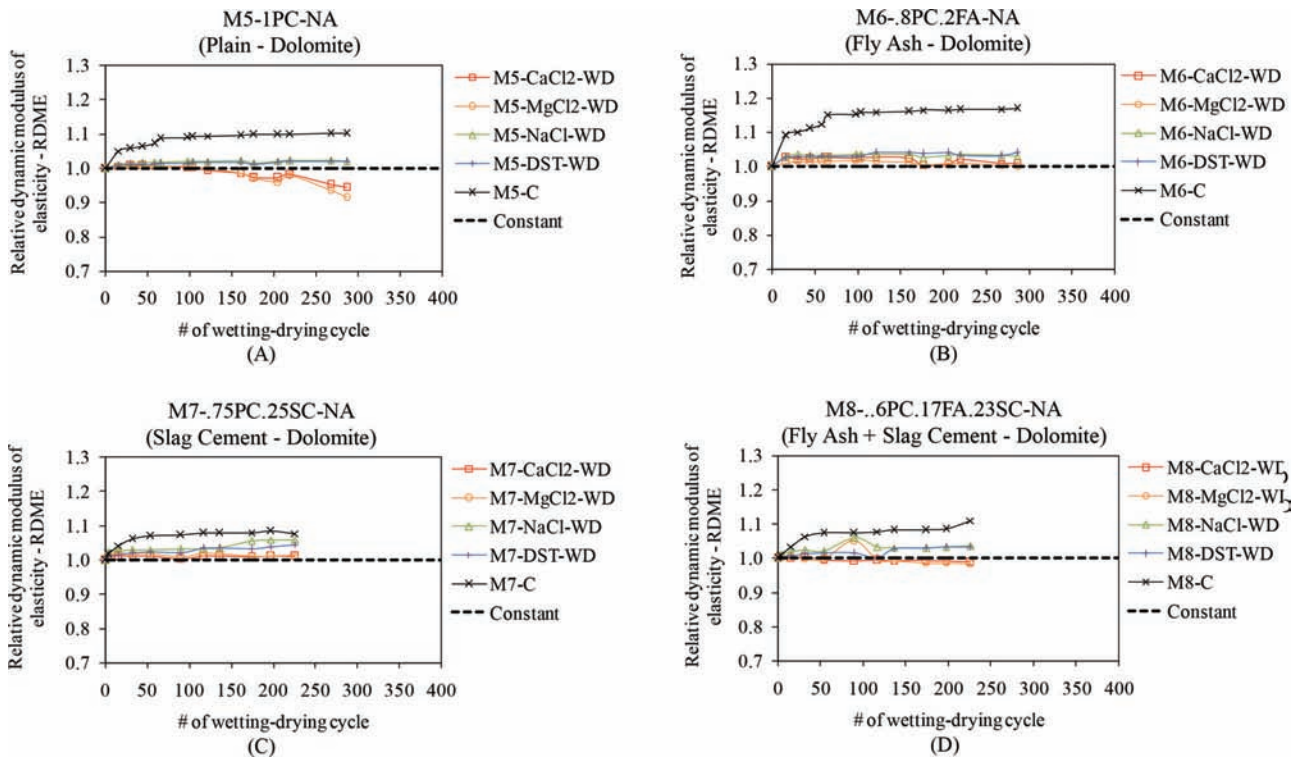


Figure C.5 Relative dynamic modulus of elasticity (RDME) of control specimens (C2) and specimens exposed to different deicers under wetting-drying (WD) cycles; (A) M5, (B) M6, (C) M7 and (D) M8.

TABLE C.2
Chloride penetration depth measurement of different concretes under freezing-thawing (FT) and wetting-drying (WD) condition.

Exposure condition	Deicers	Average chloride penetration depth (mm)							
		M1-1PC-ACBFS (plain - ACBFS)	M2-.8PC.2FA-ACBFS (fly ash - ACBFS)	M3-.75PC.25SC-ACBFS (slag cement - ACBFS)	M4-.17FA.23SC.6PC-ACBFS (ternary - ACBFS)	M5-1PC-NA (plain - dolomite)	M6-.8PC.2FA-NA (fly ash - dolomite)	M7-.75PC.25SC-NA (slag cement - dolomite)	M8-.17FA.23SC.6PC-NA (ternary - dolomite)
Freezing-thawing (FT)	NaCl	19.2	17.8	13.7	13.8	20.0	16.6	13.9	11.8
	CaCl ₂	17.4	12.4	12.9	14.5	19.8	10.5	11.8	13.0
	MgCl ₂	8.4	4.9	8.3	9.3	16.1	5.0	10.6	6.6
Wetting-drying (WD)	NaCl	21.6	19.4	14.6	21.9	16.8	21.6	16.5	18.2
	CaCl ₂	23.3	12.5	14.3	14.3	17.7	15.2	13.6	12.3
	MgCl ₂	10.6	14.1	12.2	12.0	10.5	13.7	12.3	13.1

Notes:

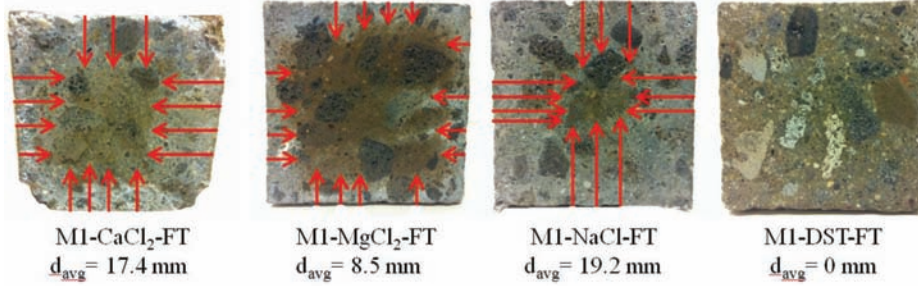
Freezing-thawing (FT):

- Specimens of M1-CaCl₂-FT failed after 111 FT cycles, the other M1 specimens were tested after 347 FT cycles.
- Specimens of M5-CaCl₂-FT failed after 151 FT cycles, the other M5 specimens were tested after 350 FT cycles.
- Specimens of M2 and M6 were tested after 347 and 350 FT cycles, respectively.
- Specimens of M3 and M4 were tested after 191 FT cycles.
- Specimens of M7 and M8 were test after 172 FT cycles

Wetting-drying (WD):

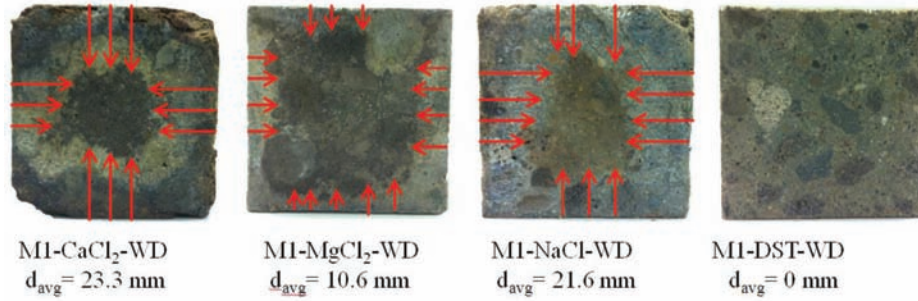
- Specimens of M1, M2, M5 and M6 were test after 286 WD cycles.
- Specimens of M3, M4, M7 and M8 were test after 226 WD cycles.

M1-IPC-ACBFS (Plain – ACBFS) – Freezing & Thawing (FT)



(A)

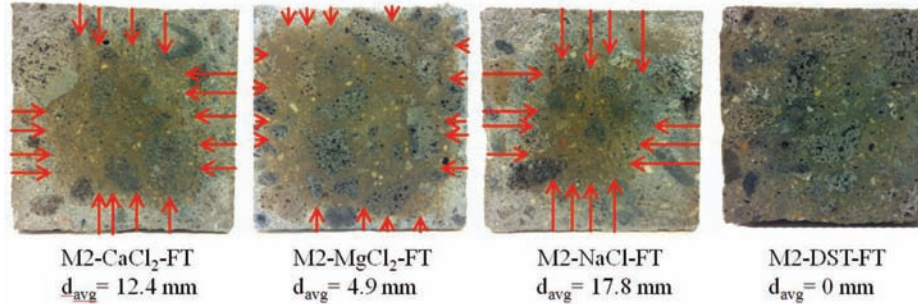
M1-IPC-ACBFS (Plain – ACBFS) – Wetting & Drying (WD)



(B)

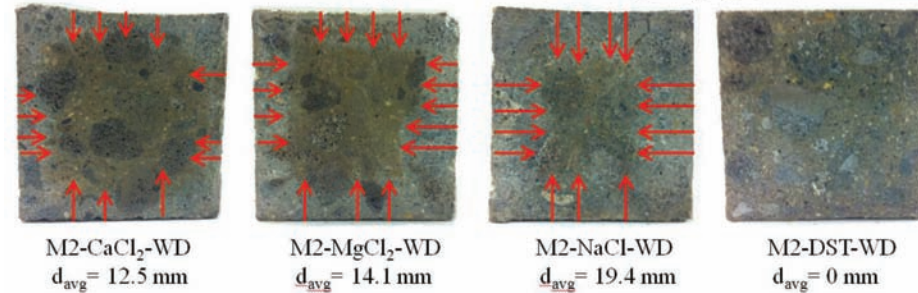
Figure C.6 Chloride penetration depths associated with different deicers in M1-IPC-ACBFS (plain-ACBFS) specimens after: (A) 347 FT cycles and (B) 286 WD cycles.

M2-8PC.2FA-ACBFS (Fly Ash – ACBFS) – Freezing & Thawing (FT)



(A)

M2-8PC.2FA-ACBFS (Fly Ash – ACBFS) – Wetting & Drying (WD)



(B)

Figure C.7 Chloride penetration depths associated with different deicers in M2-.2FA.8PC-ACBFS (fly ash-ACBFS) specimens after: (A) 347 FT cycles and (B) 286 WD cycles.

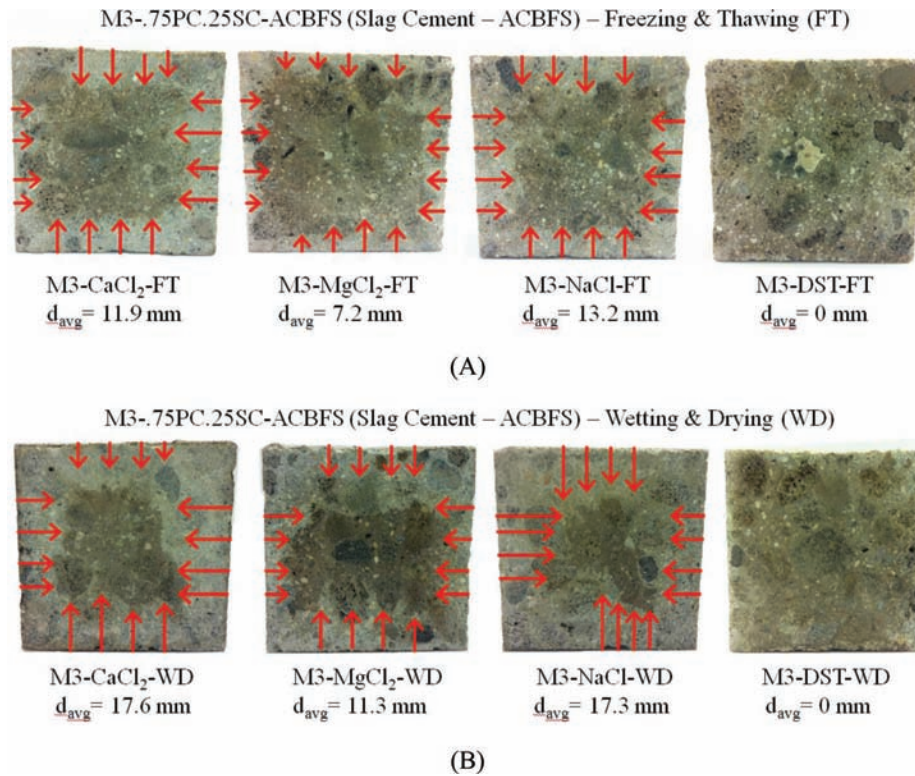


Figure C.8 Chloride penetration depths associated with different deicers in M3-.25SC.75PC-ACBFS (slag cement-ACBFS) specimens after: (A) 310 FT cycles and (B) 226 WD cycles.

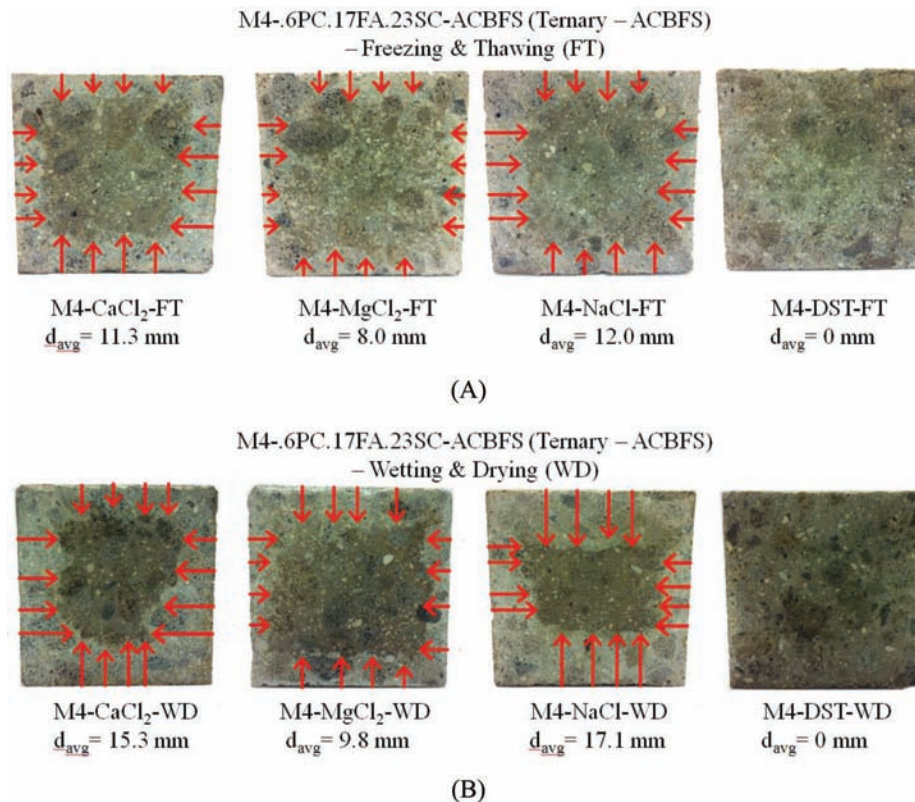


Figure C.9 Chloride penetration depths associated with different deicers in M4-.17FA.23SC.6PC-ACBFS (ternary-ACBFS) specimens after: (A) 310 FT cycles and (B) 226 WD cycles.

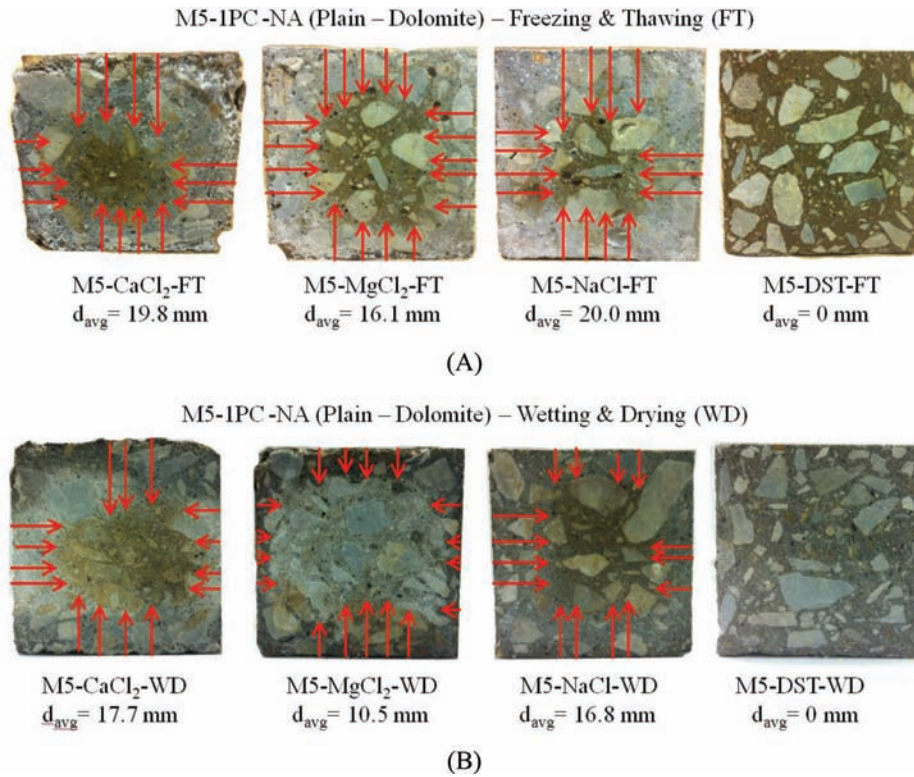


Figure C.10 Chloride penetration depths associated with different deicers in M1-1PC-NA (plain-dolomite) specimens after: (A) 350 FT cycles and (B) 286 WD cycles.

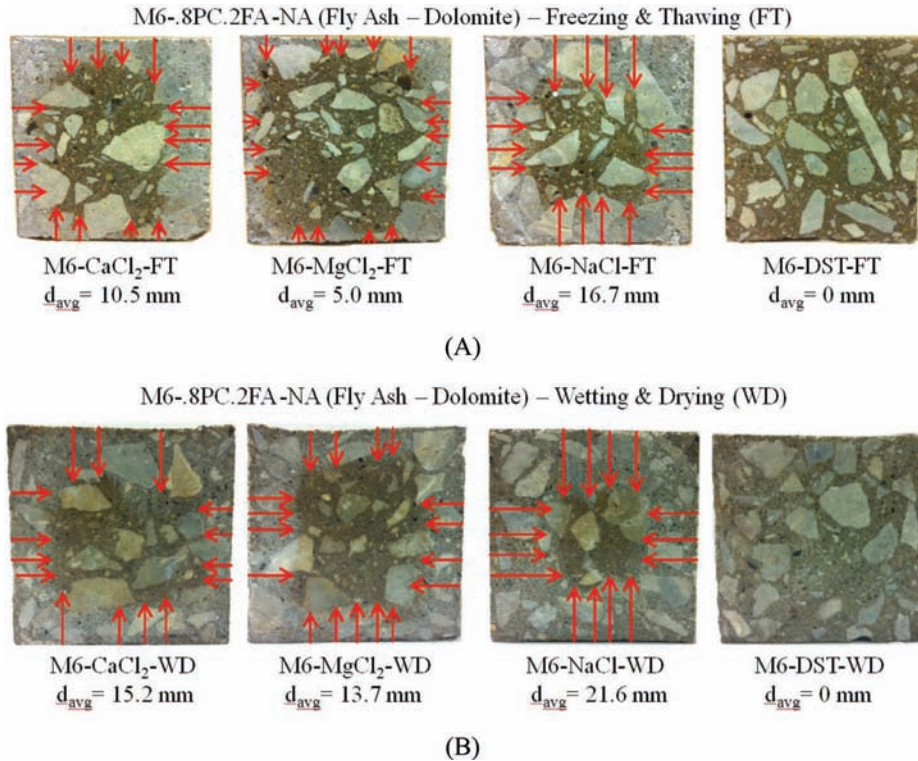


Figure C.11 Chloride penetration depths associated with different deicers in M6-.2FA.8PC-NA (fly ash-dolomite) specimens after: (A) 350 FT cycles and (B) 286 WD cycles.

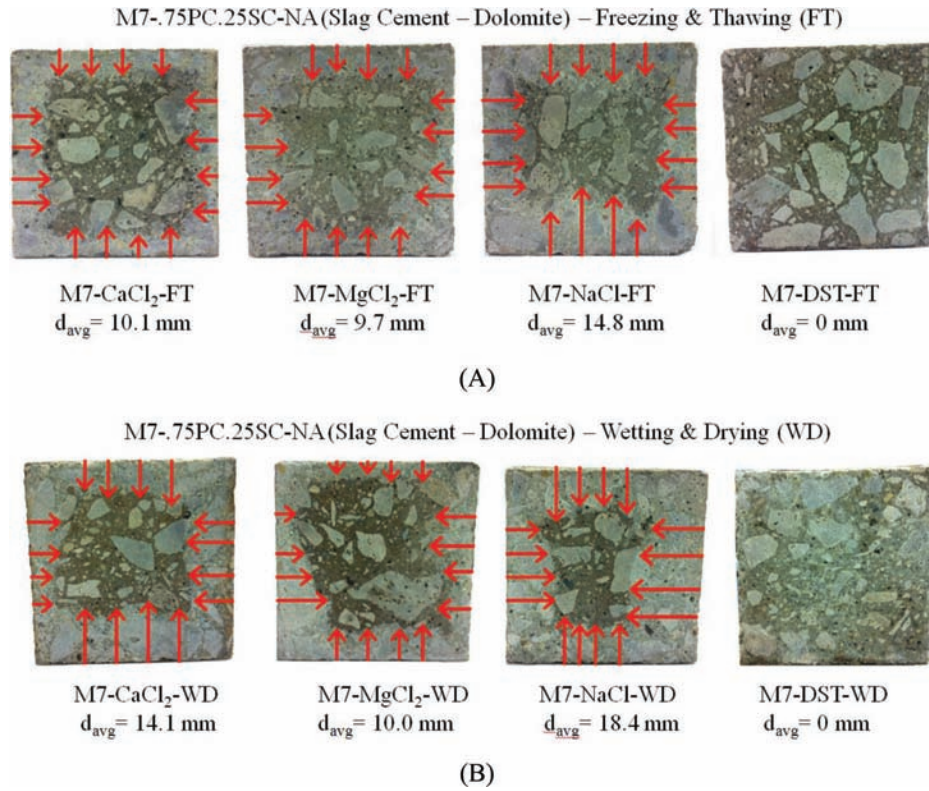


Figure C.12 Chloride penetration depths associated with different deicers in M7-.25SC.75PC-NA (slag cement-dolomite) specimens after: (A) 310 FT cycles and (B) 226 WD cycles.

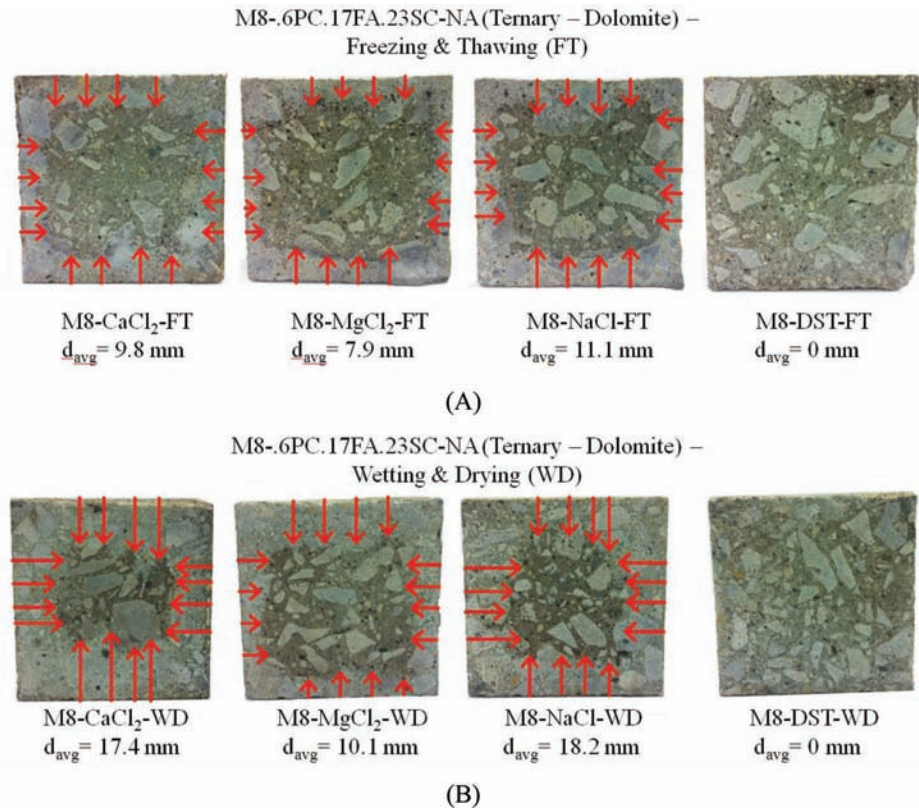


Figure C.13 Chloride penetration depths associated with different deicers in M8-.17FA.23SC.6PC-NA (ternary-dolomite) specimens after: (A) 310 FT cycles and (B) 226 WD cycles.



Figure C.14 Physical changes in the appearance of the representative sample of M1-1PC-ACBFS (plain-ACBFS) concrete specimens exposed to CaCl_2 after (from left to right) 35, 59 and 102 FT cycles.



Figure C.15 Physical changes in the appearance of the representative sample of M1-1PC-ACBFS (plain-ACBFS) concrete specimens exposed to MgCl_2 after (from left to right) 35, 59, 102 and 347 FT cycles.



Figure C.16 Physical changes in the appearance of the representative sample of M1-1PC-ACBFS (plain-ACBFS) concrete specimens exposed to NaCl after (from left to right) 35, 59, 102 and 347 FT cycles.



Figure C.17 Physical changes in the appearance of the representative sample of M1-1PC-ACBFS (plain-ACBFS) concrete specimens exposed to distilled water (DST) after (from left to right) 35, 59, 102 and 347 FT cycles.



Figure C.18 Physical changes in the appearance of the representative sample of M2-.2FA.8PC-ACBFS (fly ash-ACBFS) concrete specimens exposed to CaCl_2 after (from left to right) 35, 59, 102 and 347 FT cycles.



Figure C.19 Physical changes in the appearance of the representative sample of M2-.2FA.8PC-ACBFS (fly ash-ACBFS) concrete specimens exposed to $MgCl_2$ after (from left to right) 35, 59, 102 and 347 FT cycles.



Figure C.20 Physical changes in the appearance of the representative sample of M2-.2FA.8PC-ACBFS (fly ash-ACBFS) concrete specimens exposed to $NaCl$ after (from left to right) 35, 59, 102 and 347 FT cycles.



Figure C.21 Physical changes in the appearance of the representative sample of M2-.2FA.8PC-ACBFS (fly ash-ACBFS) concrete specimens exposed to distilled water (DST) after (from left to right) 35, 59, 102 and 347 FT cycles.



Figure C.22 Physical changes in the appearance of the representative sample of M3-.25SC.75PC-ACBFS (slag cement-ACBFS) concrete specimens exposed to $CaCl_2$ after (from left to right) 18, 191 and 310 FT cycles.

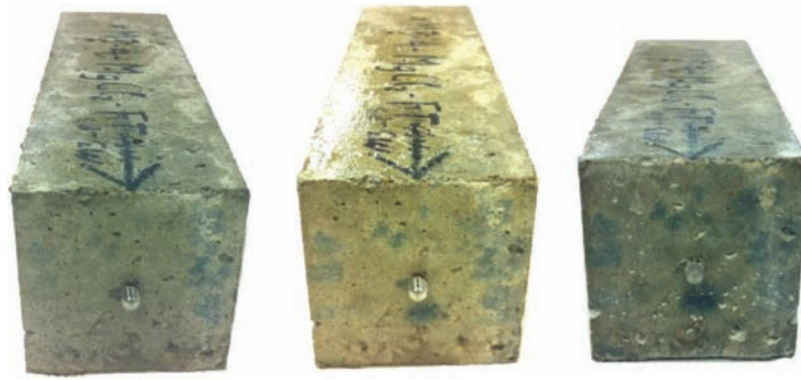


Figure C.23 Physical changes in the appearance of the representative sample of M3-.25SC.75PC-ACBFS (slag cement-ACBFS) concrete specimens exposed to $MgCl_2$ after (from left to right) 18, 191 and 310 FT cycles.



Figure C.24 Physical changes in the appearance of the representative sample of M3-.25SC.75PC-ACBFS (slag cement-ACBFS) concrete specimens exposed to $NaCl$ after (from left to right) 18, 191 and 310 FT cycles.

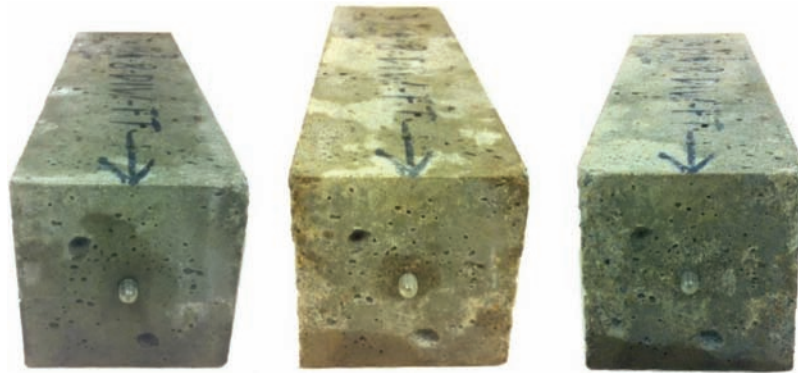


Figure C.25 Physical changes in the appearance of the representative sample of M3-.25SC.75PC-ACBFS (slag cement-ACBFS) concrete specimens exposed to distilled water (DST) after (from left to right) 18, 191 and 310 FT cycles.



Figure C.26 Physical changes in the appearance of the representative sample of M4-.17FA.23SC.6PC-ACBFS (ternary-ACBFS) concrete specimens exposed to CaCl_2 after (from left to right) 18, 191 and 310 FT cycles.



Figure C.27 Physical changes in the appearance of the representative sample of M4-.17FA.23SC.6PC-ACBFS (ternary-ACBFS) concrete specimens exposed to MgCl_2 after (from left to right) 18, 191 and 310 FT cycles.



Figure C.28 Physical changes in the appearance of the representative sample of M4-.17FA.23SC.6PC-ACBFS (ternary-ACBFS) concrete specimens exposed to NaCl after (from left to right) 18, 191 and 310 FT cycles.



Figure C.29 Physical changes in the appearance of the representative sample of M4-.17FA.23SC.6PC-ACBFS (ternary-ACBFS) concrete specimens exposed to distilled water (DST) after (from left to right) 18, 191 and 310 FT cycles.



Figure C.30 Physical changes in the appearance of the representative sample of M5-.1PC-NA (plain-dolomite) concrete specimens exposed to CaCl_2 after (from left to right) 42, 65, 118 and 139 FT cycles.



Figure C.31 Physical changes in the appearance of the representative sample of M5-.1PC-NA (plain-dolomite) concrete specimens exposed to MgCl_2 after (from left to right) 42, 65, 139 and 350 FT cycles.



Figure C.32 Physical changes in the appearance of the representative sample of M5-.1PC-NA (plain-dolomite) concrete specimens exposed to NaCl after (from left to right) 42, 65, 139 and 350 FT cycles.



Figure C.33 Physical changes in the appearance of the representative sample of M5-.1PC-NA (plain-dolomite) concrete specimens exposed to distilled water (DST) after (from left to right) 42, 65, 139 and 350 FT cycles.



Figure C.34 Physical changes in the appearance of the representative sample of M6-.2FA.8PC-NA (fly ash-dolomite) concrete specimens exposed to CaCl_2 after (from left to right) 42, 65, 139 and 350 FT cycles.



Figure C.35 Physical changes in the appearance of the representative sample of M6-.2FA.8PC-NA (fly ash-dolomite) concrete specimens exposed to MgCl_2 after (from left to right) 42, 65, 139 and 350 FT cycles.

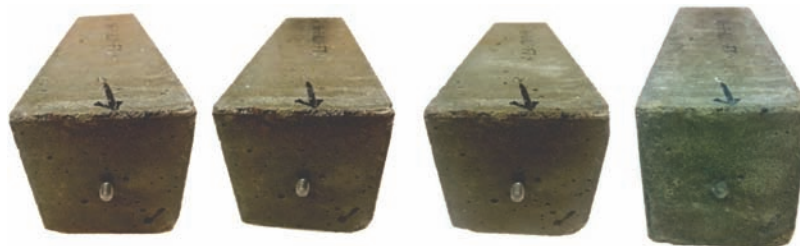


Figure C.36 Physical changes in the appearance of the representative sample of M6-.2FA.8PC-NA (fly ash-dolomite) concrete specimens exposed to NaCl after (from left to right) 42, 65, 139 and 350 FT cycles.



Figure C.37 Physical changes in the appearance of the representative sample of M6-.2FA.8PC-NA (fly ash-dolomite) concrete specimens exposed to distilled water (WD) after (from left to right) 42, 65, 139 and 350 FT cycles.



Figure C.38 Physical changes in the appearance of the representative sample of M7-.25SC.75PC-NA (slag cement - dolomite) concrete specimens exposed to CaCl_2 after (from left to right) 3, 87 and 172 FT cycles.

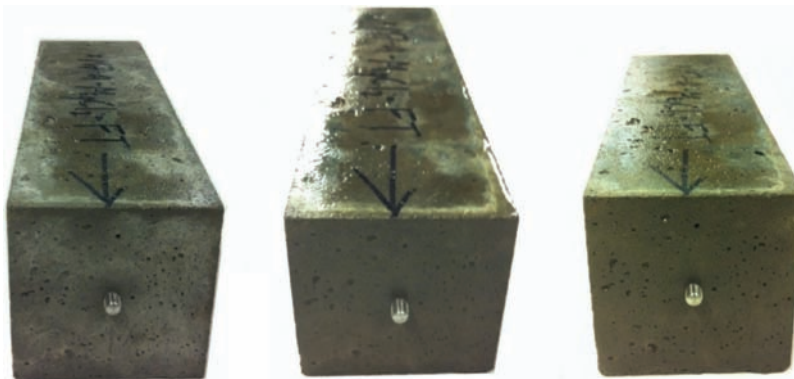


Figure C.39 Physical changes in the appearance of the representative sample of M7-.25SC.75PC-NA (slag cement - dolomite) concrete specimens exposed to MgCl_2 after (from left to right) 3, 87 and 172 FT cycles.

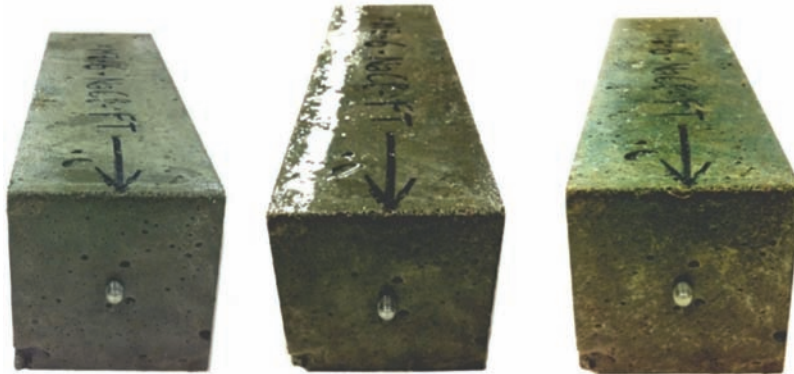


Figure C.40 Physical changes in the appearance of the representative sample of M7-.25SC.75PC-NA (slag cement - dolomite) concrete specimens exposed to NaCl after (from left to right) 3, 87 and 172 FT cycles.



Figure C.41 Physical changes in the appearance of the representative sample of M7-.25SC.75PC-NA (slag cement - dolomite) concrete specimens exposed to distilled water (DST) after (from left to right) 3 and 172 FT cycles.

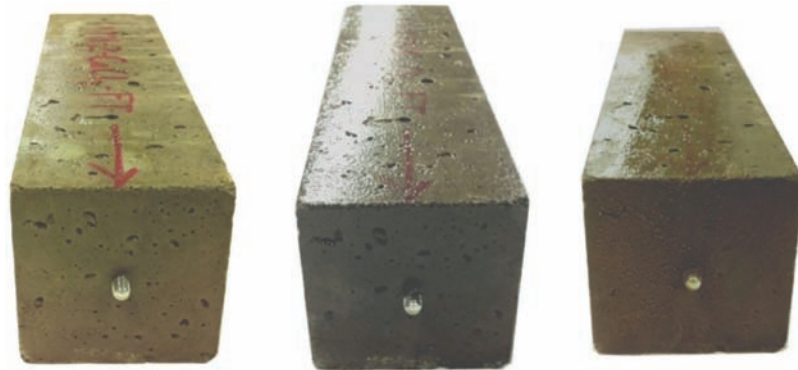


Figure C.42 Physical changes in the appearance of the representative sample of M8-.17FA.23SC.6PC-NA (Ternary - dolomite) concrete specimens exposed to CaCl_2 after (from left to right) 3, 87 and 172 FT cycles.



Figure C.43 Physical changes in the appearance of the representative sample of M8-.17FA.23SC.6PC-NA (Ternary - dolomite) concrete specimens exposed to MgCl_2 after (from left to right) 3, 87 and 172 FT cycles.



Figure C.44 Physical changes in the appearance of the representative sample of M8-.17FA.23SC.6PC-NA (Ternary - dolomite) concrete specimens exposed to NaCl after (from left to right) 3, 87 and 172 FT cycles.

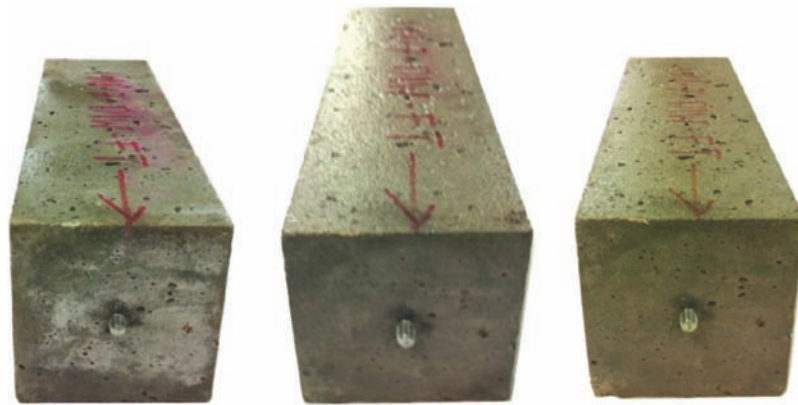


Figure C.45 Physical changes in the appearance of the representative sample of M8-.17FA.23SC.6PC-NA (Ternary - dolomite) concrete specimens exposed to distilled water (DST) after (from left to right) 3, 87 and 172 FT cycles.



Figure C.46 Physical changes in the appearance of the representative sample of M1-1PC-ACBFS (plain-ACBFS) concrete specimens exposed to CaCl_2 after (from left to right) 176, 205 and 281 WD cycles.

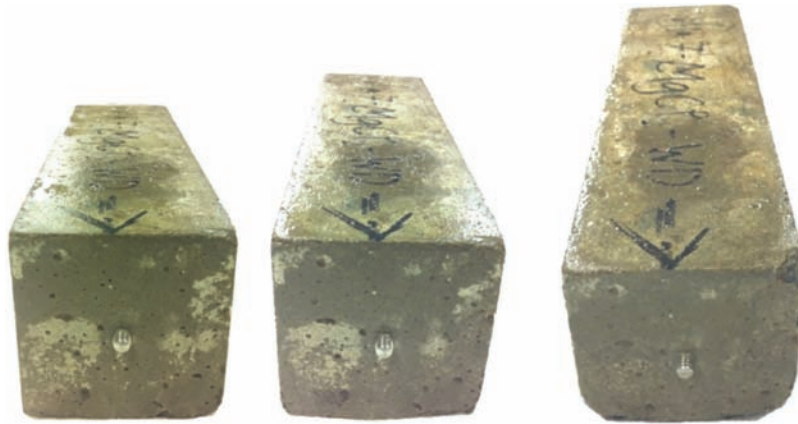


Figure C.47 Physical changes in the appearance of the representative sample of M1-1PC-ACBFS (plain-ACBFS) concrete specimens exposed to $MgCl_2$ after (from left to right) 176, 205 and 281 WD cycles.



Figure C.48 Physical changes in the appearance of the representative sample of M1-1PC-ACBFS (plain-ACBFS) concrete specimens exposed to $NaCl$ after (from left to right) 176, 205 and 281 WD cycles.



Figure C.49 Physical changes in the appearance of the representative sample of M1-1PC-ACBFS (plain-ACBFS) concrete specimens exposed to distilled water (DST) after (from left to right) 176, 205 and 281 WD cycles.



Figure C.50 Physical changes in the appearance of the representative sample of M2-.2FA.8PC-ACBFS (fly ash-ACBFS) concrete specimens exposed to CaCl_2 after (from left to right) 176, 205 and 281 WD cycles.



Figure C.51 Physical changes in the appearance of the representative sample of M2-.2FA.8PC-ACBFS (fly ash-ACBFS) concrete specimens exposed to MgCl_2 after (from left to right) 176, 205 and 281 WD cycles.



Figure C.52 Physical changes in the appearance of the representative sample of M2-.2FA.8PC-ACBFS (fly ash-ACBFS) concrete specimens exposed to NaCl after (from left to right) 176, 205 and 281 WD cycles.



Figure C.53 Physical changes in the appearance of the representative sample of M2-2FA.8PC-ACBFS (fly ash-ACBFS) concrete specimens exposed to distilled water (DST) after (from left to right) 176, 205 and 281 WD cycles.



Figure C.54 Physical changes in the appearance of the representative sample of M3-.25SC.75PC-ACBFS (slag cement-ACBFS) concrete specimens exposed to CaCl_2 after (from left to right) 0, 90 and 226 WD cycles.



Figure C.55 Physical changes in the appearance of the representative sample of M3-.25SC.75PC-ACBFS (slag cement-ACBFS) concrete specimens exposed to MgCl_2 after (from left to right) 0, 90 and 226 WD cycles.



Figure C.56 Physical changes in the appearance of the representative sample of M3-.25SC.75PC-ACBFS (slag cement-ACBFS) concrete specimens exposed to NaCl after (from left to right) 0, 90 and 226 WD cycles.



Figure C.57 Physical changes in the appearance of the representative sample of M3-.25SC.75PC-ACBFS (slag cement-ACBFS) concrete specimens exposed to distilled water (DST) after (from left to right) 0, 90 and 226 WD cycles.



Figure C.58 Physical changes in the appearance of the representative sample of M4-.17FA.23SC.6PC-ACBFS (ternary-ACBFS) concrete specimens exposed to CaCl_2 after (from left to right) 0, 90 and 226 WD cycles.



Figure C.59 Physical changes in the appearance of the representative sample of M4-.17FA.23SC.6PC-ACBFS (ternary-ACBFS) concrete specimens exposed to $MgCl_2$ after (from left to right) 0, 90 and 226 WD cycles.



Figure C.60 Physical changes in the appearance of the representative sample of M4-.17FA.23SC.6PC-ACBFS (ternary-ACBFS) concrete specimens exposed to $NaCl$ after (from left to right) 0, 90 and 226 WD cycles.

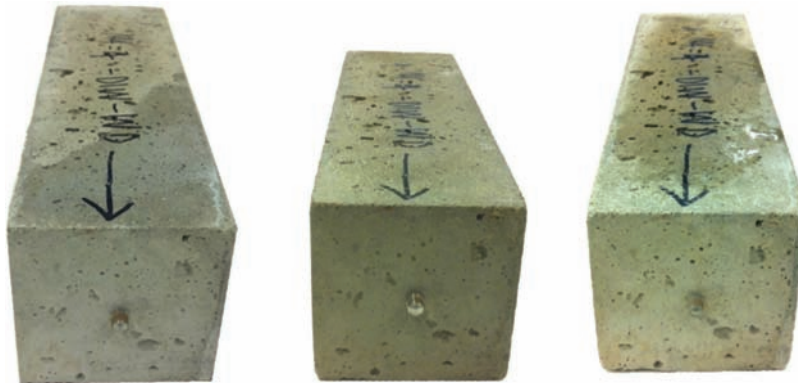


Figure C.61 Physical changes in the appearance of the representative sample of M4-.17FA.23SC.6PC-ACBFS (ternary-ACBFS) concrete specimens exposed to distilled water (DST) after (from left to right) 0, 90 and 226 WD cycles.



Figure C.62 Physical changes in the appearance of the representative sample of M5-1PC-NA (plain-dolomite) concrete specimens exposed to CaCl_2 after (from left to right) 176, 205 and 281 WD cycles.



Figure C.63 Physical changes in the appearance of the representative sample of M5-1PC-NA (plain-dolomite) concrete specimens exposed to MgCl_2 after (from left to right) 176, 205 and 281 WD cycles.



Figure C.64 Physical changes in the appearance of the representative sample of M5-1PC-NA (plain-dolomite) concrete specimens exposed to NaCl after (from left to right) 176, 205 and 281 WD cycles.



Figure C.65 Physical changes in the appearance of the representative sample of M5-1PC-NA (plain-dolomite) concrete specimens exposed to distilled water (DST) after (from left to right) 176, 205 and 281 WD cycles.



Figure C.66 Physical changes in the appearance of the representative sample of M6-.2FA.8PC-NA (fly ash-dolomite) concrete specimens exposed to CaCl_2 after (from left to right) 176, 205 and 281 WD cycles.



Figure C.67 Physical changes in the appearance of the representative sample of M6-.2FA.8PC-NA (fly ash-dolomite) concrete specimens exposed to MgCl_2 after (from left to right) 176, 205 and 281 WD cycles.



Figure C.68 Physical changes in the appearance of the representative sample of M6-.2FA.8PC-NA (fly ash-dolomite) concrete specimens exposed to NaCl after (from left to right) 176, 205 and 281 WD cycles.

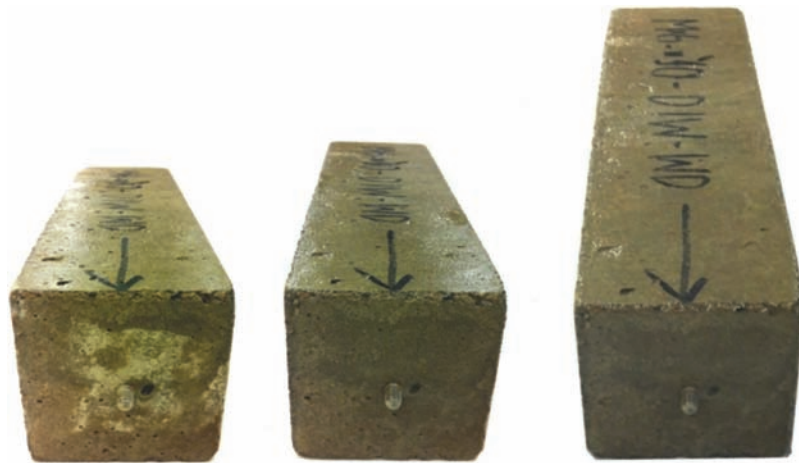


Figure C.69 Physical changes in the appearance of the representative sample of M6-.2FA.8PC-NA (fly ash-dolomite) concrete specimens exposed to distilled water (DST) after (from left to right) 176, 205 and 281 WD cycles.



Figure C.70 Physical changes in the appearance of the representative sample of M7-.25SC.75PC-NA (slag cement-dolomite) concrete specimens exposed to CaCl_2 after (from left to right) 0, 90 and 226 WD cycles.



Figure C.71 Physical changes in the appearance of the representative sample of M7-.25SC.75PC-NA (slag cement-dolomite) concrete specimens exposed to $MgCl_2$ after (from left to right) 0, 90 and 226 WD cycles.



Figure C.72 Physical changes in the appearance of the representative sample of M7-.25SC.75PC-NA (slag cement-dolomite) concrete specimens exposed to $NaCl$ after (from left to right) 0, 90 and 226 WD cycles.



Figure C.73 Physical changes in the appearance of the representative sample of M7-.25SC.75PC-NA (slag cement-dolomite) concrete specimens exposed to distilled water (DST) after (from left to right) 0, 90 and 226 WD cycles.



Figure C.74 Physical changes in the appearance of the representative sample of M8-.17FA.23SC.6PC-NA (ternary-dolomite) concrete specimens exposed to CaCl_2 after (from left to right) 0, 90 and 226 WD cycles.



Figure C.75 Physical changes in the appearance of the representative sample of M8-.17FA.23SC.6PC-NA (ternary-dolomite) concrete specimens exposed to MgCl_2 after (from left to right) 0, 90 and 226 WD cycles.



Figure C.76 Physical changes in the appearance of the representative sample of M8-.17FA.23SC.6PC-NA (ternary-dolomite) concrete specimens exposed to NaCl after (from left to right) 0, 90 and 226 WD cycles.



Figure C.77 Physical changes in the appearance of the representative sample of M8-.17FA.23SC.6PC-NA (ternary-dolomite) concrete specimens exposed to distilled water (DST) after (from left to right) 0, 90 and 226 WD cycles.

APPENDIX D. SEM RESULTS

M1-1PC-ACBFS (plain- ACBFS) – MgCl_2 + FT

Figure D.1 shows formation of Mg-O-Cl, M-S-H as the result of magnesium ion substituting the calcium ion in C-S-H. Ettringite was also found in M1 specimen exposed to MgCl_2 and FT cycles.

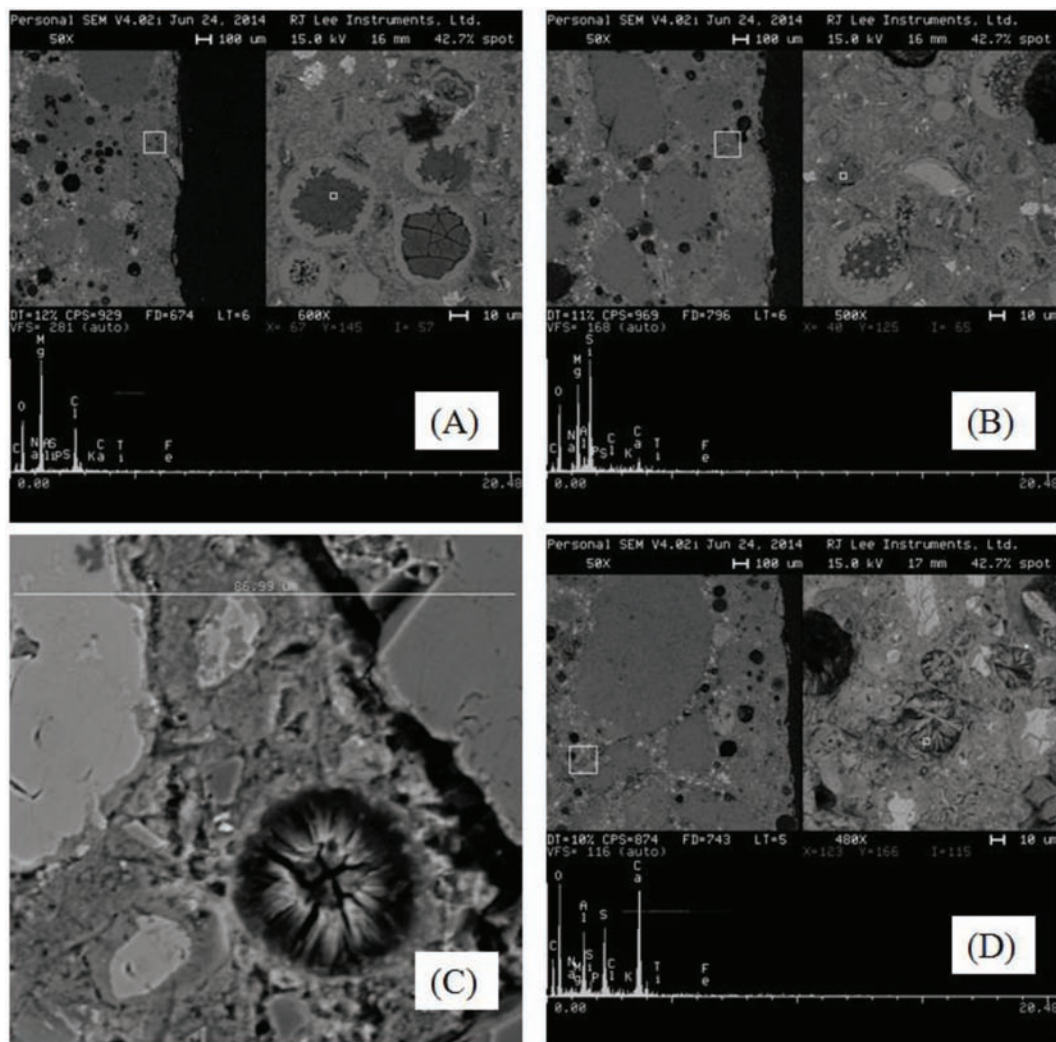


Figure D.1 SEM-EDX micrographs for M1 (plain-ACBFS) beam exposed to MgCl_2 after 347 FT cycles; (A) Mg-O-Cl, (B) M-S-H, (C) and (D) ettringite (SEM-BSE).

M1-1PC-ACBFS (plain- ACBFS) – NaCl + FT

The observation on M1 specimen exposed NaCl+FT cycles under SEM has revealed the remnant of the deicer (NaCl), ettringite, Friedel's salt and chloride ion inside the paste.

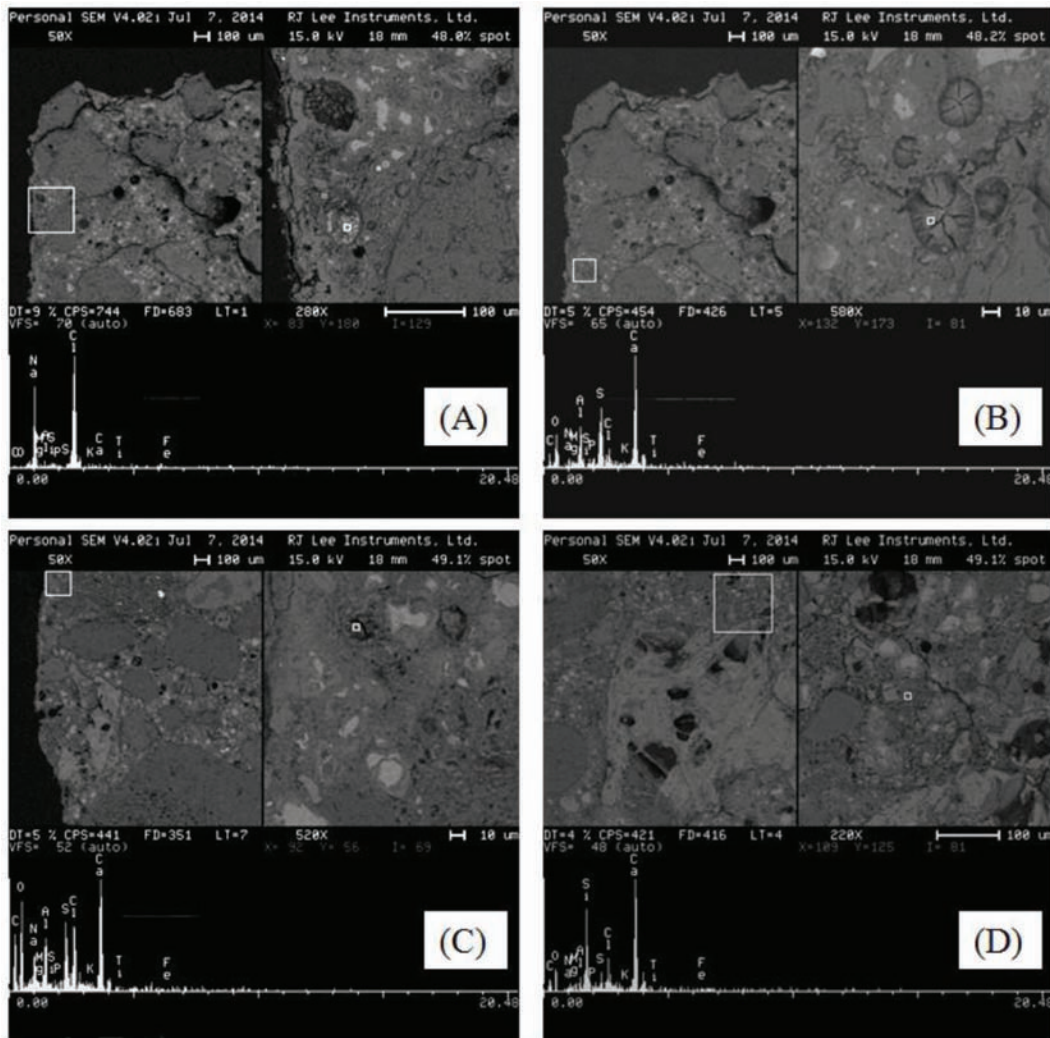


Figure D.2 SEM-EDX micrographs for M1 (plain-dolomite) beam exposed to MgCl_2 after 347 FT cycles; (A) NaCl deposit, (B) Ettringite, (C) Ettringite and Friedel's salt (D) Chloride in paste (SEM-BSE).

M1-1PC-ACBFS (plain- ACBFS) – DST + FT

Ettringite was observed in M1 specimen exposed to distilled water undergoing FT cycles in addition to the hydration products ($\text{Ca}(\text{OH})_2$ and C-S-H).

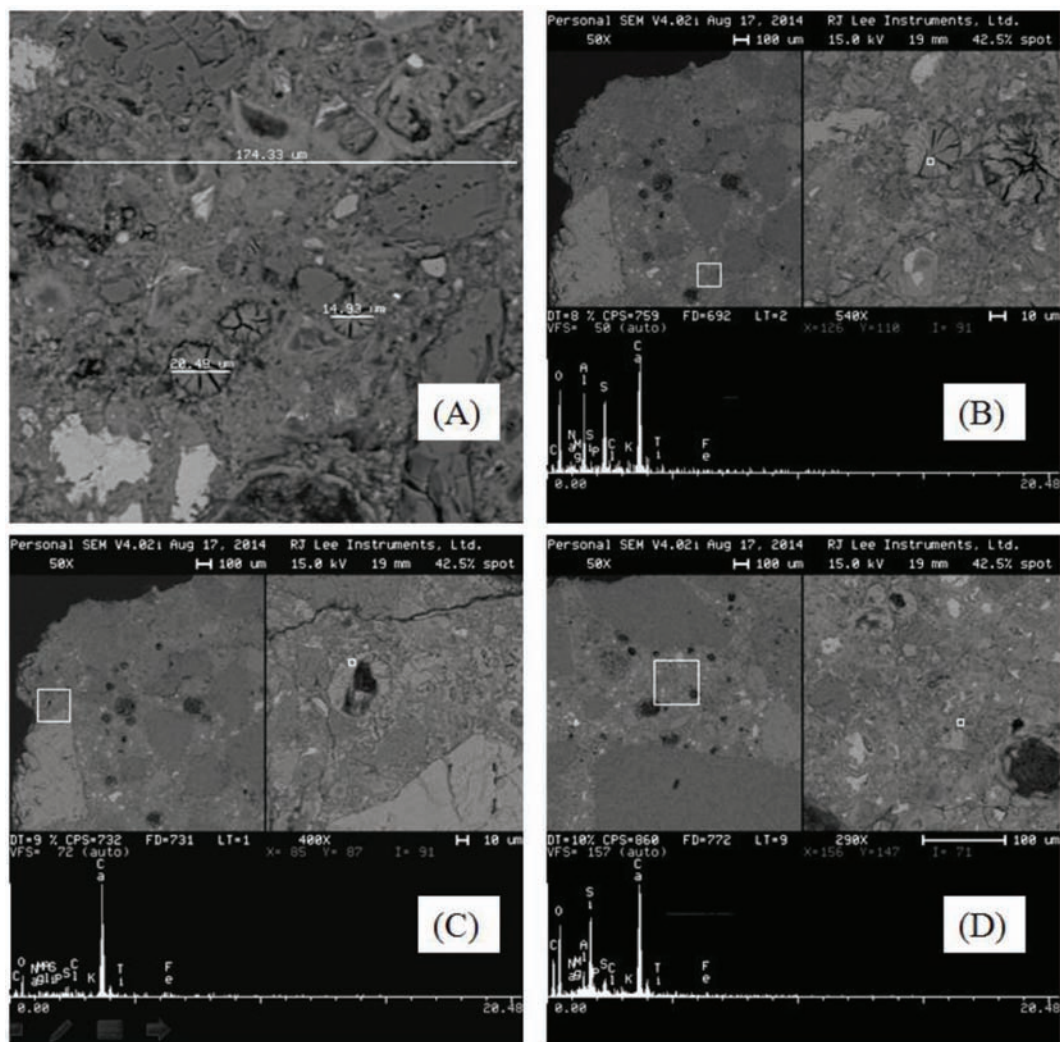


Figure D.3 SEM-EDX micrographs for M1 (plain-NaCl) specimen exposed to distilled water (DST) after 347 FT cycles; (A) and (B) ettringite, (C) Portlandite/ $\text{Ca}(\text{OH})_2$, (D) C-S-H (SEM-BSE).

M2-.2FA.8PC-ACBFS (fly ash-ACBFS) – CaCl_2 + FT

SEM results for M2 specimen exposed to CaCl_2 and 347 FT cycles are presented in Figure D.4.

Remnant of CaCl_2 was found inside the cracks of the concrete matrix. Deposits of Friedel's salt and ettringite were found inside the pores. In addition, intrusion of Cl^- was found within the paste.

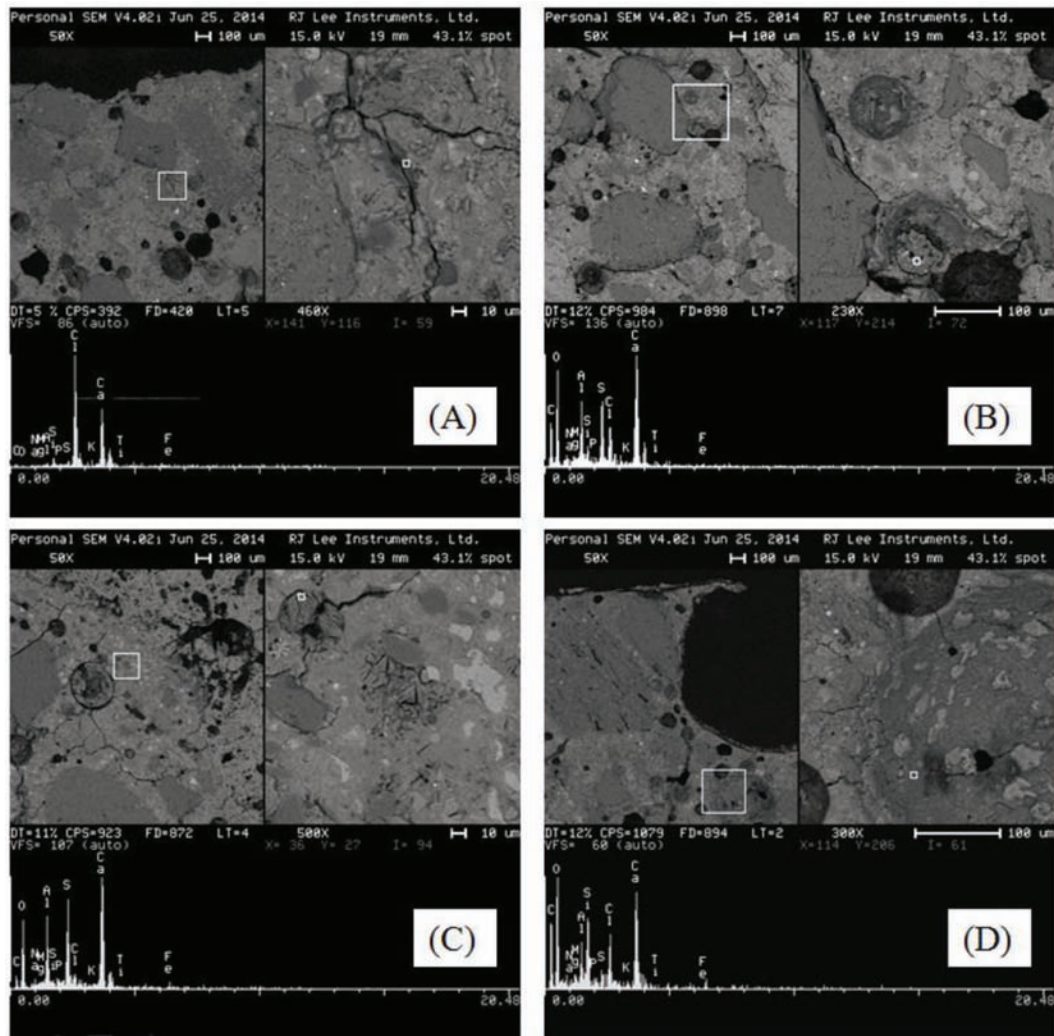


Figure D.4 SEM-EDX micrographs for M2 (fly ash-ACBFS) specimen exposed to CaCl_2 after 347 FT cycles; (A) CaCl_2 , (B) Friedel's salt and ettringite, (C) Ettringite (D) Cl^- intrusion in the paste (SEM-BSE).

M2-.2FA.8PC-ACBFS (fly ash-ACBFS) – MgCl_2 + FT

SEM results for M2 after 347 FT cycles in the presence of MgCl_2 are shown in Figure D.5.

Traces of Cl- and sulfate were found near the cracks in the matrix. Brucite layer was found on the surface of the specimen exposed to MgCl_2 as the result of dissolution of Portlandite by Mg ion. The presence of ettringite and Friedel's inside the pores was observed. In addition, void surrounded by Mg-O-Cl was observed.

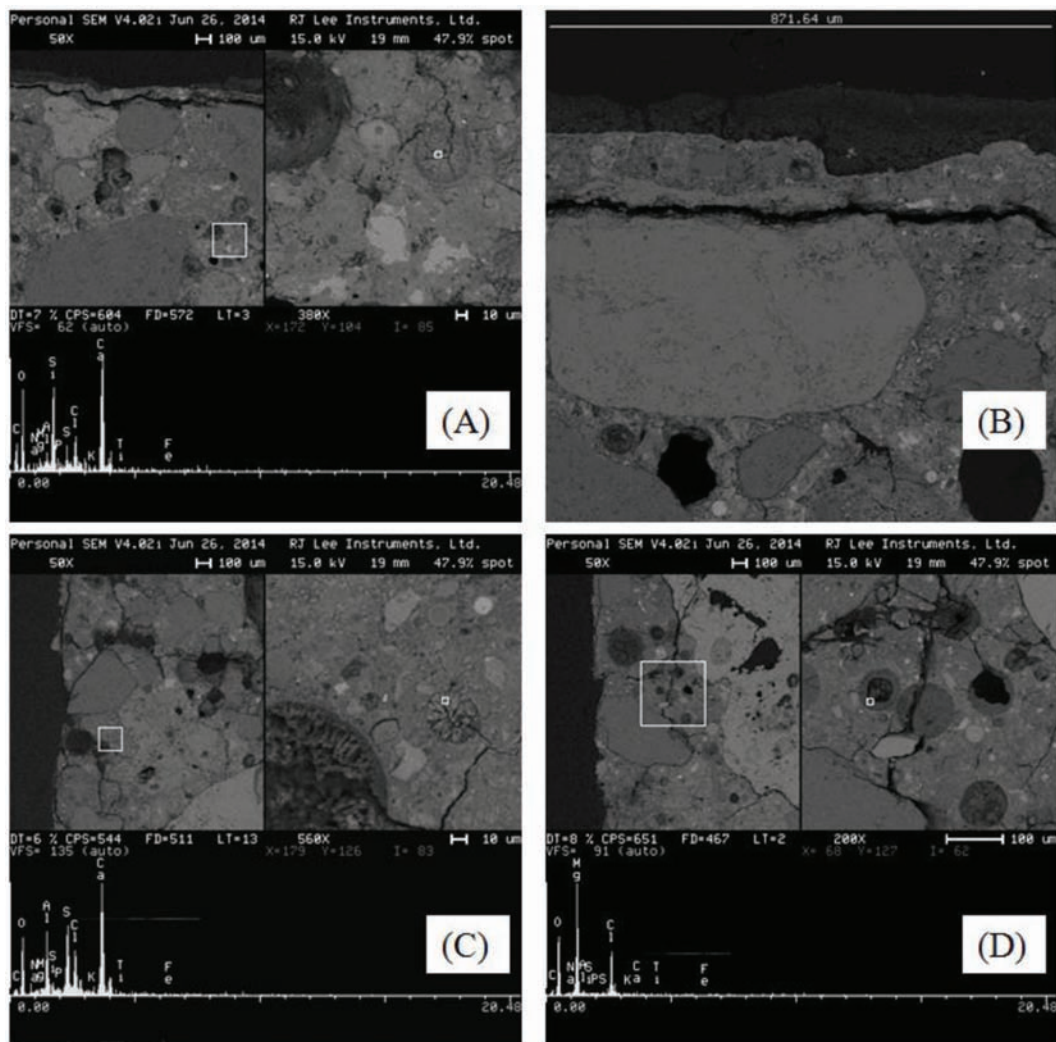


Figure D.5 SEM-EDX micrographs for M2 (fly ash-ACBFS) specimen exposed to MgCl_2 after 347 FT cycles; (A) Cl- and sulfate in the matrix, (B) Brucite layer, (C) Ettringite and Friedel's salt in void, (D) Mg-O-Cl (SEM-BSE).

M2-.2FA.8PC-ACBFS (fly ash-ACBFS) – NaCl + FT

SEM results for M2 after 347 FT cycles in the presence of NaCl are shown in Figure D.6.

No extensive cracks were observed on the surface of the specimens. However, chloride ingress, Friedel's salt and NaCl deposits were found near the surface of the specimen, indicating the penetration of NaCl deicer into the matrix. Moreover, the presence of ettringite inside the pores was observed.

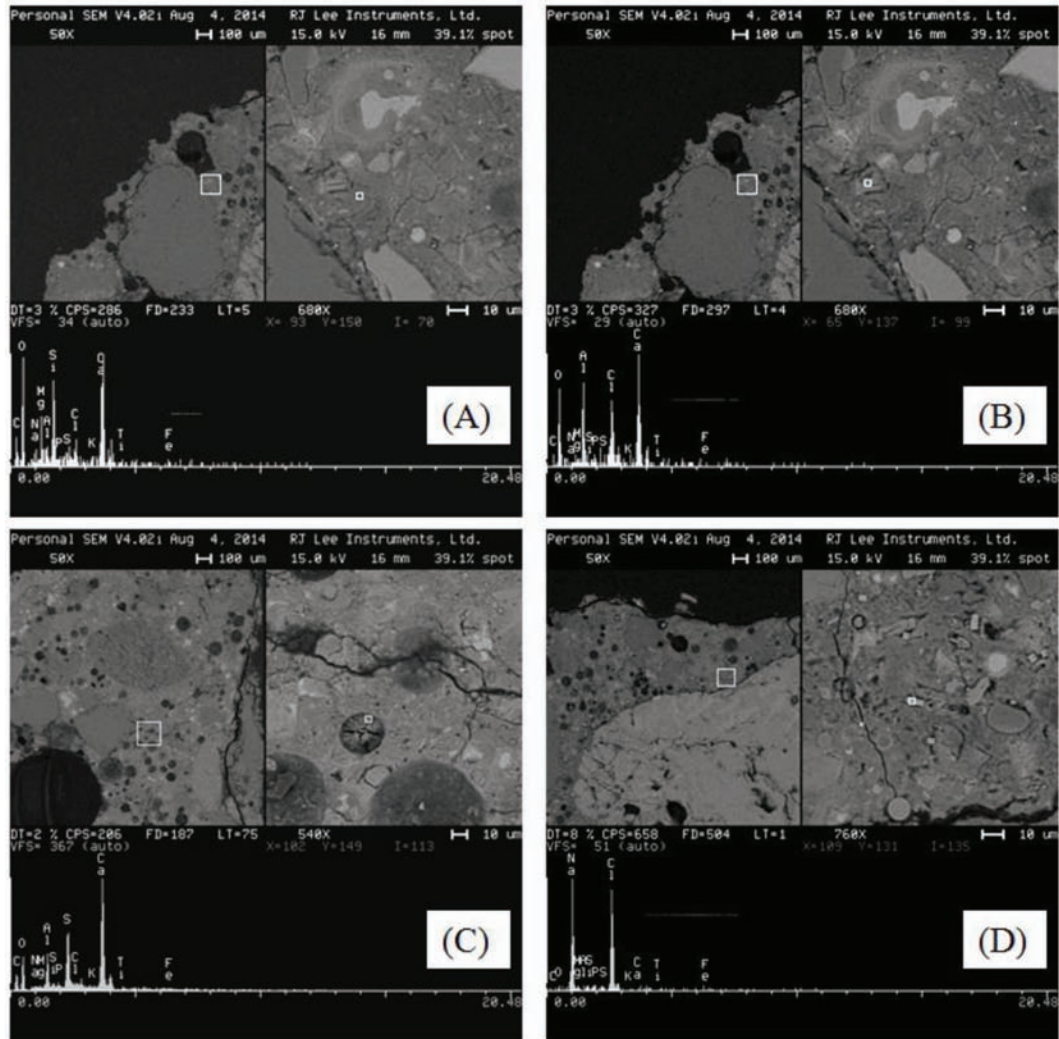


Figure D.6 SEM-EDX micrographs for M2 (fly ash-ACBFS) specimen exposed to NaCl after 347 FT cycles; (A) Cl- ingress in the matrix, (B) Friedel's salt, (C) Ettringite and (D) NaCl deposit (SEM-BSE).

M3-.25SC.75PC-ACBFS (slag cement-ACBFS) – CaCl_2 + FT

SEM results for M3 after 310 FT cycles in the presence of CaCl_2 are shown in Figure D.7.

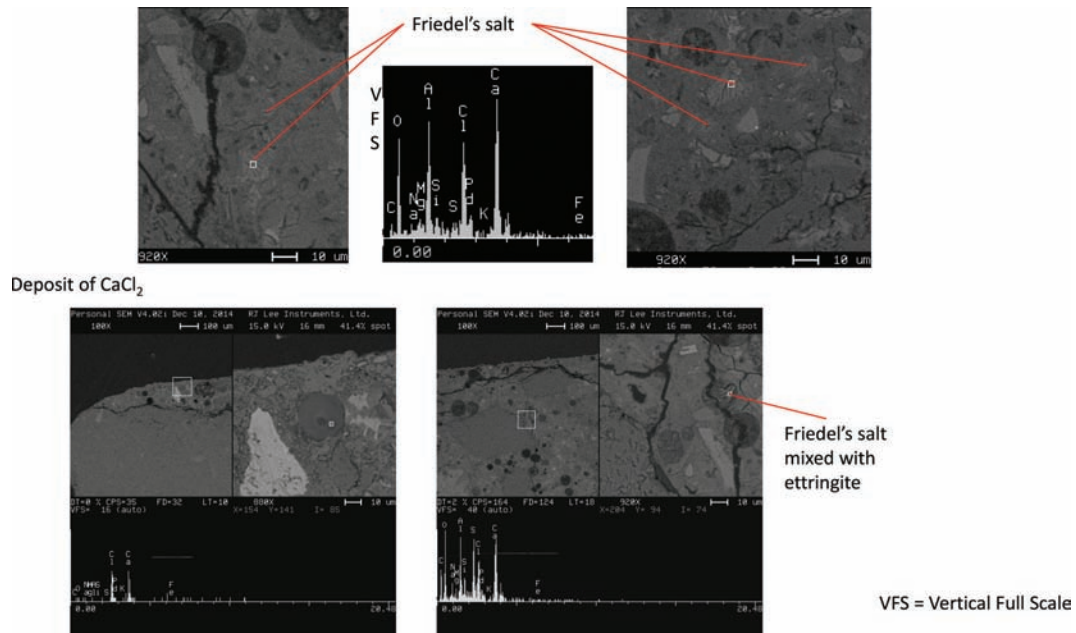


Figure D.7 SEM-EDX micrographs for M3 (slag cement-ACBFS) specimen exposed to CaCl_2 after 310 FT cycles have shown deposits of Friedel's salt, ettringite and CaCl_2 deicer in the matrix (SEM-BSE).

M4-.17FA.23SC.6PC-ACBFS (ternary-ACBFS) – MgCl_2 + FT

SEM results for M4 after 310 FT cycles in the presence of MgCl_2 are shown in Figure D.8.

Figure C.8 shows the presence of M-S-H as the results of Mg ion replacing Ca ion in C-S-H. Layer of carbonation product (calcium carbonate) was found at the surface of the specimen exposed to deicer. Calcium sulfide (CaS) appears as bright dots within the matrix of ACBFS.

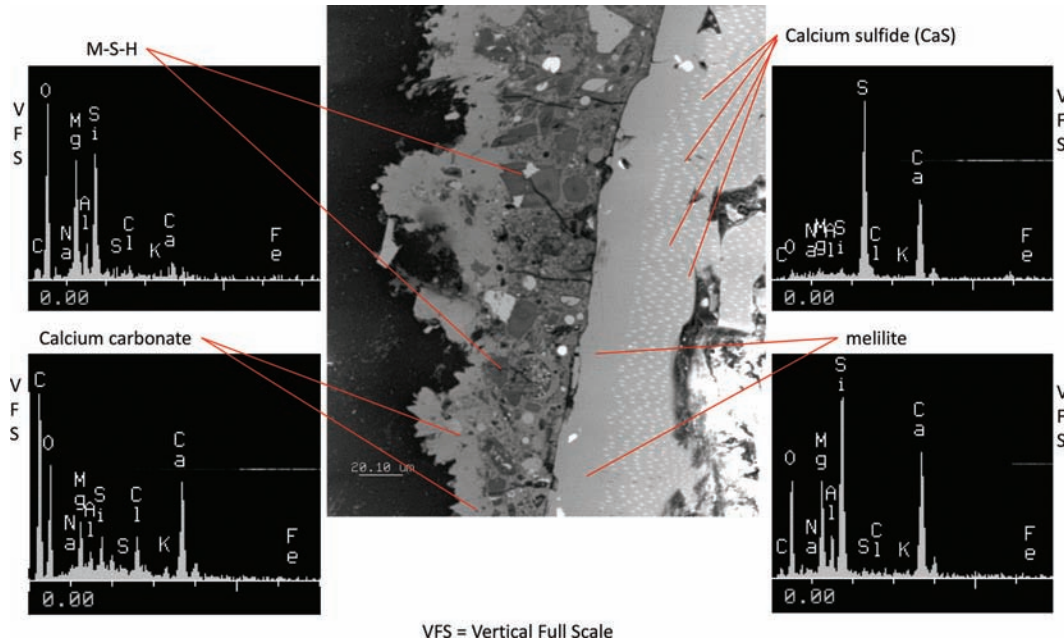


Figure D.8 SEM-EDX micrographs for M4 (ternary-ACBFS) specimen exposed to MgCl_2 after 310 FT cycles (SEM-BSE).

M4-.17FA.23SC.6PC-ACBFS (ternary-ACBFS) – NaCl + FT

SEM results for M4 after 310 FT cycles in the presence of NaCl are shown in Figure D.9.

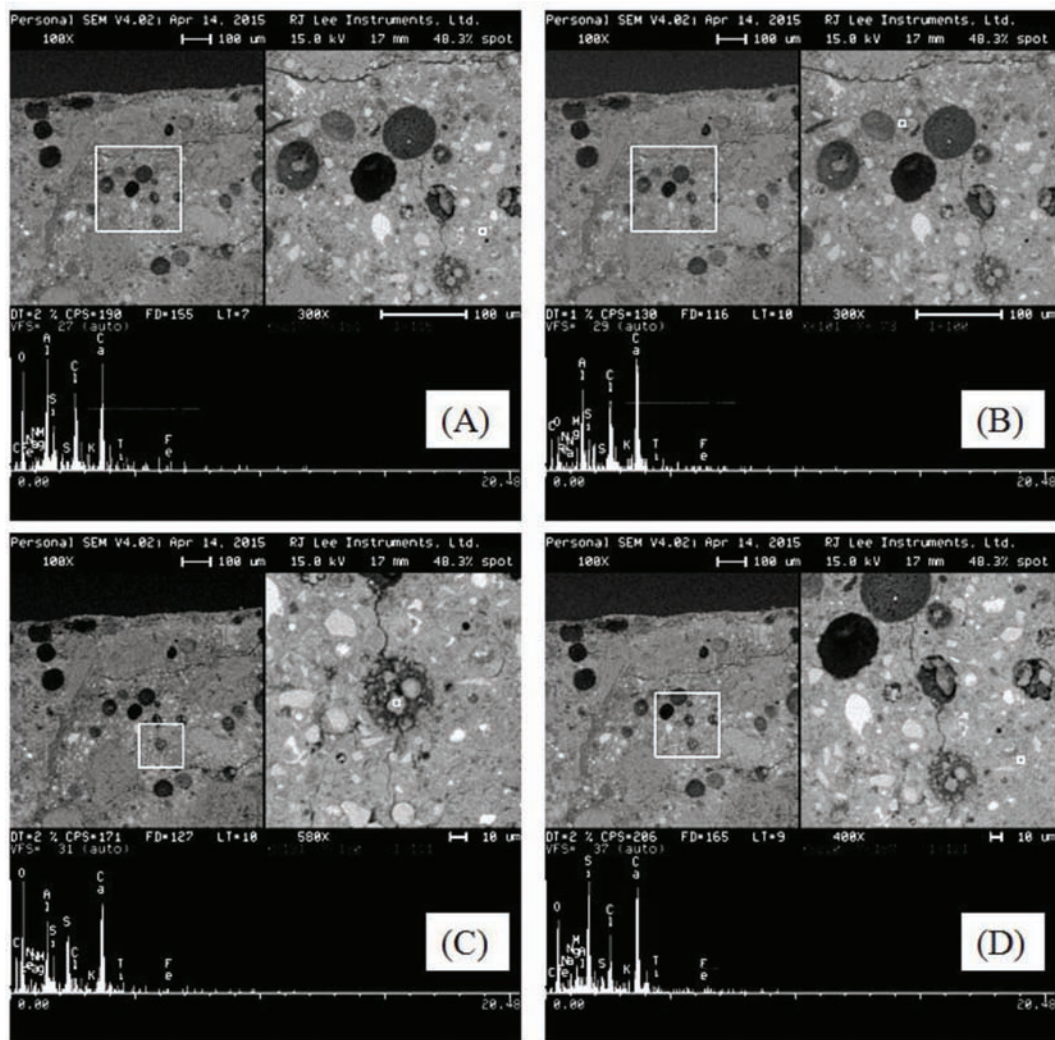


Figure D.9 SEM-EDX micrographs for M4 (ternary-ACBFS) specimen exposed to NaCl after 310 FT cycles; (A) and (B) Friedel's salt, (C) ettringite deposit in pore (D) Cl deposits within the matrix (SEM-BSE).

M4-.17FA.23SC.6PC-ACBFS (ternary-ACBFS) – DST + FT

SEM results for M4 after 310 FT cycles in the presence of distilled water (DST) are shown in Figure D.10.

SEM analysis on M4 specimen exposed to DST and FT cycles has indicated the presence of ettringite filling the pore. Monosulfate and Friedel's salt were also observed in the matrix.

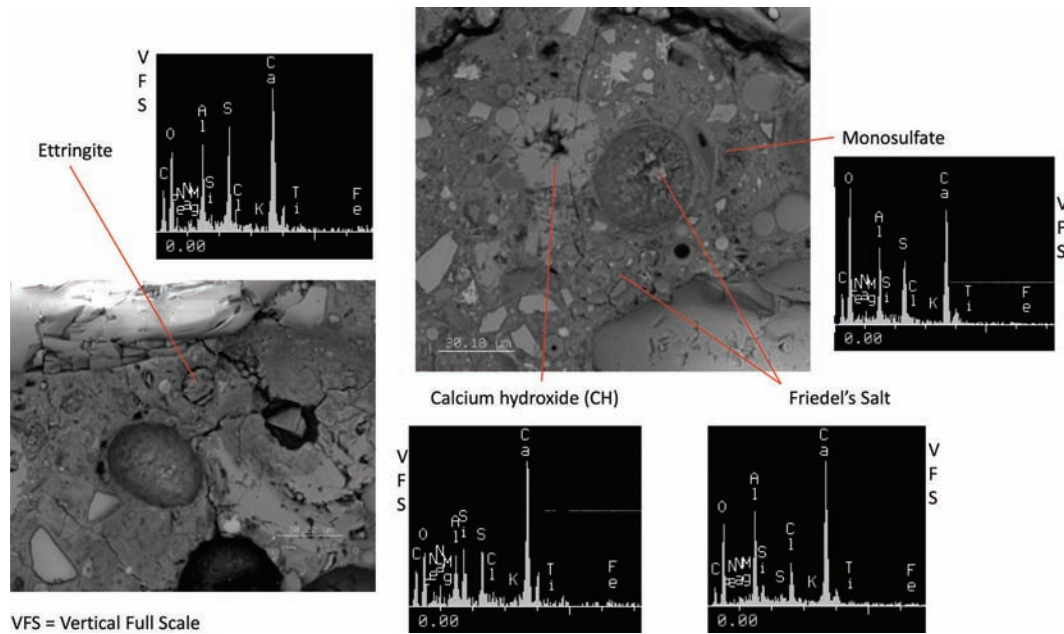


Figure D.10 SEM-EDX micrographs for M4 (ternary-ACBFS) specimen exposed to distilled water (DST) after 310 FT cycles (SEM-BSE).

M5-1PC-NA (plain-dolomite) – CaCl_2 + FT

SEM results for M5 after 151 FT cycles exposed to CaCl_2 are shown in Figure D.11.

It can be seen that the matrix of M5 specimen exposed to CaCl_2 +FT has experienced extensive cracks as the specimen was failed after 151 FT cycles. Chloride deposits and Friedel's salts were found within the matrix.

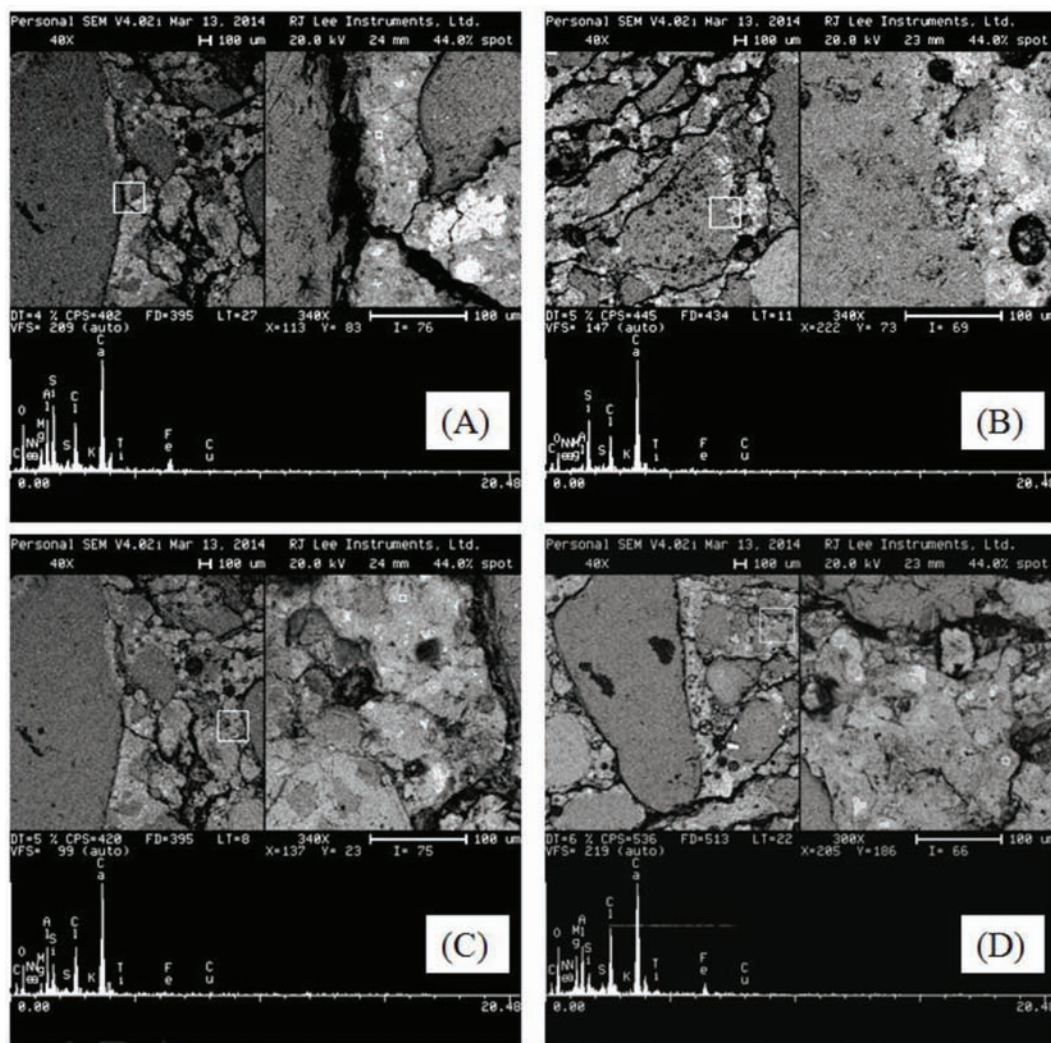


Figure D.11 SEM-EDX micrographs for M5 (plain-dolomite) specimen exposed to CaCl_2 after 151 FT cycles; (A) and (B) Deposits of Cl within the matrix, (C) & (D) Friedel's salt (SEM-BSE).

M5-1PC-NA (plain-dolomite) – MgCl_2 + FT

SEM results for M5 after 350 FT cycles and exposed to MgCl_2 are shown in Figure D.12.

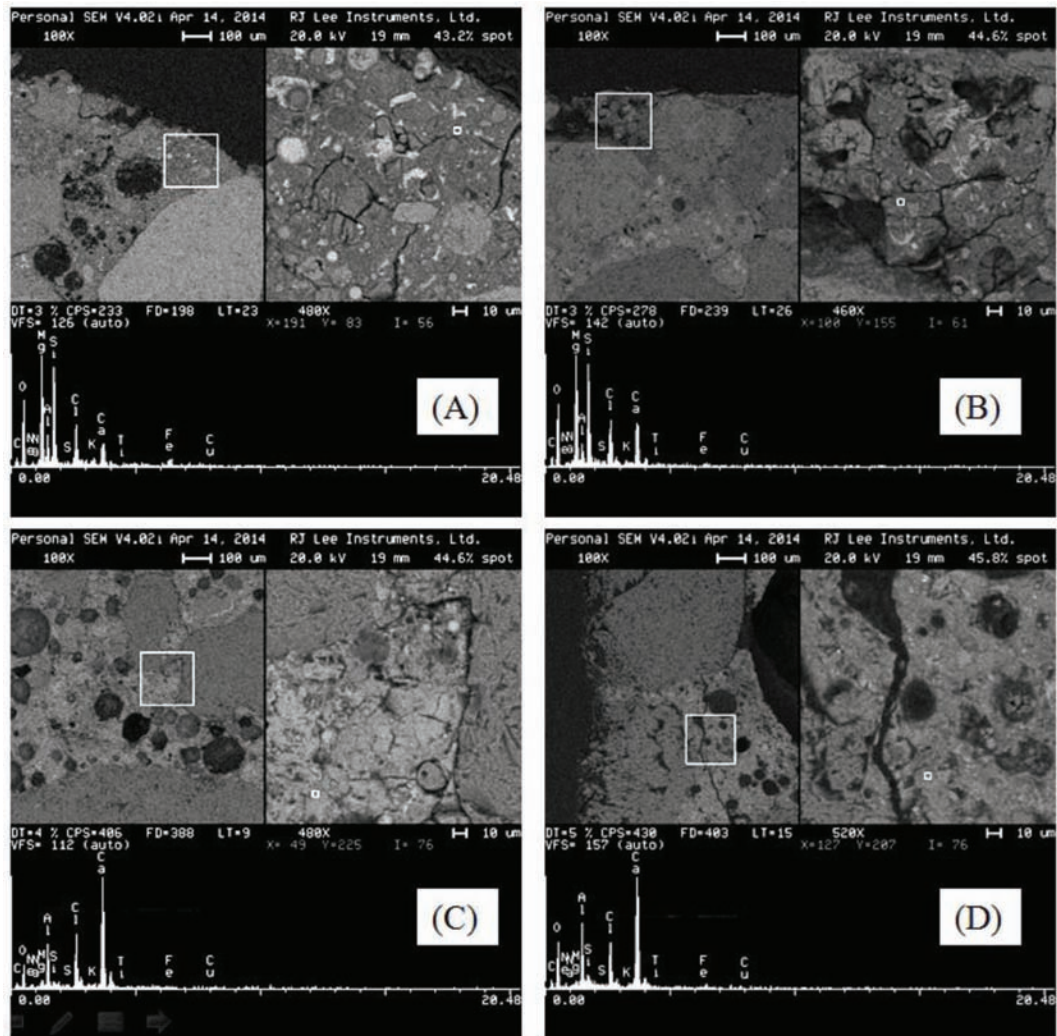


Figure D.12 SEM-EDX micrographs for M5 (plain-dolomite) specimen exposed to MgCl_2 after 350 FT cycles; (A) and (B) Chloride infused M-S-H, (C) & (D) Friedel's salt (SEM-BSE).

M5-1PC-NA (plain-dolomite) – NaCl + FT

SEM results for M5 after 350 FT cycles and exposed to NaCl are shown in Figure D.13.

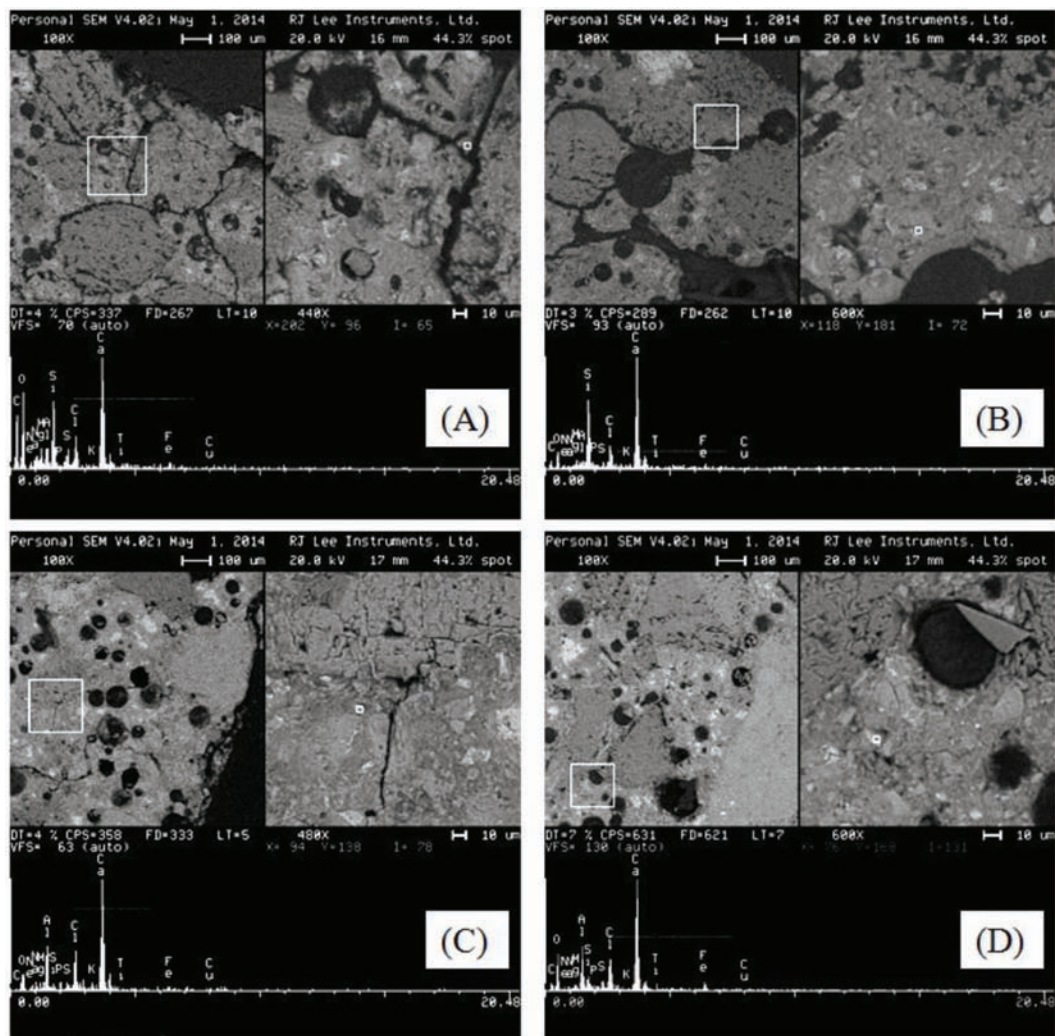


Figure D.13 SEM-EDX micrographs for M5 (plain-dolomite) specimen exposed to NaCl after 350 FT cycles; (A) and (B) Chloride deposits within C-S-H, (C) & (D) Friedel's salt (SEM-BSE).

M6-.2FA.8PC-NA (fly ash-dolomite) – MgCl_2 + FT

SEM results for M6 after 350 FT cycles and exposed to MgCl_2 are shown in Figure D.14.

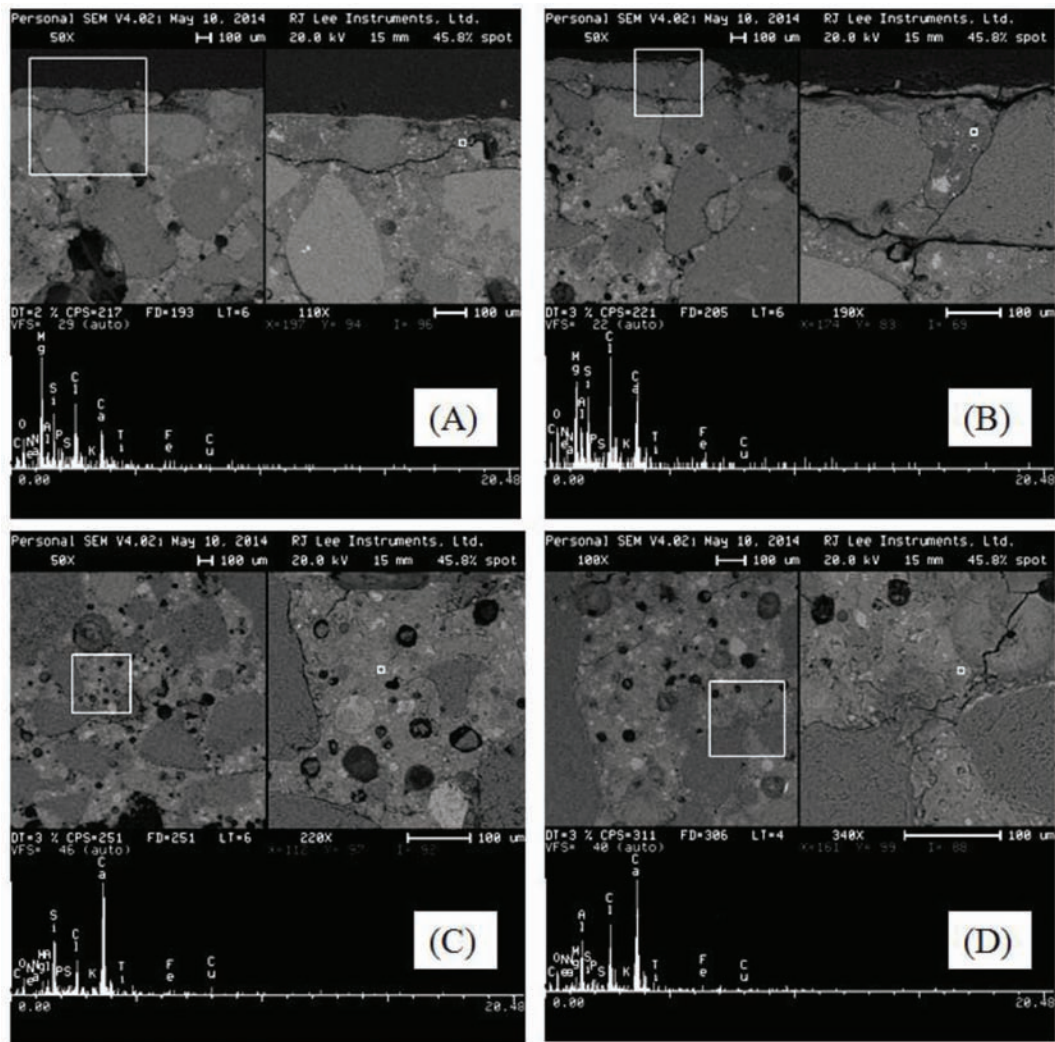


Figure D.14 SEM-EDX micrographs for M6 (fly ash-dolomite) specimen exposed to MgCl_2 after 350 FT cycles; (A) and (B) Chloride infused M-S-H, (C) Cl deposits within C-S-H and (D) Friedel's salt (SEM-BSE).

M7-.25SC.75PC-NA (slag cement-dolomite) – CaCl_2 + FT

SEM results for M7 after 310 FT cycles and exposed to CaCl_2 are shown in Figure D.15.

The traces of chloride ingress were found within the carbonation and hydration products in the concrete matrix.

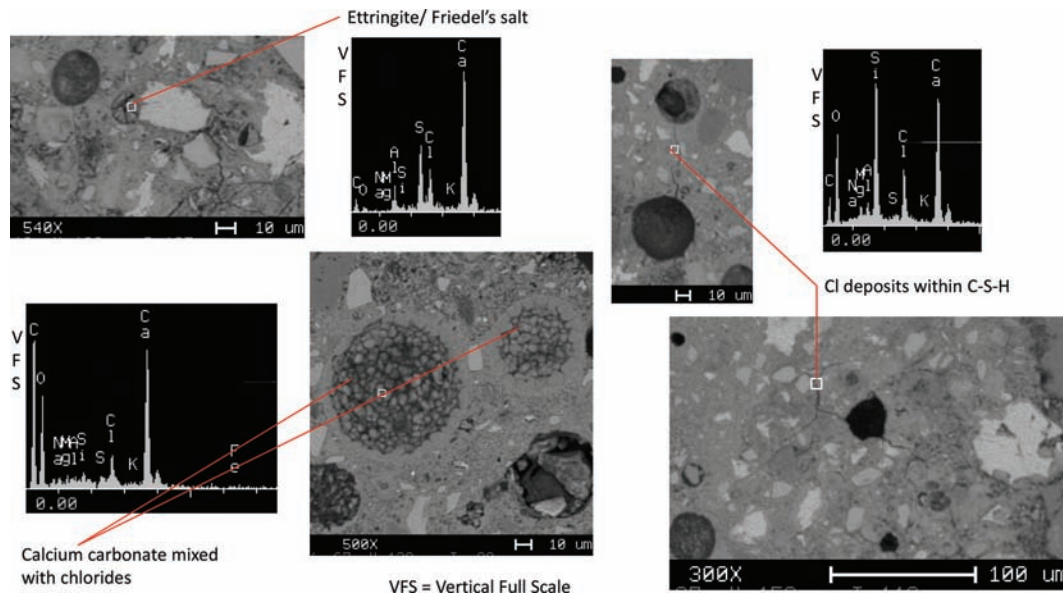


Figure D.15 SEM-EDX micrographs for M7 (slag cement-dolomite) specimen exposed to CaCl_2 after 310 FT cycles (SEM-BSE).

M7-.25SC.75PC-NA (slag cement-dolomite) – MgCl_2 + FT

SEM results for M7 after 310 FT cycles and exposed to MgCl_2 are shown in Figure D.16.

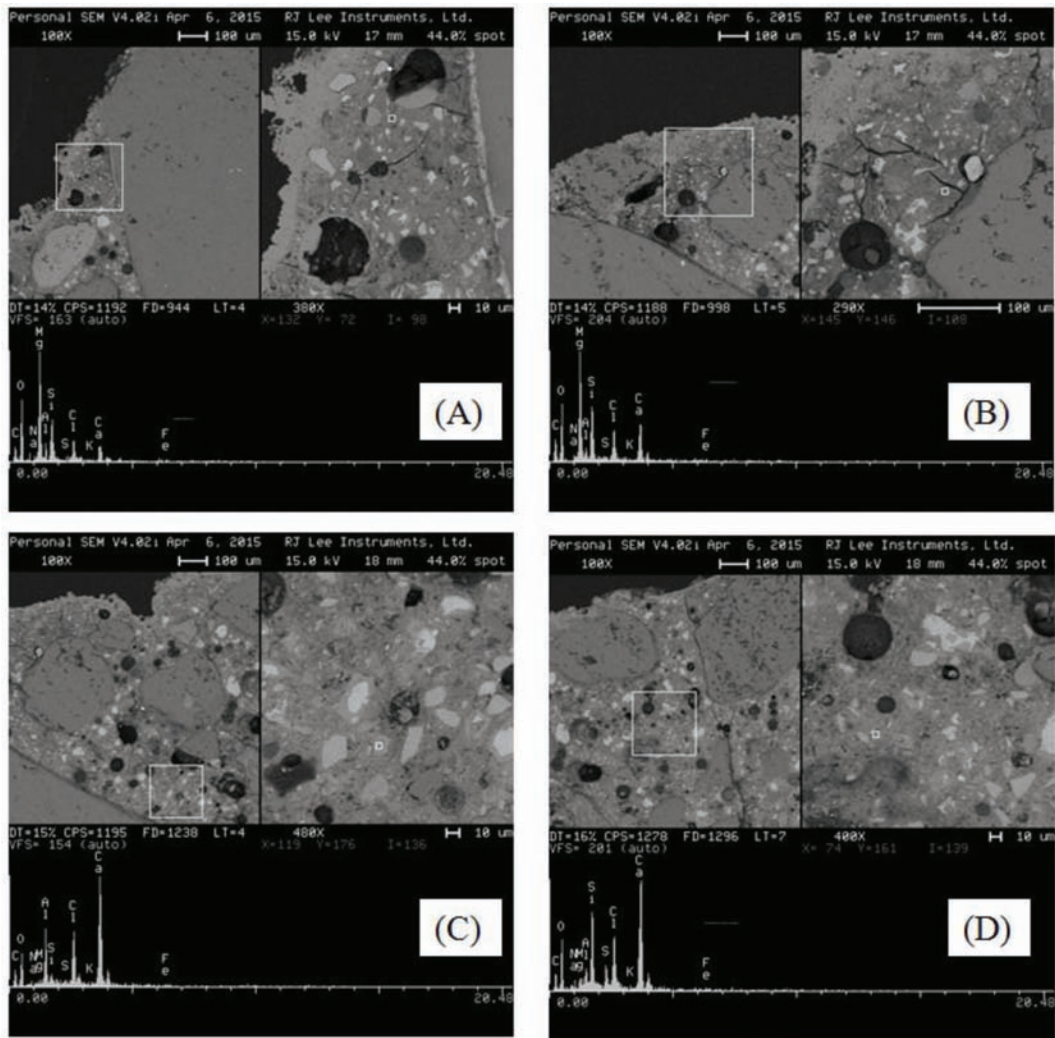


Figure D.16 SEM-EDX micrographs for M7 (slag cement-dolomite) specimen exposed to MgCl_2 after 350 FT cycles; (A) and (B) M-S-H, (C) Friedel's salt and (D) chloride deposits within C-S-H (SEM-BSE).

M8-.17FA.23SC.6PC-NA (ternary-dolomite) – CaCl_2 + FT

SEM results for M8 after 310 FT cycles and exposed to CaCl_2 are shown in Figure D.17.

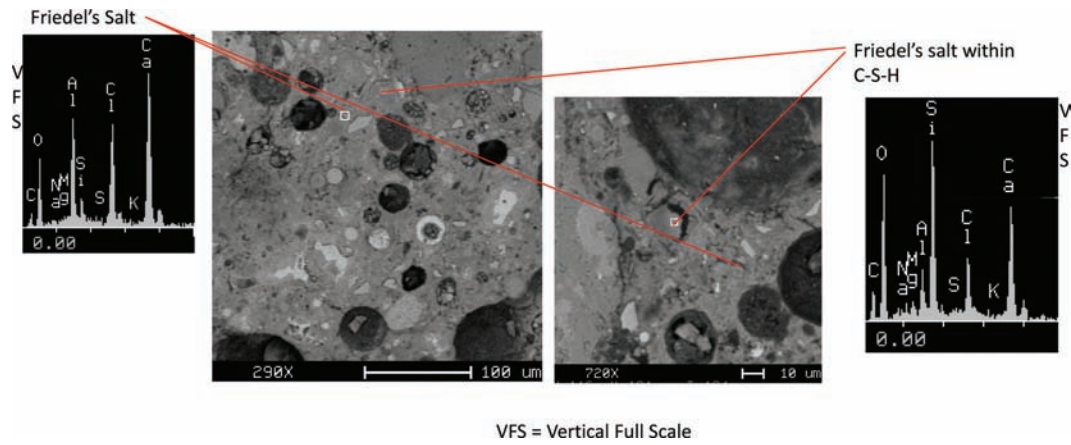


Figure D.17 SEM-EDX micrographs for M8 (ternary-dolomite) specimen exposed to CaCl_2 after 310 FT cycles (SEM-BSE).

M8-.17FA.23SC.6PC-NA (ternary-dolomite) – MgCl_2 + FT

SEM results for M8 after 310 FT cycles and exposed to MgCl_2 are shown in Figure D.18.

Brucite ($\text{Mg}(\text{OH})_2$) and M-S-H appeared to be darker than the normal concrete matrix due to the high content of magnesium.

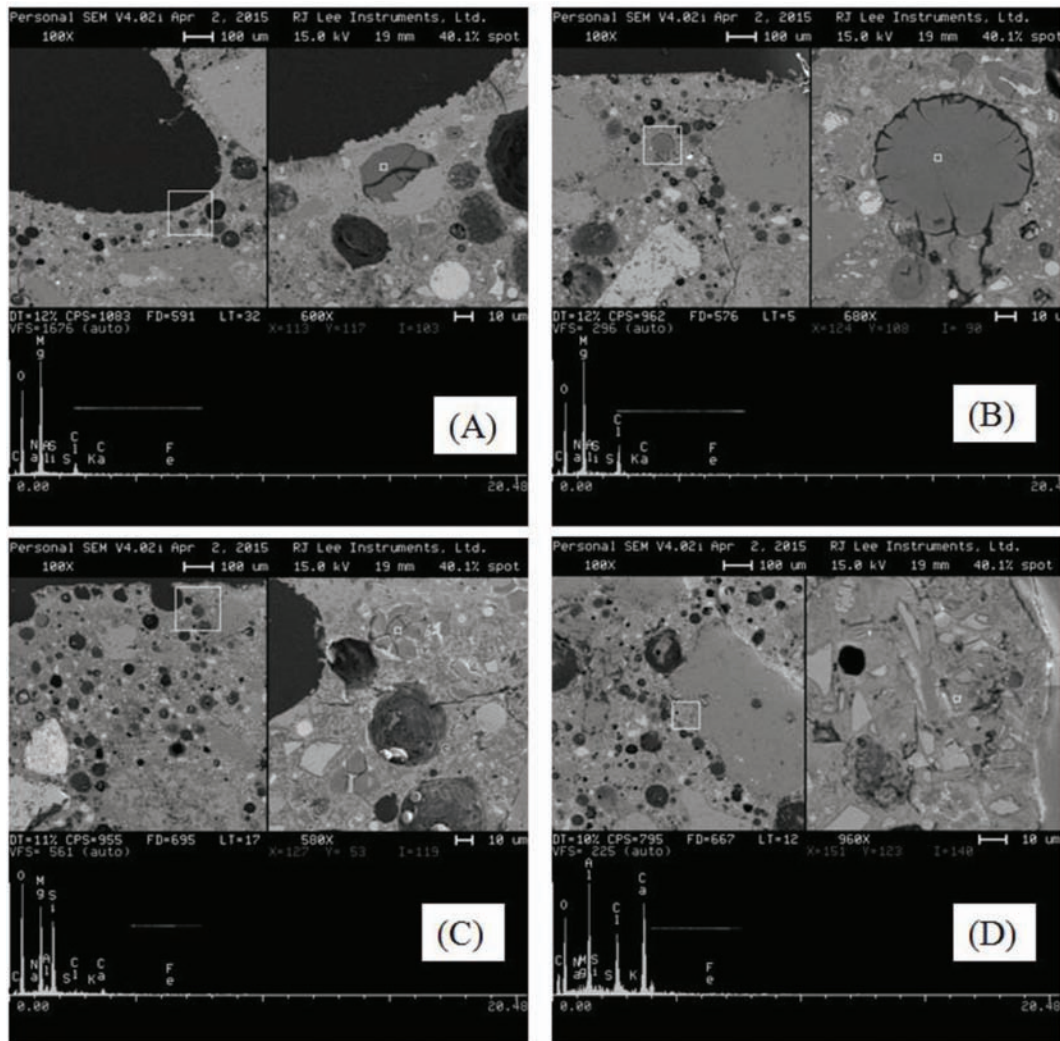


Figure D.18 SEM-EDX micrographs for M8 (ternary-dolomite) specimen exposed to MgCl_2 after 310 FT cycles; (A) and (B) brucite, (C) M-S-H and (D) Friedel's salt (SEM-BSE).

M8-.17FA.23SC.6PC-NA (ternary-dolomite) – NaCl + FT

SEM results for M8 after 310 FT cycles and exposed to NaCl are shown in Figure D.19.

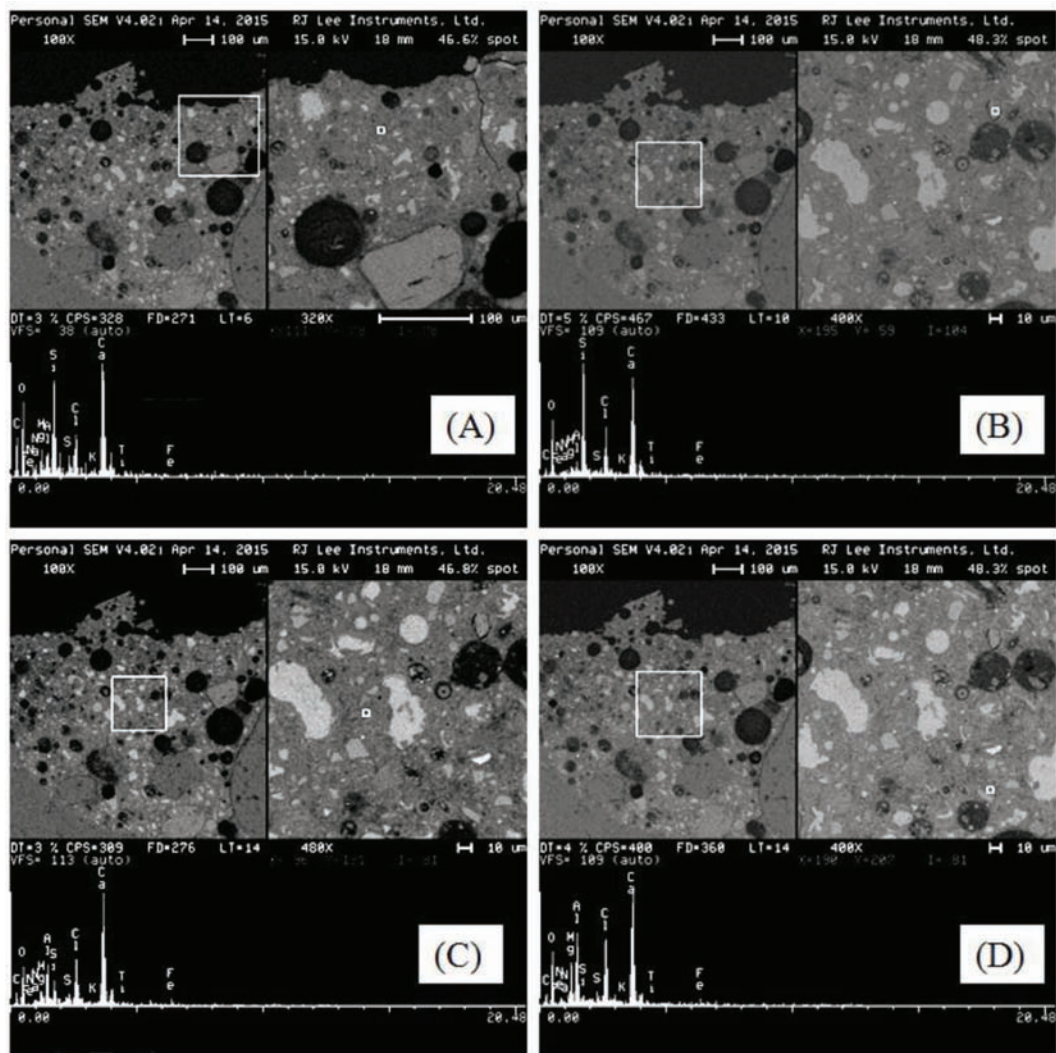


Figure D.19. SEM-EDX micrographs for M8 (ternary-dolomite) specimen exposed to NaCl after 310 FT cycles; (A) and (B) chloride deposits within the matrix C-S-H, (C) & (D) Friedel's salt (SEM-BSE).

M8-.17FA.23SC.6PC-NA (ternary-dolomite) – DST+ FT

SEM results for M8 after 310 FT cycles and exposed to distilled water (DST) are shown in Figure D.20.

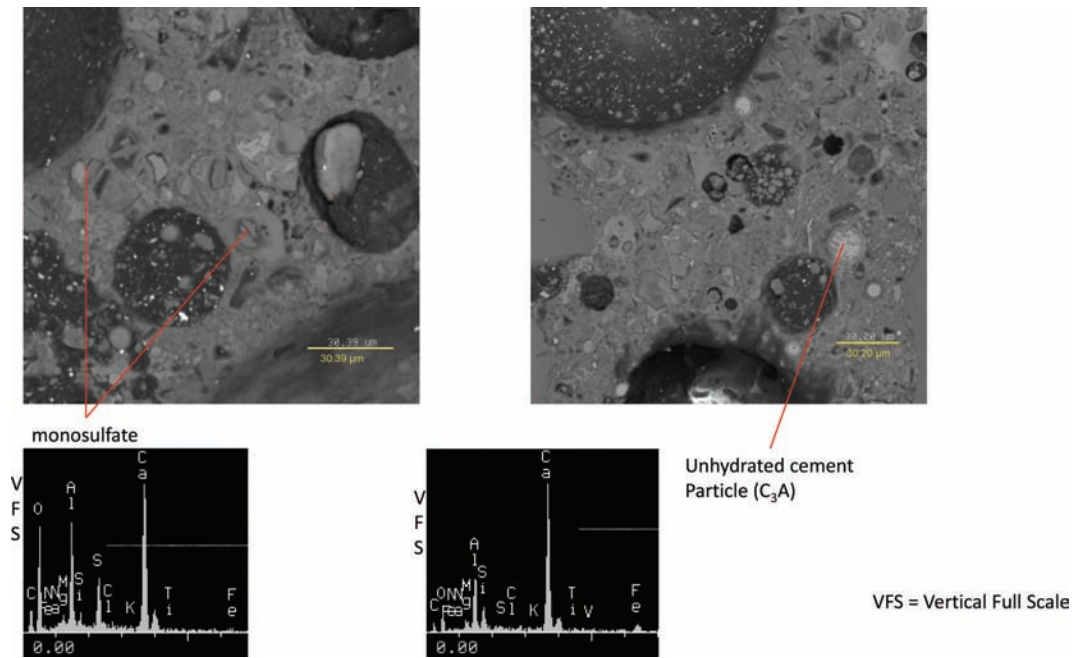


Figure D.20 SEM-EDX micrographs for M8 (ternary-dolomite) specimen exposed to distilled water (DST) after 310 FT cycles (SEM-BSE).

APPENDIX E. PORE SOLUTION ANALYSIS

TABLE E.1
Oxide composition of cement, class C fly ash and GGBFS used in the study.

Oxides	OPC	Class C fly ash	GGBFS slag ^a
Silicon Dioxide (SiO ₂)	18.94	36.9	32–42
Aluminum Oxide (Al ₂ O ₃)	5.65	20.14	7–11
Ferric Oxide (Fe ₂ O ₃)	3.29	7.01	0.1–0.7 ^b
Calcium Oxide (CaO)	63.2	24.6	35–45
Magnesium Oxide (MgO)	3.13	5.47	7–15
Sulfur Trioxide (SO ₃)	3.43	1.58	1–2.5 ^c
Loss on Ignition (LOI)	1.13	Not available	Not available
Sodium Oxide (Na ₂ O)	0.34	Not available	Not available
Potassium Oxide (K ₂ O)	0.78	Not available	Not available
Total Alkali as Na ₂ O	0.86	1.21	Not available

^aThe oxide composition for slag was obtained from the manufacturer and is presented as a range of values, rather than a single value.

^bThe reported value represents FeO instead of Fe₂O₃.

^cThe reported value represents sulfides (S²⁻) and sulfates (SO₄²⁻) instead of SO₃.

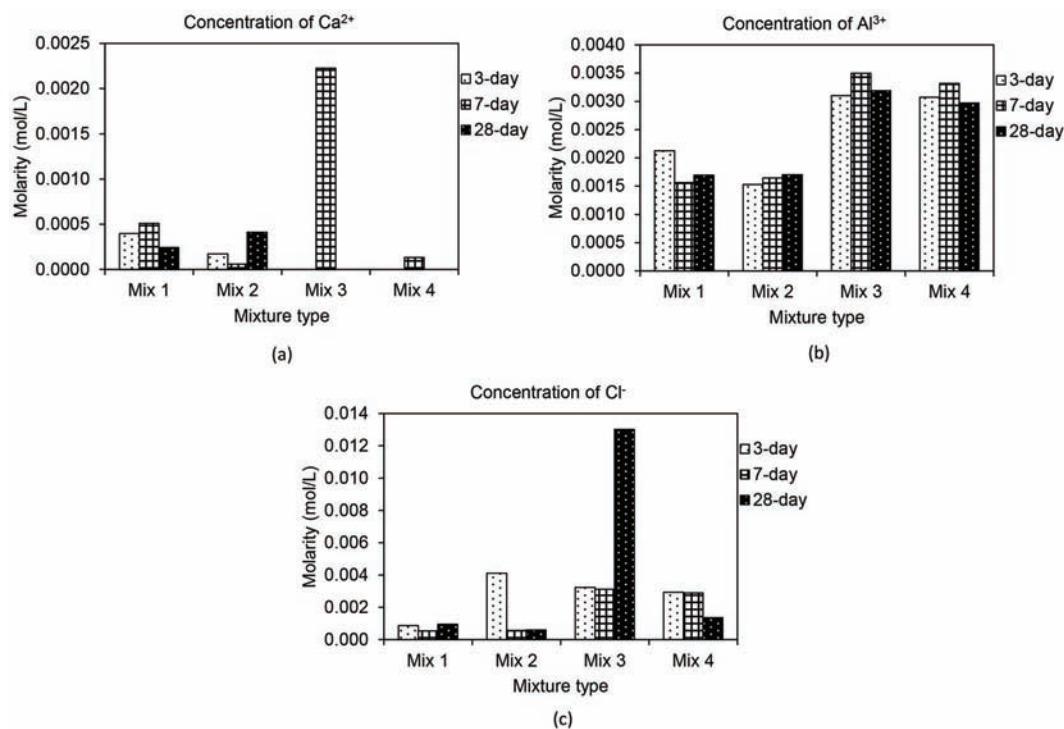


Figure E.1 Concentration variation of (a) calcium, (b) aluminum and (c) chloride ions.

APPENDIX F. BENEFIT COST ANALYSIS

New Pavement	Driving Lanes				PCC Shoulder	Area of Pavement	Total Volume	ACBFS in Base Course	Estimated quantity required ^a					
	No.	Width (ft)	Thickness (in)	PCCP Length (mi.)	Width (ft)	(ft ²)	(cyd)	%	Cement	F.A.	GGBFS	Dolomite (#8)	ACBFS Agg.	Sand (#23)
												(US tons)		
Concrete	1	12	10	1	0	63360	1955.6	N.A.	573.0	0.0	0.0	1681.8	0.0	1290.7
Base (#8)	1	12	3	1	0	63360	586.7	100%	N.A.	N.A.	N.A.	0.0	586.7	N.A.
Base (#53)	1	12	6	1	0	63360	1173.3	100%	N.A.	N.A.	N.A.	0.0	1173.3	N.A.
Mix Design*	Cement	F.A.	GGBFS	Dolomite (#8)	ACBFS Agg.	Sand (#23)		Total	573.0	0.0	0.0	1681.8	1760.0	1290.7
(lbs/cy)	586	0	0	1720	0	1320								

^aThe estimated quantity required shown has been calculated for the mix design marked with an asterisk (*).

Figure F.1 Example of calculation of quantities of raw materials required.

	Haul Distance between					Hauling Cost	Landfill Cost						
Cost of #53 dolomite aggregate	ACBFS agg. production plant and landfill	ACBFS agg. production plant and concrete batching plant	Dolomite production plant and concrete batching plant	Dolomite production plant and project site	ACBFS production plant and project site	(typically \$ 0.3-0.4/ton)	(typically \$ 1-2/ton)	Cost of # 8 dolomite agg. (typically \$8.5-10.5/ton)	Cost of ACBFS agg. (typically \$9.5-10.5/ton)	Cost of Cement (typically \$40 - 70/ton)	Cost of FA (typically \$15 - 40/ton)	Cost of GGBFS (typically \$25 - 45/ton)	Cost of #23 Sand
	(\$/ton)	(mi.)	(mi.)	(mi.)	(mi.)	(\$/ton/mile)	(\$/ton)	(\$/ton)	(\$/ton)	(\$/ton)	(\$/ton)	(\$/ton)	(\$/ton)
	9	10	70	60	65	75	0.35	1.5	9.5	10	55	27.5	35

Figure F.2 Input variables for calculation of cost of concrete pavement.

About the Joint Transportation Research Program (JTRP)

On March 11, 1937, the Indiana Legislature passed an act which authorized the Indiana State Highway Commission to cooperate with and assist Purdue University in developing the best methods of improving and maintaining the highways of the state and the respective counties thereof. That collaborative effort was called the Joint Highway Research Project (JHRP). In 1997 the collaborative venture was renamed as the Joint Transportation Research Program (JTRP) to reflect the state and national efforts to integrate the management and operation of various transportation modes.

The first studies of JHRP were concerned with Test Road No. 1 — evaluation of the weathering characteristics of stabilized materials. After World War II, the JHRP program grew substantially and was regularly producing technical reports. Over 1,600 technical reports are now available, published as part of the JHRP and subsequently JTRP collaborative venture between Purdue University and what is now the Indiana Department of Transportation.

Free online access to all reports is provided through a unique collaboration between JTRP and Purdue Libraries. These are available at: <http://docs.lib.purdue.edu/jtrp>

Further information about JTRP and its current research program is available at: <http://www.purdue.edu/jtrp>

About This Report

An open access version of this publication is available online. This can be most easily located using the Digital Object Identifier (doi) listed below. Pre-2011 publications that include color illustrations are available online in color but are printed only in grayscale.

The recommended citation for this publication is:

Verian, K. P., Panchmatia, P., & Olek, J. (2017). *Investigation of use of slag aggregates and slag cements in concrete pavements to reduce the maintenance cost* (Joint Transportation Research Program Publication No. FHWA/IN/JTRP-2017/17). West Lafayette, IN: Purdue University. <https://doi.org/10.5703/1288284316362>